ANKARA YILDIRIM BEYAZIT UNIVERSITY

GRADUATE SCHOOL OF NATURAL AND APPLIED SCIENCES

ENHANCING THE PERFORMANCE OF RAYLEIGH BACKSCATTERING BASED FIBER OPTIC SENSORS

Ph.D. Thesis by

Abdullah Erkam GÜNDÜZ

Department of Electrical and Electronic Engineering

January, 2024

ANKARA

ENHANCING THE PERFORMANCE OF RAYLEIGH BACKSCATTERING BASED FIBER OPTIC SENSORS

A Thesis Submitted to

The Graduate School of Natural and Applied Sciences of

Ankara Yıldırım Beyazıt University

In Partial Fulfillment of the Requirements for the Degree of Doctor of

Philosophy in Electrical and Electronic Engineering, Department of Electrical and Electronic Engineering

by

Abdullah Erkam GÜNDÜZ

January, 2024

ANKARA

Ph.D. THESIS EXAMINATION RESULT FORM

We have read the thesis entitled "**ENHANCING THE PERFORMANCE OF RAYLEIGH BACKSCATTERING BASED FIBER OPTIC SENSORS**" completed by **ABDULLAH ERKAM GÜNDÜZ** under the supervision of **PROF.DR. HALİM HALDUN GÖKTAŞ** and we certify that in our opinion it is fully adequate, in scope and in quality, as a thesis for the degree of Doctor of Philosophy.

Prof. Dr. Halim Haldun GÖKTAŞ

(Supervisor)

Prof. Dr. İlyas ÇANKAYA

(Jury Member)

Prof. Dr. İsa NAVRUZ

(Jury Member)

Prof. Dr. Murat YÜCEL

(Jury Member)

Assoc. Prof. Dr. Ömer KARAL

(Jury Member)

Prof. Dr. Sadettin ORHAN

(Director)

Graduate School of Natural and Applied Sciences

ETHICAL DECLARATION

I hereby declare that, in this thesis which has been prepared in accordance with the Thesis Writing Manual of Graduate School of Natural and Applied Sciences,

- All data, information and documents are obtained in the framework of academic and ethical rules,
- All information, documents and assessments are presented in accordance with scientific ethics and morals,
- All the materials that have been utilized are fully cited and referenced,
- No change has been made on the utilized materials,
- All the works presented are original,

and in any contrary case of above statements, I accept to renounce all my legal rights.

Date: **Signature:**

Name & Surname: Abdullah Erkam GÜNDÜZ

ACKNOWLEDGEMENTS

I would like to express my gratitude to my supervisor, Prof Dr. Halim Haldun GÖKTAŞ. He supported and motivated me endlessly during this study. He pointed me to right direction whenever I was lost. Also, I would like to thank committee members Prof. Dr. İlyas ÇANKAYA and Prof. Dr. İsa NAVRUZ who always kindly supported and guided me.

I would like to thank Prof. Dr. Murat YÜCEL for providing me with access to his laboratory and his continuous support.

I would also like to thank my colleagues Özgün ERSOY and İrfan Alp GÜRKAYNAK for their help and suggestions during this study.

Most importantly, I would like to thank my family, my father and my mother for their continuous support. They have always supported me when I was in despair about the thesis. This thesis and other achievements in my life would not have been possible without them.

Finally, I would like to thank The Scientific and Technological Research Council of Turkey (TUBITAK) for supporting this thesis study under the National Ph.D. Scholarship Program Grant with Code (2211-A).

ENHANCING THE PERFORMANCE OF RAYLEIGH BACKSCATTERING BASED FIBER OPTIC SENSORS

ABSTRACT

In this thesis, firstly, an Optical Time Domain Reflectometer (OTDR) system was simulated using OptiSystem which was successful at locating connector positions along a 10 km test fiber. Then the simulated OTDR system is constructed in laboratory to successfully detect connector positions along a 22 km fiber. Furthermore, the effects of laser pulse width and peak to peak voltage of low frequency (LF) trigger signal over the received signal are observed. The detection capabilities of biased and non-biased photo detectors are observed. A MATLAB remote control code is created to fully automate data acquisition process and parameter changes. Standard Commands for Programmable Instruments (SCPI) command protocol is utilized in the remote-control code.

Then, the performance of the OTDR system is tried to be improved. The high reflection loss effects of connectors are negated using splices. The effect of an isolator at the end of the test fiber is observed. A GUI is designed to improve OTDR monitoring.

Finally, an investigation of different types of fiber for their compatibility in a Rayleigh based optical time domain reflectometer (R-OTDR) temperature sensor setup is conducted. A reference test setup consisting of standard single mode fiber (SMF) is observed to constitute a background for comparison. In this setup, the Rayleigh response of -50.25 dBm and a temperature sensitivity of 0.002 dB/°C is achieved. Then Rayleigh responses for highly nonlinear fiber (HNLF), dispersion shifted fiber (DSF) and polarization maintaining fiber (PMF) are observed. The Rayleigh responses were: HNLF had -39.83 dBm, DSF had -34.03 dBm and PMF had -31.34 dBm. Since PMF showed the best Rayleigh response it was selected to be observed as fiber under test (FUT) in a classical R-OTDR temperature sensor setup. With the PMF used in temperature R-OTDR setup a temperature sensitivity of 0.018 dB/°C was achieved. As a result, it has been determined that PMF fiber has high temperature sensitivity in R-OTDR installations compared to SMF. It has been shown that temperature measurements can be made on

shorter lengths of fiber with a much simpler setup using PMF as opposed to the more complex alternatives.

Keywords: Rayleigh scattering, OTDR, Temperature sensor, Nonlinear fiber

RAYLEIGH GERİ SAÇILMA TABANLI FİBER OPTİK SENSÖRLERDE PERFORMANS İYİLEŞTİRİLMESİ

ÖZ

Bu tez çalışmasında, öncelikle, 10 km'lik bir test fiberi boyunca konnektör konumlarını bulmada başarılı olan OptiSystem kullanılarak bir Optik Zaman Alanı Reflektometre (OTDR) sistemi simüle edildi. Daha sonra simüle edilmiş OTDR sistemi, 22 km'lik bir fiber boyunca konnektör konumlarını başarılı bir şekilde tespit etmek için laboratuvarda oluşturuldu. Ayrıca, düşük frekanslı (LF) tetikleme sinyalinin darbe genişliğinin ve tepeden tepeye voltajının alınan lazer sinyali üzerindeki etkileri gözlemlenmiştir. Biased ve non-biased foto dedektörlerin algılama yetenekleri gözlemlenmiştir. Veri toplama sürecini ve parametre değişikliklerini tamamen otomatikleştirmek için bir MATLAB uzaktan kumanda kodu oluşturuldu. Uzaktan kumanda kodunda Programlanabilir Araçlar için Standart Komutlar (SCPI) komut protokolü kullanıldı.

Daha sonra OTDR sisteminin performansı artırılmaya çalışıldı. Konektörlerin yüksek yansıma kaybı etkileri fiber eklemeler kullanılarak ortadan kaldırıldı. Test fiberinin ucundaki bir yalıtkanın etkisi gözlemlendi. OTDR izlemeyi geliştirmek için bir GUI tasarlanmıştır.

Son olarak, Rayleigh tabanlı optik zaman alanı reflektometre (R-OTDR) sıcaklık sensörü kurulumunda farklı fiber türlerinin uyumlulukları açısından bir araştırma yapılmıştır. Standart tek modlu fiberden (SMF) oluşan bir referans test kurulumunun karşılaştırma için bir arka plan oluşturdu. Bu kurulumda -50.25 dBm Rayleigh tepkisi ve 0.002 dB/°C sıcaklık hassasiyeti elde edildi. Daha sonra yüksek derecede doğrusal olmayan fiber (HNLF), dispersiyonu kaydırılmış fiber (DSF) ve polarizasyonu koruyan fiber (PMF) için Rayleigh tepkileri gözlemlendi. Rayleigh saçılımları: HNLF -39.83dBm, DSF -34.03 dBm ve PMF -31.34dBm olarak kaydedildi. PMF en iyi Rayleigh tepkisini gösterdiğinden, klasik bir R-OTDR sıcaklık sensörü kurulumunda fiber test altında (FUT) olarak gözlemlenmek üzere seçildi. Sıcaklık R-OTDR kurulumunda kullanılan PMF ile 0,018dB/°C sıcaklık hassasiyeti elde edildi. Sonuç olarak PMF fiberin R-OTDR kurulumlarında SMF'ye göre yüksek sıcaklık hassasiyetine sahip olduğu tespit edilmiştir.

Daha karmaşık alternatiflerin aksine, PMF kullanılarak çok daha basit bir kurulumla daha kısa fiber uzunluklarında sıcaklık ölçümlerinin yapılabileceği gösterilmiştir.

Anahtar Kelimeler: Rayleigh saçılması, OTDR, Sıcaklık sensörü, Doğrusal olmayan fiber

NOMENCLATURE

Acronyms

AOM	Acousto-Optic Modulation
BOTDA	Brillouin Optical Time Domain Analysis
BOTDR	Brillouin Optical Time Domain Reflectometer
C-OFDR	Coherent Optical Frequency Domain Reflectometer
CW	Continuous Wave
DSF	Dispersion Shifted Fiber
EDFA	Erbium Doped Fiber Amplifier
FBG	Fiber Bragg Grating
HNLF	Highly Nonlinear Fiber
I-FMCW	Incoherent Frequency-Modulated Continuous Wave
I-OFDR	Incoherent Optical Frequency Domain Reflectometer
LF	Low Frequency
MZM	Mach Zehnder Modulator
OSA	Optical Spectrum Analyzer
OTDR	Optical Time Domain Reflectometer
PD	Photo Diode
PMF	Polarization Maintaining Fiber
R-OTDR	Rayleigh Optical Time Domain Reflectometer
SMF	Single Mode Fiber
TLS	Tunable Laser Source

CONTENTS

TABLE OF FIGURES

CHAPTER 1

INTRODUCTION

The simplicity, accuracy and higher sustainability of optical fiber sensors have attracted many researchers to apply them in temperature sensing applications [1,2]. Various methods of optical fiber sensors have been investigated in the literature, mainly; Fiber Bragg Grating (FBG) based [3-6], Brillouin backscattering based [7-11] and Raman backscattering based [12-14]. However, Rayleigh backscattering based [15-17] fiber optic temperature sensors offer more advantages as they are much simpler and cheaper.

Brillouin backscattering based temperature sensors offer advantages in sensitivity [18,19]. However, the frequency analysis in Brillouin sensors require many filters, window fittings, complex calculations of reverse Fourier transform even before the data becomes usable for processing [20,21]. FBG based sensors also suffer from the same frequency analysis complexity [22]. Although they are mainly used in fiber amplifiers [23-25], Raman backscattering can also be utilized in temperature sensing. However, Raman sensors need powerful amplifiers and polarization controllers [26], which add to the overall cost the sensor setup. In Rayleigh based setups, on the other hand, especially in classical OTDR's, depending on the selection of the test fiber type good temperature results can be achieved even with shorter lengths of FUT [27]. Thereby, Rayleigh based sensors offer more accessible and easier alternatives to inelastic backscattering sensors.

1.1 Background

D. Hazarika and D.S. Pegu's work describes a microcontroller-based instrumentation system for monitoring air pressure using fiber optic sensors. The instrumentation system includes a laser source, a beam distributor, two multi-mode fiber optic cables, two light dependent resistor (LDR) based timer circuits and the AT89S8252 microcontroller. The beam splitter is used to divide the laser beam into two parts and are sent to two multimode fibers. One of the multimode fibers is used as a sensing fiber and the other as a reference fiber. The purpose of using reference fiber is to eliminate environmental impacts during

air pressure measurement. The two laser beams in the sensor and reference fibers are applied to two equivalent LDR based timer circuits. The LDR-based timer circuits are connected to the microcontroller via timer pins. The microcontroller samples the frequencies of the timer circuits using its counter-0 and counter-1 circuits. Counter values are used to measure the air pressure magnitude [28].

In the study of Alberto J. Palma et al., an optical sensor comprising a new opto-chemical portable electronic device for the determination of atmospheric oxygen is presented. Optical sensors based on luminescence quenching are designed for sufficient accuracy and high stability. The portable device is based on a microcontroller. Its main features are single optical sensor channel, optical filter, fully digital signal processing capacity, reprogramming, data saving, low power consumption, computer communication capability. With the use of a digital output photodetector, there is no need for analog processing with less circuit elements and better noise immunity. The parameter measured in the transmission process is like the luminescence lifetime. Instrument characteristics are temperature effect correction, low drift and 0.5% accuracy of oxygen concentration [29].

A. F. Omar and M. Z. Matjafri use the method of spectroscopy analysis fiber sensor for detection of water quality. The system is capable of detecting scattered 180 ° from light that is reflected from light when there is an interaction between light and solids suspended in water. Empirical analysis is performed by measuring clay capacity (mg / L) suspended in water. The system consists of two separate light detector circuits that are sensitive to blue (470Nm) and red (635nm) monochromatic light. The result of the detection is sent to the microcontroller with Basic Stamp 2 for processing and analysis. The turbidity level is defined and displayed by the microcontroller [30].

Qiuhong Zhang and Qian Liu proposed to make a smart home control system to improve the high-tech living environment, computer, network, control and integration technology which integrates domain family and even the whole city. It detects ambient temperature and stress change by scattering from the fiber optic sensor. In this study, microcontroller, GSM, fiber optic sensor and smart home control system are explained. In this study,

wireless data transmission networks have been built by using GSM for wireless communication [31].

Oleg Uzenkov et al. presented an FPGA-based measuring system to measure the output of a fiber-Bragg grating-based tension sensor. The system can track up to 10 light source outputs generated by the fiber Bragg grating sensor and separate them using a miniaturized monochromator. The center of the light sources can be measured using a 2048-pixel linear CCD array controlled by Xilinx FPGA. The system scans the linear array with a frequency of 2 MHz and a sub-pixel resolution of 1 micro-stress. The control circuit can be realized in an XCS40 circuit with 58% less logic resources [32].

In this study, Graham Wild and Steven Hinckley presented an Intelligent Converter Interface Module (STIM) for distributed optical fiber intelligent sensors. STIM is a general-purpose interface designed for use with intensiometric optical fiber sensors. The interface consists of two optical fiber PIN receivers, a differential amplifier, and a digital signal processor. The two received signals are differentially amplified to increase sensitivity and signal-to-noise ratio. STIM has been successfully used as an embedded system in both temperature and strain monitoring, and these measurements can be used to alert when a predetermined threshold is exceeded. The sensing system can be used to detect dynamic stress signals successfully even without DSP [33].

In this dissertation study by Qin, a distributed optical fiber vibration sensor based on Rayleigh scattering was developed. Pen breaking was used as the vibration source and the spatial resolution was 1 m and the maximum distance between the maximum vibration point and detection point was measured as 18 cm. Distributed vibration measurements of 500 Hz up to 1 kHz were performed on a 20 cm single-mode fiber [34].

In the study of Bao and Chen, the recent developments on scattering based fiber sensors were investigated. It was observed that Rayleigh, Brillouin, and Raman scattering in the fiber occurred because of interactions of photons within the fiber due to density, temperature and stress. For example, an acoustic/mechanical wave forms a dynamic intensity diversity. It has been observed that these and similar variations are caused by

changes in local temperature, stress, and vibrations. Measurements such as temperature and vibration can be detected by detecting changes in the phase, frequency or amplitude of light scattered from the fiber, which is several meters to hundreds of meters in length. In these and similar measurements, it has been found that it is possible to access location information by using time domain or frequency domain analysis [35].

In this study by Barrios et al., Brillouin sensors which provide innovative solutions for temperature and stress measurements in large structures were investigated. Typically, the effective measuring range of these sensors is in the range of 20-30 km. In this study, Brillouin optical time domain analysis (BOTDA) was used to extend the measuring distance. The measuring distance could be extended with some strengthening methods and the quality of the measurement could be improved [36].

In this study by Soto et al., optimization of Brillouin time domain analysis (BOTDA) sensors using Raman amplification was investigated to make longer distance and higher resolution measurements. Stress/temperature measurements were performed with a 120-km single mode fiber with Raman amplifier, with an error of 2 meters and an accuracy of 45με / 2.1°C [37].

In the study of Chen et al., a new diffuse sensor system based on harmonious interaction in Brillouin gain and loss was investigated. 0.5 m spatial resolution and 6 με stress accuracy were experimentally obtained using 20/15 ns Stokes and Anti-Stokes pulses on a 15 m long polarization protected fiber [38].

In Mafang's thesis, a new technique called Brillouin Echoes Distributed Sensing (BEDS) has been developed. In the first part, the classic Brillouin sensor configuration is updated. Then, the limitations of the conventional Brillouin sensors are measured. In the second part, the BEDS approach that describes spatial resolutions in Brillouin scattered measurements is presented. By using BEDS technology, it was possible to obtain great accuracy in the laboratory tests. In addition, the geometric structure fluctuation along a photonic crystal fiber was modeled using BEDS [39].

In this study by Frazao et al., a Raman fiber Bragg grating laser sensor for stress/temperature measurements is presented. Using a pump laser, it was possible to obtain a Raman Bragg grating sensor in the class of 35nm. Bragg gratings were fixed to 10 km [40].

In the study by Martins et al., a temperature-insensitive strain sensor with Rayleigh scattering based on Four-Wave Mixing (FWM) using a Raman fiber Bragg grating laser was studied. Two fiber Bragg gratings were used to form two linear cavity laser sensors that were strengthened together by Raman and Rayleigh scattering. Due to the low scattering coefficient of the fiber, it was possible to use two lasers using FWM. In this configuration, only one of the two sensors is sensitive to strain. The difference between the incident signal's wavelength and the converted signal offers a tensile coefficient with a sensitivity of 2 pm/με [41].

In the study of Bolognini et al., the behavior of random Raman scattering and coded OTDR based distributed temperature sensors were studied theoretically and experimentally. A high-performance design has been implemented using amplitude modulation with simplex coding. The detection range is extended using segmented Raman amplification and direct detection. Along a 30 km scattering shifted fiber, a spatial resolution of 17 m and a temperature resolution of 5 °K was achieved. Hence an efficient and economical distributed temperature sensor is theoretically and experimentally proved [42].

In the study of Stokes and Vo-Dinh, fiber sensors based on Surface Enhanced Raman Scattering (SERS) in a single fiber system were observed for remote and on-site measurements. The heart of the sensor is designed with a special single mode optical fiber. This design uses a single fiber under test which offers practicality for on-site measurements in the microenvironment. Since the laser excitation and SERS signal radiation in a single fiber are carried together, the remote sensor type parameters are simpler and more stable [43].

In the study of Palmieril and Schenato, the properties of distributed fiber sensors based on Rayleigh scattering were examined. These distributed optical fiber sensors are based on scattering processes resulting from the interaction between light and object. For a certain optical frequency, Rayleigh-based sensors use the three basic characteristics of light: intensity, phase and polarization. In this study, all these detection mechanisms are examined in terms of basic principles, basic flow techniques and possible application areas [44].

A. Wosniok et al. developed a distributed fiber optic imaging system for the determination of stress and temperature along single mode fiber. The system is based on the BOFDA technique, and the side band technique is used to reduce cost. No tunable laser source was required [45].

In this study, Hyungwoo Kwon and colleagues developed a long-distance distributed fiber senor system using coherent (single-phase) sensing along a 36 km long fiber. Calculated using the Lorentzian algorithm, Brillouin frequency shift was also measured successfully [46].

A.H. Reshak and colleagues examined Brillouin and Rayleigh scattering behavior in optical fiber. Simulations were done to observe the coherent Rayleigh scattering. A new algorithm was presented to effectively determine the backscattered Brillouin signal for certain incident light wavelength [47].

Y. D. Gong in his study, introduced analysis of distributed temperature and strain sensor based on the stimulated Brillouin scattering effect in optical fiber. It offers some new considerations for short and long-distance distributed temperature and strain sensors, such as optimizing incident power and optimizing pump power [48].

In their study, V. Lecoeuche et al. presented a new study for a single-terminated fiber sensor based on stimulated Brillouin scattering with the sensitivity of sensing fast enough temperature or tension on a 25 km long sensing fiber with spatial resolution of 2 m. The system reveals the effect of phase modulation as an important limiting factor for probe wave power [49].

P.C. Wait and colleagues in their study observed advances in narrow-band pulse laser technology and using low-loss fiber filters to separate Rayleigh signal from the Brillouin signal [50].

A. Perez-Herrera and M. Lopez-Amo identified and compared different types of multiplexing networks used in fiber optic sensors, including networks using optical amplifying and lasing multiplexing systems. Multiplexed and dispersed sensor networks using strong, longer, and distributed Brillouin signals have been shown [51].

Sorin et al., used a 1320 nm, 2 kHz linewidth Nd:YAG laser to diagnose optical communication networks. The long coherence length of the laser allowed for measurements up to 50 km, whereas the spatial resolution was limited to 380 meters [52].

Venkatesh et al., used a piezoelectric tuning of a single-mode Nd:YAG ring laser by varying the gap between the two pieces of the laser resonator. 5 cm apart Fresnel reflections were obtained over 20 m [53].

Shimizu et al., using a multi-quantum well distributed feedback laser diode, obtained 50 cm spatial resolution over 500 m. The laser frequency was swept by a control current [54].

Huang et al., used a GaAs quantum well laser diode which was spliced to a grating wrapped around a piezoelectric transducer cylinder. This laser was tuned by strain and the length of the cavity yielded a wavelength change. Spatial resolution of 2 m was obtained over 115 m [55].

Passy et al. [56] obtained a resolution of 400 μm over 10 cm by using a three-electrode DFB laser at 1550 nm coupled to an external cavity. Observing Rayleigh backscattering over 400 m was provided due to the 200 kHz linewidth [57].

Tsuji et al., achieved spatial resolution of 5 m over 30 km by using an electro-optic phase modulator with 1.55 μm Er-Yb laser [58].

Oberson et al., used Er/Yb codoped fiber spliced with a pair of fiber Bragg gratings as laser resonator. 10 kHz linewidth and 16 cm spatial resolution over 150 m was demonstrated [59].

Geng et al., was able to measure Rayleigh backscattering over 95 km [60].

Oh et al., used a mode-locked fiber laser in unidirectional ring configuration with an EDF and a Fiber Fabry-Pérot Filter (FPF). 100 μm spatial resolution over several centimeters was achieved [61].

Ndiaye et al., obtained 50 μm spatial resolution over 1 m using FPF laser [62].

Juan Clement et al., proposed an I-OFDR system based on low-bandwidth direct detection and balanced bidirectional phase modulation. The system provides negligible amplitude and phase imbalances in frequency conversions. Spatial resolution of 2.3 cm was achieved [63].

Youngwoong Kim et al., proposed a bi-directional determination technique of Rayleigh C-OFDR system for distributed strain and temperature sensing. The system uses phase-shifting method with a 3 × 3 fiber coupler to double the measurement range. Strain and temperature sensing over 200 m was achieved [64].

Fan Ai et al., proposed an ultra-weak FBG (UWFBG) based C-OTDR that provides simultaneous temperature and vibration sensing. The system utilizes 63 UWFBGs. Very high temperature accuracy of 0.05℃ over 30 cm was achieved [65].

There are various types of Rayleigh based fiber optic temperature sensors. Yang Zhi et al., proposed a system that utilized the jagged appearance of Rayleigh backscatter traces from an SMF measured with a coherent OTDR (COTDR) that was dependent on the reproducibility and restorability of the Rayleigh backscatter traces. When the system was simulated the frequency compensation for strain and temperature change is detected through cross correlation of reference OTDR signal and measured OTDR signal [66].

Leonardo Marcon et al., proposed an OTDR system modelled with the virtual perturbation induced by the cumulative round-trip time delay change. The model works by comparing the theoretical results obtained from the first section of the fiber which is subjected to temperature change to the virtual perturbations measured on the second section of the fiber. For each measured disturbance an algorithm can compute and correct the corresponding virtual perturbation, improving the quality of the CP phase-OTDR [67].

Tao Liu et al., demonstrated an ultra-high resolution distributed strain sensor assisted with Rayleigh-scattering enhanced optical fiber and phase noise compensation scheme. They achieved a static strain resolution of 1.89 nε and dynamic resolution of 97.5 pε/√Hz over 1Hz [68].

Chengli Li et al., proposed an enhanced distributed optical fiber sensor based on broadband ultra-weak fiber Bragg grating array (UWFBG) to measure dynamic strain using −50 dB reflectivity and with reflected signal 17 dB higher than the Rayleigh backscattering. They successfully managed to observe a temperature range of 20 ℃ to 200 ℃ with minimum phase detection of 1.02×10−3 rad/Hz, and SNR above 59.2 dB at 100 Hz [69].

1.2 Problem Statement

In fiber optic sensing systems, Reflectometry based sensors are used to detect various environmental factors such as: temperature, pressure, strain and vibration. These environmental factors change very rapidly along a long distance. Both the amount of change and the location can affect system health. Especially for security, these rapid changes need to be sensed over a long distance with precision.

To meet these requirements, distributed fiber sensors have been developed. These sensors are acquired by using the backscattering phenomena happening on the fiber. The incident light travelling from one end of the fiber experiences reflections, scatterings along its journey. Mainly these scatterings can be elastic or inelastic. The elastic scattering is of the same frequency with the incident light. They are caused by the collision of light with molecular inhomogenities formed during manufacture along the fibers. The main elastic

backscattering is Rayleigh backscattering [15,16]. The inelastic scatterings have different frequencies compared to incident light. They are mainly caused by interference with the acoustic [8,9] and dielectric effects along the fiber [13]. Brillouin and Raman are the main inelastic backscatterings.

Utilizing these backscatterings, time domain reflectometry systems have been constructed to sense environmental changes over a fiber. The light sent from one end of the fiber as short strong pulses, and arriving the backscattered light is observed. The arriving light experiences losses with respect to environmental factors along the fiber. These losses are observed to determine the amount ambient factor changes. The arrival time of the backscattered light is used to pinpoint the location of these ambient changes, as every loss arrives back at different times [27].

Brillouin OTDR systems have been used for measuring both temperature and strain changes. The backscattered signal is very weak and has different frequencies compared to the incident light. The frequency of the backscattered light is very close to incident light. Therefore, the arriving signal needs to be amplified heavily and processed to be meaningful [11]. To solve these problems, Brillouin optical time domain analysis systems (BOTDA) have been developed. In this setup a CW light is sent from the other end of the fiber to boost the scattered pulse travelling on the opposite direction [10]. Although the incoming light is boosted, the noise on signal is boosted as well.

Raman OTDR systems are mainly used for monitoring temperature change [24]. The Raman backscattered light has wavelength difference of 100nm with respect to the incident light. Therefore, filtering is needed to observe the arriving light. Also, the arriving signal is very weak compared to the incident light and needs to be boosted [26]. All the filters and powerful amplifiers increase the cost of the overall system.

In this thesis work, Rayleigh OTDR system will be studied as an alternative to Brillouin and Raman OTDR systems. This decreases the cost of the sensor system considerably. Also, the arriving signal does not need heavy processing since the backscattered light is of the same frequency. Different nonlinear fibers will be observed to see how they work as temperature sensing medium.

1.3 Intended Purpose

1. Simulating a Rayleigh OTDR system to detect lossy events along a fiber
2. Realizing the simulated system in laboratory and lossy event locations along a fiber
3. Observing the effects of splicing, isolators, trigger signal parameters on the quality of the backscattered light
4. Investigation of performance of R-OTDR as temperature sensor
5. Investigation of performance of Polarization Maintaining fiber (PMF) as temperature sensing medium

1.4 Scope of Research

The main aim of this thesis work is to design a simple and cheap distributed temperature sensor utilizing Rayleigh OTDR. At the beginning, a Rayleigh OTDR is simulated to detect loss events across a fiber to provide the proof of concept. Then this setup is realized in laboratory. The Rayleigh responses are observed. Then optimization is done on the input signal parameters. Various elements such as: isolators and splices are added to see their effects on the performance of the Rayleigh OTDR setup.

Investigation of different nonlinear fibers in a Rayleigh OTDR temperature sensor setup is conducted to determine which is the most efficient nonlinear fiber for the temperature testing medium to replace SMF. PMF is chosen as the temperature test medium.

1.5 Thesis Outline

Within the scope of the thesis, performance enhancement studies in terms of improving the backscattered signal power and increasing the temperature sensitivity for Rayleigh OTDR are provided with the addition of various optical elements and different nonlinear fibers as testing medium. Thesis organization is divided into five different chapters as follows:

In Chapter 1, the historical development of OTDR systems is mentioned and a summary is given together with the literature studies.

In Chapter 2, backscatterings and how OTDR systems work is explained theoretically. Brillouin OTDR, BOTDA, Raman OTDR and Rayleigh OTDR systems are mentioned.

In Chapter 3, Rayleigh backscattering based OTDR system is simulated using OptiSystem program. A lossy event detection system is observed to see the viability of the proposed setup.

In Chapter 4, the simulated Rayleigh OTDR setup is realized in laboratory. Various loss events and their locations are successfully detected and classified. Effects of input laser signal parameters, namely: Voltage peak to peak (Vpp) and pulse width on the OTDR performance are observed and optimal parameter values are chosen.

In Chapter 5, optical isolators are added to see their effects on the performance of the OTDR system. The Rayleigh OTDR temperature test setup is constructed and nonlinear fibers: HNLF, DSF, PMF are observed as potential test medium. PMF and SMF are compared on their temperature sensitivity responses.

CHAPTER 2

MAIN DISTRIBUTED SENSING MECHANISMS IN OPTICAL FIBERS

2.1 Introduction

In this section, main backscatterings in optical fibers, namely: Brillouin, Raman and Rayleigh are mentioned. Theoretical modeling of BOTDR, BOTDA, Raman OTDR and Rayleigh OTDR sensors are given.

2.2 Scattering in Optical Fibers

Scattering is the interaction of light with fiber core. As a result, the optical properties of the core are modified [70]. Only small amount of incident light suffers scattering after interacting with particles or doping materials in the fiber. The scattering happens in many random directions. Scattering phenomena is shown in figure 2.1.

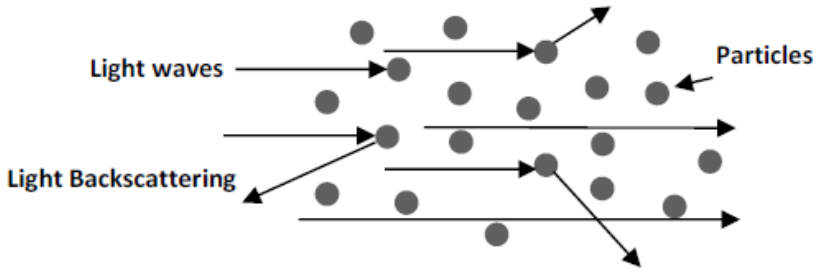

Figure 2.1 - Scattering and backscattering into the core of an optical fiber [70]

During scattering, some photons return to the source. This is called backscattering. These photons experience energy change. When the photon frequency does not shift, this is called an elastic scattering. When the photons suffer frequency shift, this is called an inelastic scattering. There are three main scatterings in optical fiber: Rayleigh (elastic), Raman (inelastic) and Brillouin (inelastic) scattering. Figure 2.2 shows these scatterings.

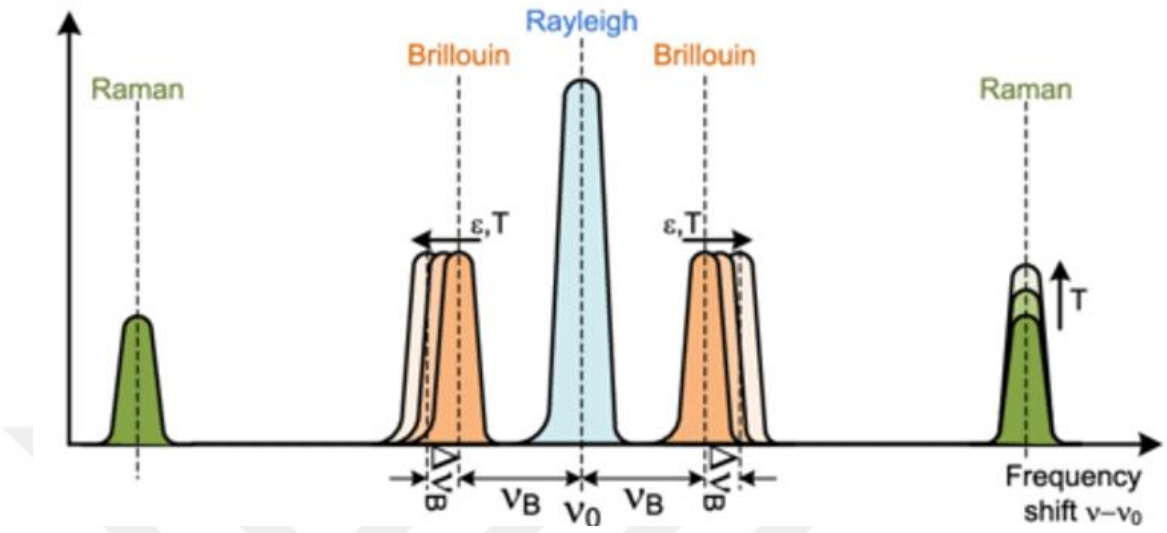

Figure 2.1 – Main backscatterings in optical fiber [71]

2.2.1 Brillouin Backscattering

Brillouin scattering occurs when materials experience compression due to an electric field, known as electrostriction [72]. When an electric field oscillates at the pump frequency Ωp, it generates an acoustic wave at a different frequency Ω. Spontaneous Brillouin scattering happens when the pump wave scatters from this acoustic wave, producing a new wave at the pump frequency Ωs, where both energy and momentum are conserved. This means that the Stokes shift Ω must be equal to $\omega_p - \omega_s$, due to energy conservation, whereas wave vector $\mathbf{k_A}$ should be $\mathbf{k_A} = \mathbf{k_p} - \mathbf{k_s}$ due to momentum conservation. The dispersion relation is given as $|\mathbf{k_A}| = \Omega/v_A$, ($v_A$: acoustic velocity). This gives us the acoustic frequency as [73]

$$\Omega = |k_A| v_A = 2 v_A |k_p| \sin\left(\frac{\theta}{2}\right) \tag{2.1}$$

Stimulated Brillouin scattering (SBS) happens in backwards direction. The back scattered Brillouin signal's frequency shift is given by $\Omega_B = 2 v_A |k_p|$. Using this, the Brillouin shift can be written as

$$\nu_B = \frac{\Omega_B}{2\pi} = \frac{2 n \nu_A}{\lambda_p} \tag{2.2}$$

2.2.2 Raman Backscattering

Raman scattering happens when the incident light collides with silica molecules. During these collisions, some of the incident photons transfer their energy to new photons at a lower frequency with reduced. Since the scattering is caused by energy transfer from molecular collisions, and not by a moving field of acoustic grating field, the Raman scattering can happen in forward and backward directions.

Similarly, the stimulated Raman scattering (SRS) happens in both forward and backward directions. The interaction between the incident and scattered light generates a frequency component $\boldsymbol{\omega_p - \omega_s}$ [73].

The Raman gain in optical fibers is usually around 10 THz. The vibrational energy levels of silica molecules create a band, which causes the Stokes frequency $\boldsymbol{\omega_s}$ to differ from incident light as $\boldsymbol{\Omega_R = \omega_p - \omega_s}$ [74].

2.2.3 Rayleigh Backscattering

In Rayleigh scattering the incident light interacts with very small particles in the fiber core. Here only minuscule variations happen in refraction index [75]. So, the backscattered light has the same frequency as the incident light. Therefore, Rayleigh scattering is elastic [70]. The Rayleigh backscattering has the highest amplitude out of the three main scatterings [76].

The density fluctuations in the silica molecules changes the refractive index of the fiber smaller than the incident wavelength $\boldsymbol{\lambda}$, which cause backscattering. The scattering cross-section scales inversely with $\boldsymbol{\lambda^4}$. The Rayleigh scattering loss can be written as

$$\alpha_R = \frac{C}{\lambda^4} \qquad \textbf{(2.3)}$$

where the constant C is in between 0.7-0.9 (dB/km)-(μm^4).

2.3 Brillouin Optical Time Domain Reflectometer (BOTDR)

In BOTDR sensing system, a CW laser is modulated with an AOM or EOM. The modulated optical pulse is sent to the sensing fiber via a circulator or coupler make a stimulated Brillouin scattering signal. The power and the frequency of the backscattered light is affected by the ambient temperature and strain along the sensing fiber [77]. A typical setup for BOTDR is given in figure 2.3.

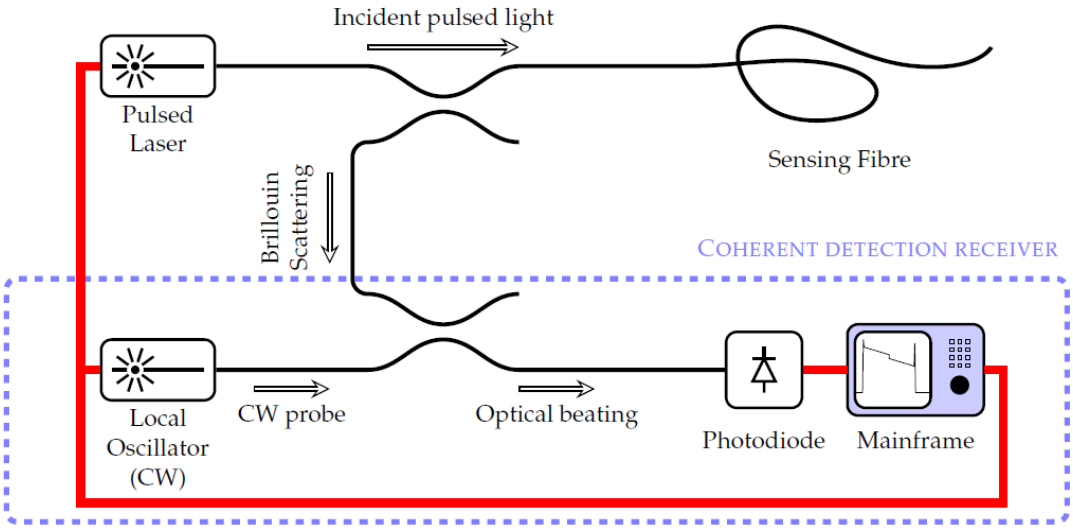

Figure 2.3 - BOTDR Setup [78]

The Brillouin frequency shift is affected by the ambient temperature and strain by

$$v_B = \omega_B(T_0, \varepsilon_0) + C_T(T - T_0) + C_\varepsilon(\varepsilon - \varepsilon_0) \quad \textbf{(2.4)}$$

Where T_0: initial temperature, ε_0: initial strain, C_T: BFS temperature coefficient and $C\varepsilon$: BFS strain coefficient.

However, the BOTDR has low Signal-to-Noise Ratio (SNR) as only backscattered incident pulse is read for temperature and strain data. SNR needs to be improved to effectively increase a sensor's range. Also, the measurements will become much more accurate with better SNR [77]. The measurement error can be found as

$$\Delta\alpha = \frac{W_{BGS}}{\sqrt{2}(SNR)^{\frac{1}{4}}} \quad \textbf{(2.5)}$$

To improve the BOTDR's sensing capabilities BOTDA systems have been proposed.

2.4 Brillouin Optical Time Domain Analysis (BOTDA)

The BOTDR sends the incident light through one end of the fiber. However, the resulting backscattered signal is very weak. To overcome this, a CW signal is interjected from other end of the fiber. The CW signal boosts the backscattered pulse signal [77]. This method is called Brillouin Optical Time Domain Analysis (BOTDA). The setup of a BOTDA is given in figure 2.4.

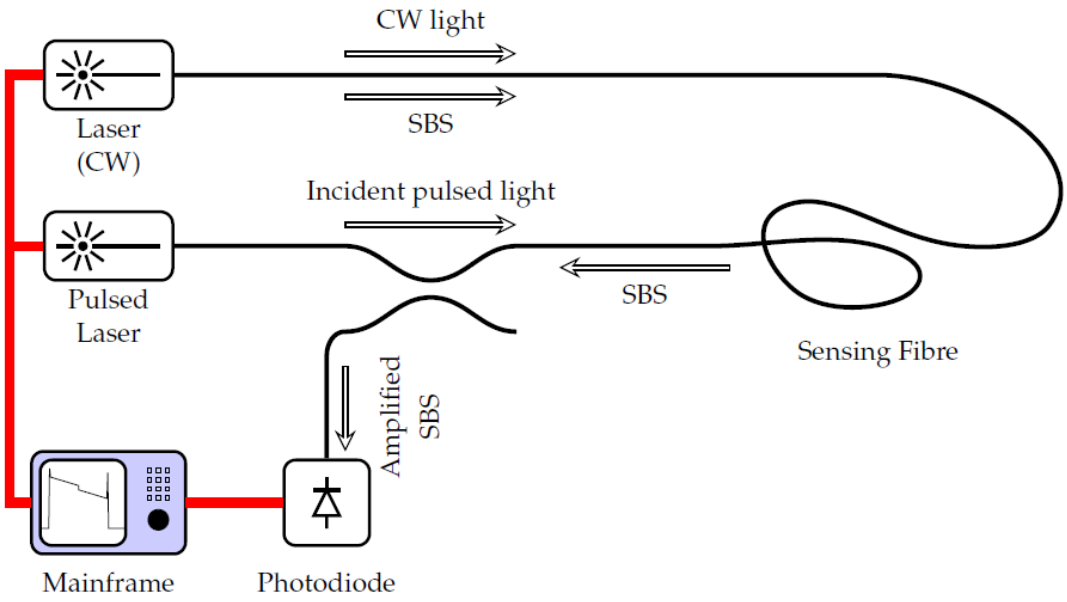

Figure 2.4 – BOTDA setup [78]

The frequency and power of the amplified backscattered light depends on ambient temperature and strain. Although, with this setup, the sensor needs access at both ends of the testing fiber, the received signal has much higher SNR, effectively increasing the sensing length.

2.5 Raman Optical Time Domain Reflectometer (Raman OTDR)

Unlike Brillouin, the Raman backscattered signal is only temperature dependent. Also, Raman stokes signals are much further away than Brillouin stokes, in the orders of 100

nm. To detect the temperature dependent Raman backscatter signals, a different type of OTDR technique is used, where the ratio of stokes to anti-stokes levels of backscattered light is examined [79]. The ratio is given as

$$R_r = \left(\frac{\lambda_S}{\lambda_a}\right)^4 \exp\left(-\frac{hcv}{kT}\right) \quad \textbf{(2.6)}$$

Where h: Planck's constant, c: velocity of light, v: frequency of incident light, k: Boltzmann constant and T: temperature.

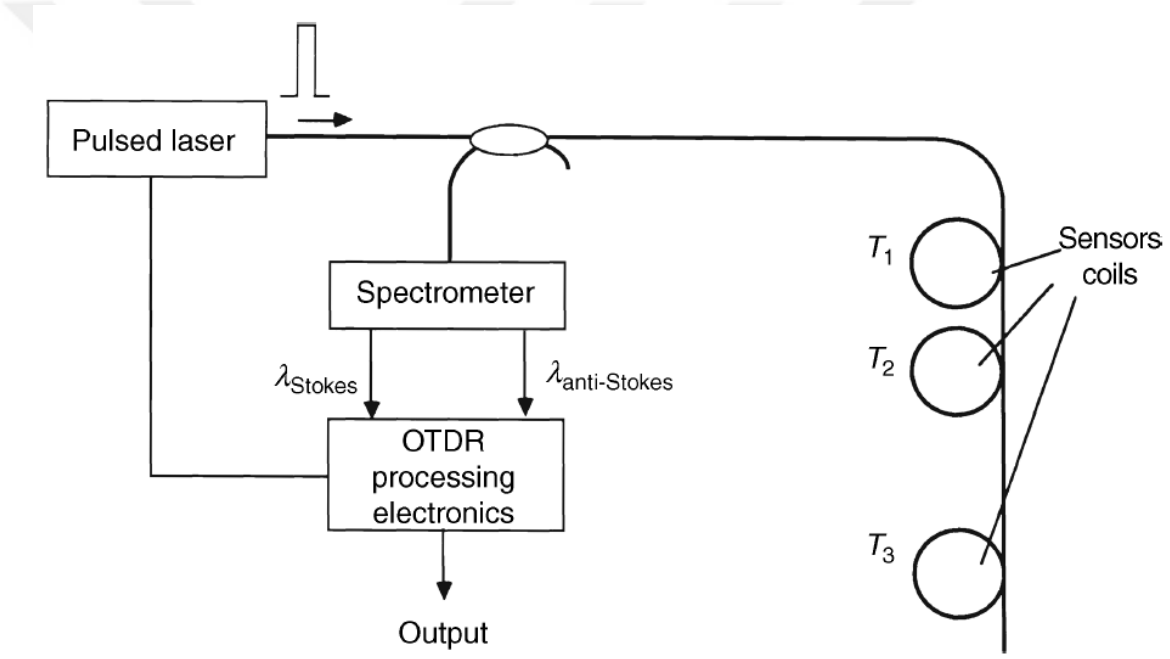

Figure 2.5 – Raman OTDR distributed temperature sensor [79]

2.6 Rayleigh Optical Time Domain Reflectometer (R-OTDR)

In OTDR, scattered signal's attenuation is measured. OTDR plots the attenuation of the backscattered light as a function of the time [80]. Light attenuation occurs due to Rayleigh backscattering. When a pulse of light is launched into an optical fiber, the attenuation decays exponentially with time due to the intrinsic loss in the fiber [75]. This is one of the principal reasons that OTDR is considered a linear backscattering system [76].

The light source sends out pulses of laser with a specific duration or pulse width and send them into FUT. Rayleigh backscattering happens in FUT and backscattered pulses are

sent to the photodetector [81]. The photodetector measures the attenuation of the scattered pulses and assign an electric level accordingly. The round-trip pulse travel time light multiplied by the speed of light in the FUT, is used to calculate the round-trip distance. The distance from the OTDR to the measured point is the half of the round-trip distance [82]. Using above, distance-attenuation graphics are obtained. In OTDR systems the spatial resolution is in the order of meters. The spatial resolution is given by below equation, where c is the speed of light, n is the fiber refractive index and τ is the pulse width

$$\Delta z = \frac{C\tau}{2n} \tag{2.7}$$

Stimulated emission in the gain environment of the amplifier amplifies the incident light in the linear gain amplifier erbium doped fiber amplifier [83]. As the second type of optical signal amplifier, Raman fiber amplifier is a non-linear gain amplifier. Photons in the incoming light interact with the phonons in the environment and produce photons with new energy level [84].

2.6.1 Incoherent Optical Frequency Domain Reflectometry (I-OFDR)

In this method, a CW probe signal is modulated by a constant amplitude RF signal whose frequency is changed periodically over a certain frequency range either stepwise (step-frequency method) [85] or continuously (sweep frequency method) [86] and sent into DUT. Rayleigh backscattered and back reflected optical signals are detected as a function of frequency. Network analyzer is used to observe this frequency domain. Hence these systems are called Network Analysis OFDR (NA-OFDR). Inverse Fourier transform of the frequency response gives the time-domain impulse response if scanned frequency range is sufficiently large. NA-OFDR is shown represented in figure 2.3(a).

Alternatively for Incoherent Frequency-Modulated Continuous Wave (I-FMCW), the modulating RF signal is swept in frequency and the detected probe signal is mixed with the modulating RF signal in the electrical domain [87]. Resulting output is observed by an electrical spectrum analyzer. The frequency axis represents the delay times

experienced by the probe signal. The time axis is converted into physical distance as in OTDR. I-FMCW is shown in figure 2.3(b).

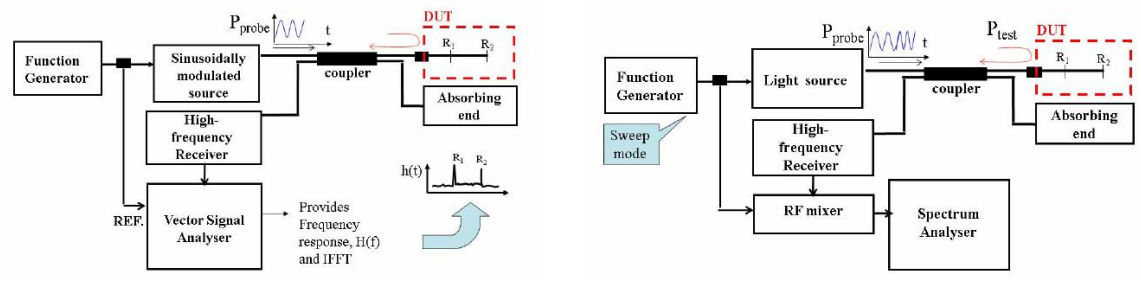

Figure 2.6 - Operation principles of (a) NA-OFDR, (b) I-FMCW [87]

2.6.2 Coherent Optical Frequency Domain Reflectometry (C-OFDR)

In the C-OFDR, the frequency of TLS is swept linearly in time then probe signal is split into two, where one goes to DUT whereas the other is used as reference signal in detection. This provides coherent detection of the backscattered signal. Then the interference signal containing beat frequencies with peaks is observed in network analyzer. The inverse Fourier transform of this signal gives the time domain response.

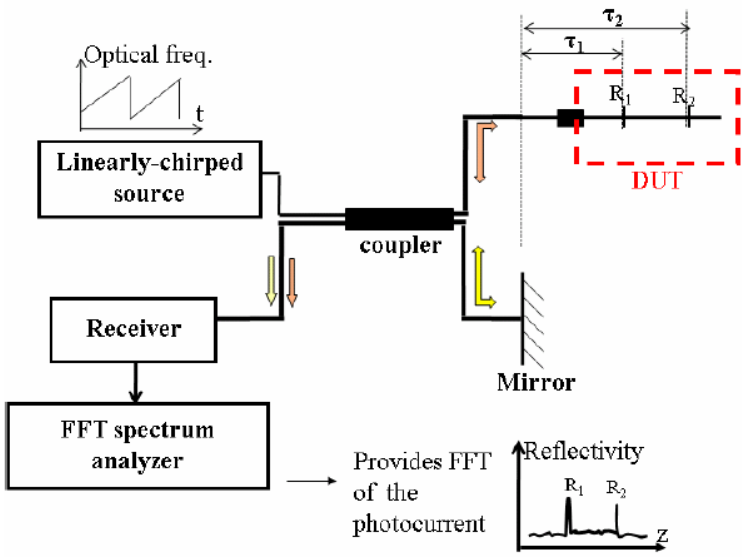

Figure 2.7 - Operation principle of C-OFDR [88]

The time domain response can be converted to distance scale as in OTDR. The squared magnitude of the signal at each beat frequency shows the reflectivity of each point [88]. C-OFDR is shown in figure 2.7.

C-OFDR has got some advantages [88]. The measured photocurrent is proportional to the square root of reflected optical power, which allows for measuring large power differences. Also, the RF frequencies are lower compared to other OTDR techniques. Therefore, the overall noise is reduced whereas dynamic range is increased. However, C-OFDR cannot be applied to long measurement distances. The measurement distance is limited by the coherence length of the TLS. Therefore, very expensive and precise TLS are needed to increase the measurement length.

2.7 Summary

The theoretical background of backscattering based OTDR systems is given in this section. The mechanisms of Brillouin, Raman and Rayleigh based distributed sensors are explained.

CHAPTER 3

DESIGN AND SIMULATION OF RAYLEIGH OTDR FOR LOSSY EVENT DETECTION

3.1 Introduction

In this section, a Rayleigh OTDR sensor setup will be simulated using OpstiSystem. This simulation study will provide a background Rayleigh scattering gain figure for the latter laboratory tests.

3.2 Electrical Pulse Generation

To create an electrical pulse, PRBS and Not Return Zero Pulse Generator (NRZ PG) is used. The PRBS creates a discrete output of electrical signal, utilizing overall system bit rate. PRBS parameters are given in figure 3.2. The operation mode has, Probability, Order, Alternate, Ones and Zeros modes. Probability mode uses Random number generator, with parameter Mark probability specifying the probability of ones in the sequence. Order mode [89] uses Order k to generate a sequence with period of 2k-1. In Alternate mode alternate sequence of ones and zeros is generated. Ones and Zeros modes generate a PRBS signal with 1's or 0's in between leading and trailing zeros. Here Ones order is chosen to generate a discrete electrical pulse with 1's in 0% to 5% of the time window of simulation.

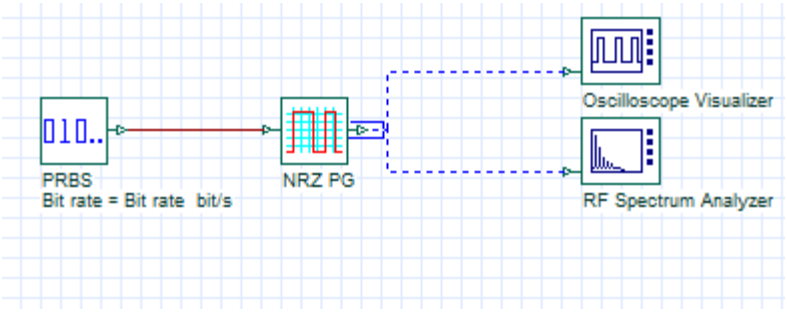

Figure 3.1 Electrical Pulse Generation in OptiSystem

Disp	Name	Value	Units	Mode
☑	Bit rate	Bit rate S	bit/s	Script
☐	Operation mode	Ones		Normal
☐	Order	log(Sequence length)/log(2 S		Script
☐	Mark probability	0.5		Normal
☐	Number of leading zeros	(Time window * 0 / 100) * S		Script
☐	Number of trailing zeros	(Time window * 95/ 100) * S		Script

Figure 3.2 Pseudo Random Bit Generator (PRBS) Parameters

Then the discrete pulse is sent to NRZ PG. NRZ PG takes a discrete set of 1's and 0's and creates a continuous pulse signal. Different from return zero (RZ), the NRZ PG does not return to 0 at 1's. Therefore 1's next to each other create a pulse signal. Parameters for NRZ PG is given in figure 3.3. Default parameter values are used.

Label: NRZ PG

Main | Simulation | Custom order

Disp	Name	Value	Units	Mode
☐	Rectangle shape	Exponential		Normal
☐	Format for pulse range	Min/Max		Normal
☐	Maximum	1	a.u.	Normal
☐	Minimum	0	a.u.	Normal
☐	Amplitude (wrt DC)	1	a.u.	Normal
☐	DC bias	0	a.u.	Normal
☐	Position	0	bit	Normal
☐	Rise time	0.05	bit	Normal
☐	Fall time	0.05	bit	Normal

Figure 3.3 NRZ PG Parameters

Finally, the output electrical pulse is achieved and given in figure 3.4.

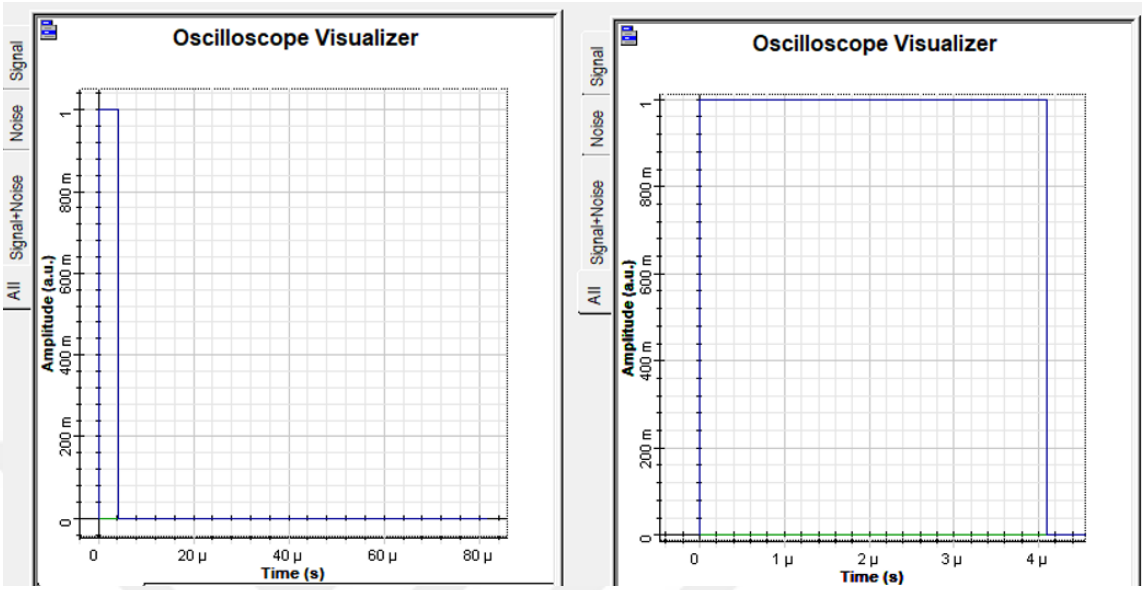

Figure 3.4 Electrical pulse signal 4μs pulse width

3.3 Optical Pulse Generation

Previously generated electrical pulse is used to generate optical pulse signal. The simulation setup is given in figure 3.5. To create an optical pulse, a continuous wave (CW) laser input is modulated with an electrical pulse signal. For modulation a Mach-Zender modulator (MZM) is used.

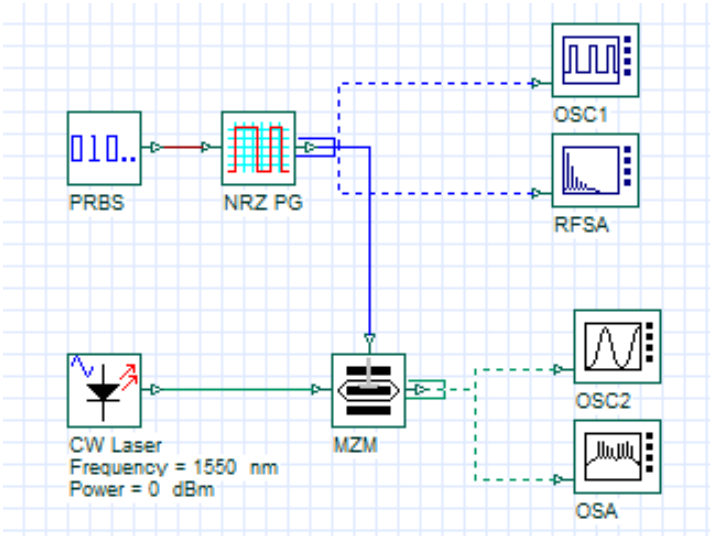

Figure 3.5 Optical Pulse Generation Simulation Setup

The CW laser and MZM parameters are given in figure 3.6 and figure 3.7 respectively.

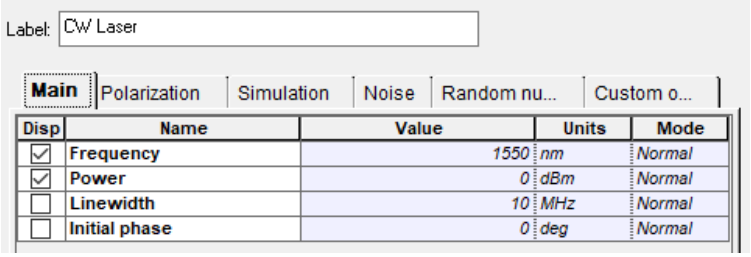

Figure 3.6 CW laser parameters

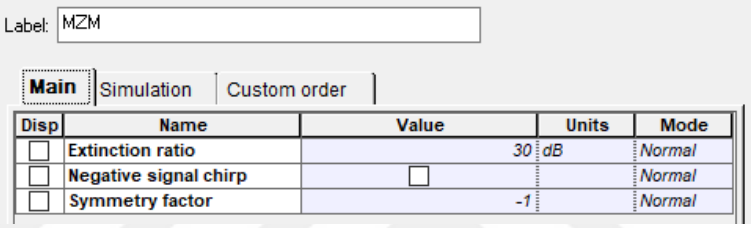

Figure 3.7 MZM parameter

The generated optical pulse signal is given in figure 3.8. Here the peak power of pulse is determined by CW laser power and the minimum power of the pulse is determined by the ER of the MZM. It is possible to lower noise power level by increasing the ER.

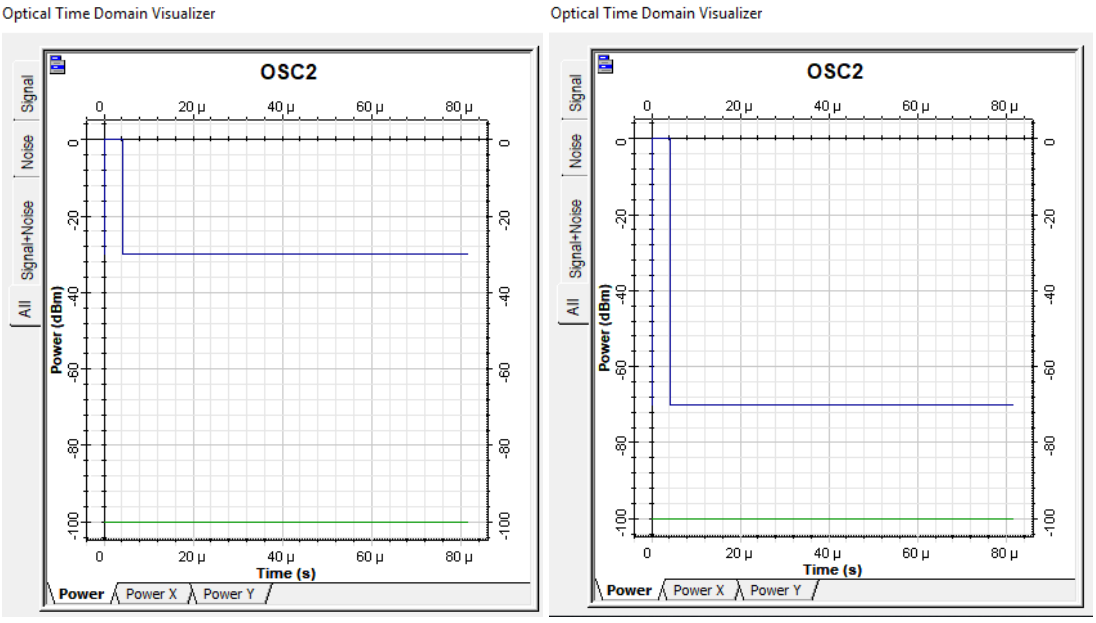

(a) (b)

Figure 3.8 Optical Pulse with (a) 30dB, (b) MZM Extinction Ratio (ER)

3.4 Rayleigh Backscattering Simulation

The simulation setup for observing Rayleigh backscattering over a 1 km optical fiber is given in figure 3.9. Here the further end of the optical fiber is attached to an Optical Null (ON) to enable bi-directional analysis.

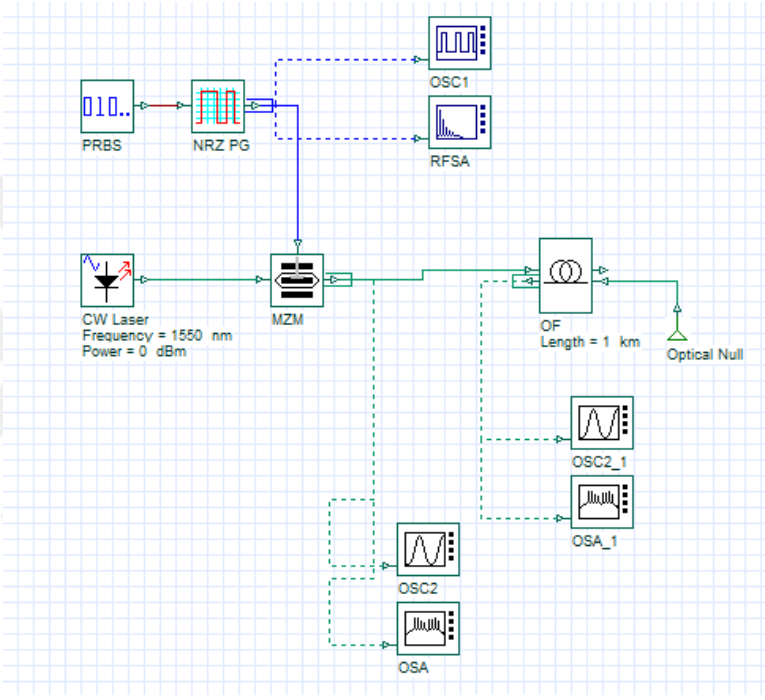

Figure 3.9 Rayleigh Backscattering Simulation Setup

For the optical fiber only the Rayleigh backscattering is enabled as enabling Brillouin and Raman backscattering will considerably increase the simulation time.

Label: OF

Main | Dis... | PMD | No... | En... | Nu... | Gr... | Si... | N... | Ra... | Cu...

Disp	Name	Value	Units	Mode
☐	Rayleigh scattering	☑		Normal
☐	Rayleigh data type	Constant		Normal
☐	Rayleigh backscattering	50.00000000000001e-006	1/km	Normal
☐	Rayleigh vs. wavelength	Rayleigh.dat		Normal
☐	Brillouin scattering	☐		Normal
☐	Brillouin gain data	Constant		Normal
☐	Brillouin gain constant	46.00000000000001e-012	m/W	Normal
☐	Brillouin gain file name	Brillouin.dat		Normal
☐	Brillouin linewidth	31.7	MHz	Normal
☐	Frequency shift	11	GHz	Normal
☐	Max. power reference	50	mW	Normal
☐	Min. power reference	0.1	mW	Normal

Figure 3.20 Optical Fiber Rayleigh Backscattering Constant

The backscattered signal power is given in figure 3.11. The Rayleigh backscattering coefficient directly affect the amount of reflected signal power.

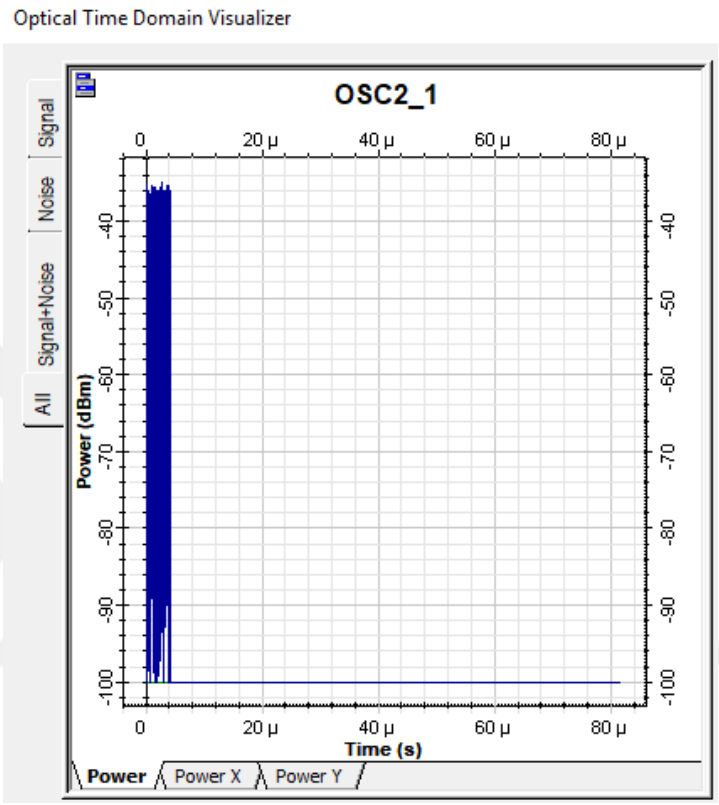

Figure 3.31 Backscattered signal power with 50e-6 Rayleigh coefficient

The propagation power equation used in the simulation program is given as [90]

$$\frac{dP_f(z,v_i)}{dz} = -\alpha(v_i)P_f(z,v_i) + \gamma(v_i)P_\delta(z,v_i) + P_f(z,v_i).$$

$$\sum_{v_j<\delta} \frac{g_\gamma(v_i - v_j)}{K_{eff}A_{eff}}\left[P_f(z,v_j) + P_b(z,v_j)\right] +$$

$$h\Delta v_i \sum_{v_i<v_j} \frac{g_\gamma(v_i-v_j)}{A_{eff}}\left[P_f(z,v_j) + P_b(z,v_j)\right]\left[1 + \left(\exp\left[\frac{h(v_i-v_j)}{kT}\right] - 1\right)^{-1}\right] -$$

$$P_f(z,v_i) \sum_{v_i>v_j} \frac{g_\gamma(v_i-v_j)}{K_{eff}A_{eff}} \frac{v_i}{v_j}\left[P_f(z,v_j) + P_b(z,v_j)\right] -$$

$$2hv_i\Delta v_i P_f(z,v_i) \sum_{v_i>v_j} \frac{g_\gamma(v_i-v_j)}{A_{eff}}\left[1 + \left(\exp\left[\frac{h(v_j-v_i)}{kT}\right] - 1\right)^{-1}\right] \quad \textbf{(2.8)}$$

where α: attenuation, γ: Rayleigh backscattering coefficient, P_δ: Backward propagating power (including sampled, parameterized and noise bin signals), P_f: Forward propagating power (including sampled, parameterized and noise bin signals), g_γ: Raman gain coefficient for v_i-v_j and K_{eff}: Polarization factor [90].

Then the Rayleigh backscattering coefficient is set to 0.5 and 0.05 to show this behavior directly. The resulting power spectrum is given in figure 3.12.

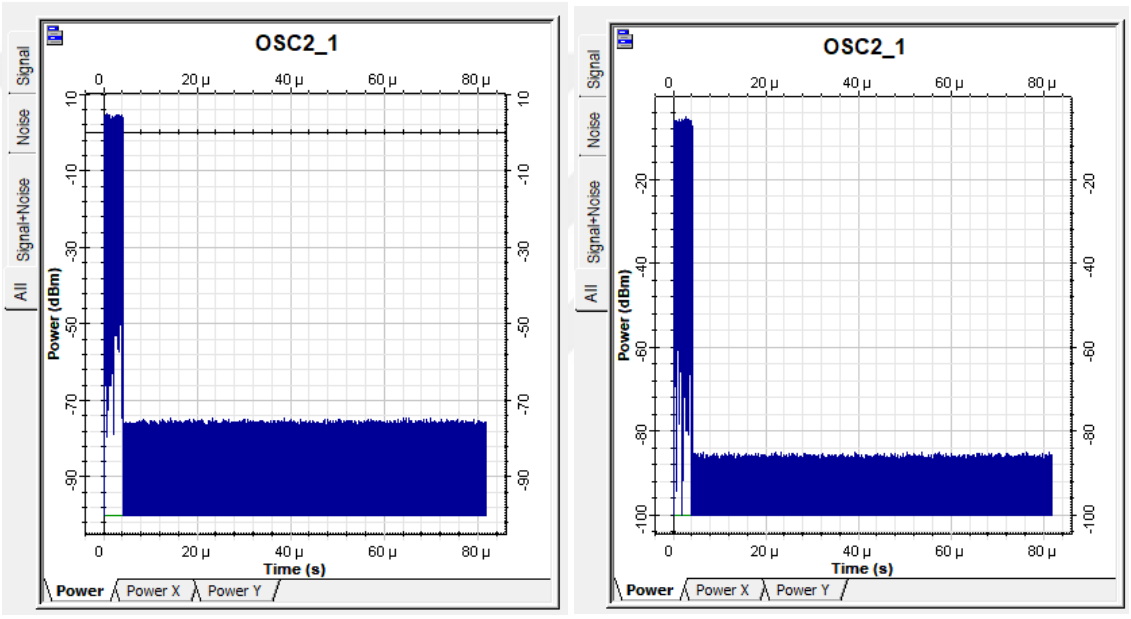

(a) (b)

Figure 3.12 Rayleigh backscattered signal with (a) 0.5 1/km and (b) 0.05 1/km Rayleigh coefficient

3.5 Rayleigh Backscattering Simulation

The OptiSystem program does not allow direct time domain analysis over a single fiber segment. Also, the program parametrizes the power spectrum meaning it averages fiber response over time. Therefore, you will not be able to distinguish the time domain distribution of power.

To work around this behavior, we can divide a 10 km FUT into 10 equal length 1km segments. Also, we can put time delays in forward and backward directions in between to simulate a more realistic time domain analysis. The suggested simulation setup is given in figure 3.13.

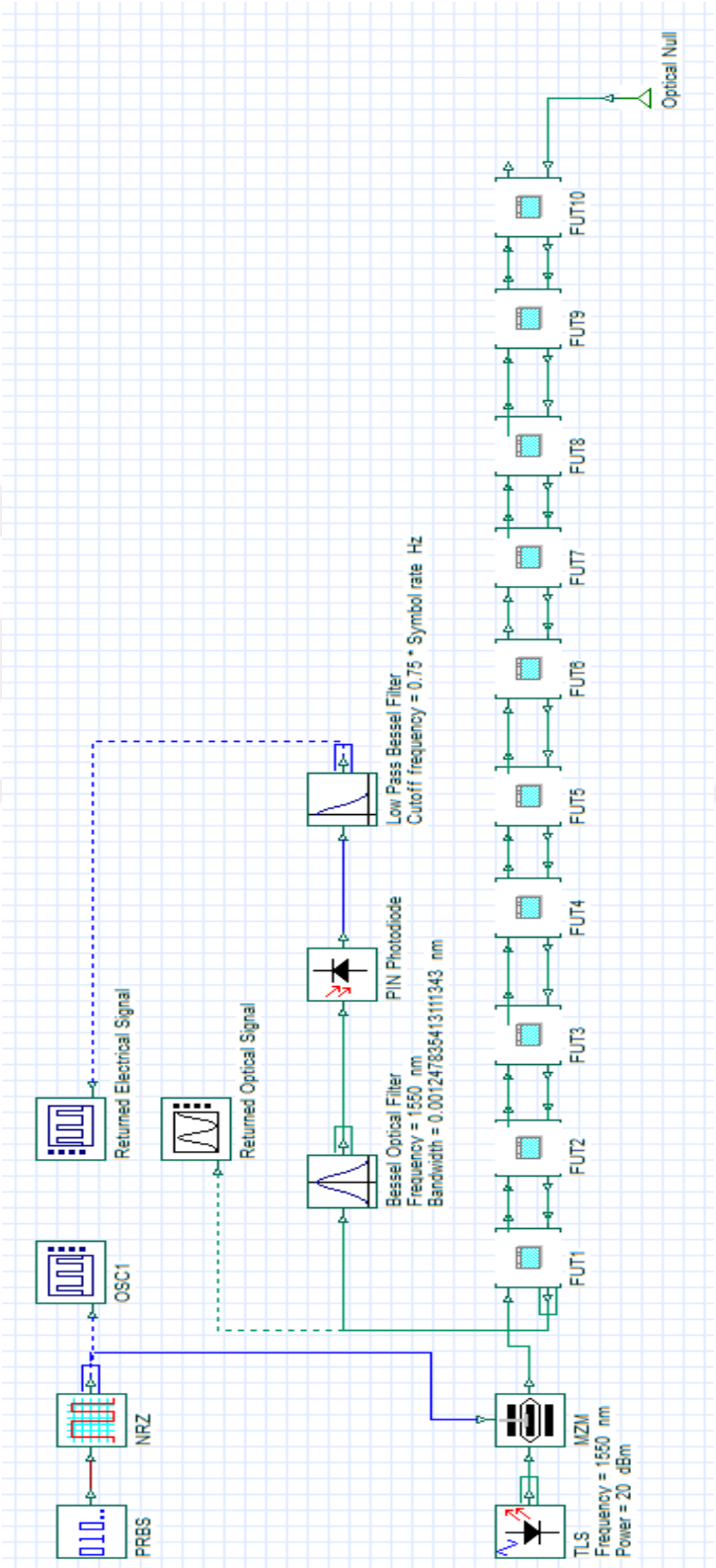

Figure 3.13 Rayleigh backscattering analysis with time delayed fiber segments

The returned signal is sent to a Bessel filter centered around laser wavelength 1550 nm, to negate out band harmonics. Then the signal is sent to a pin photodiode receiver to get the electrical backscattered signal. Then finally a lowpass Bessel filter is applied to further negate down out of band harmonics.

The fiber segment with time delays is given in figure 3.14. The time delay is arranged so that the fiber segment length determines it. The time delay parameter is given in figure 3.18. Here time delay is equal to Segment Length/($3x10^5$/1.45). Fiber refractive index is 1.45, speed of light in a vacuum is $3x10^5$ km/s and segment length is in km. In this simulation the fiber segment length is taken as 1 km, which in turn comes to a 4.83 µs one way delay. Therefore in between 2 fiber segments we have a 9.66 µs delay.

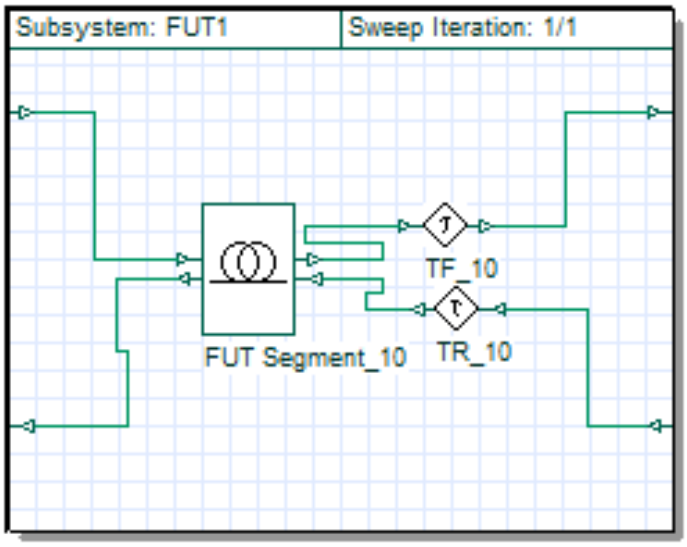

Figure 3.14 Rayleigh backscattering analysis with time delays over segmented fiber under test

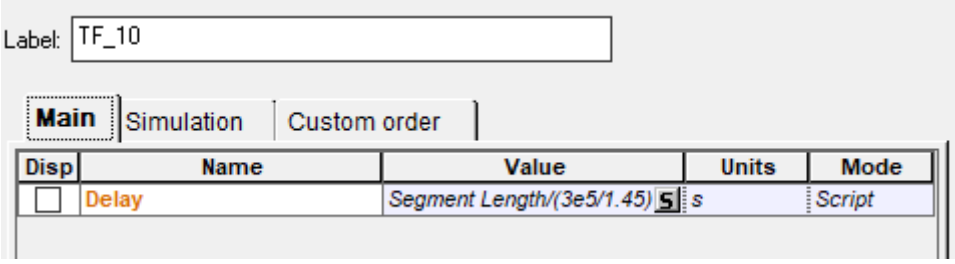

Figure 3.15 Time delay parameters

The simulation result is given in figure 3.16. The backscattered signal is achieved exactly as expected, with the ten peaks having around 9.66 us delay in between and the returned signal peak is decreasing slightly.

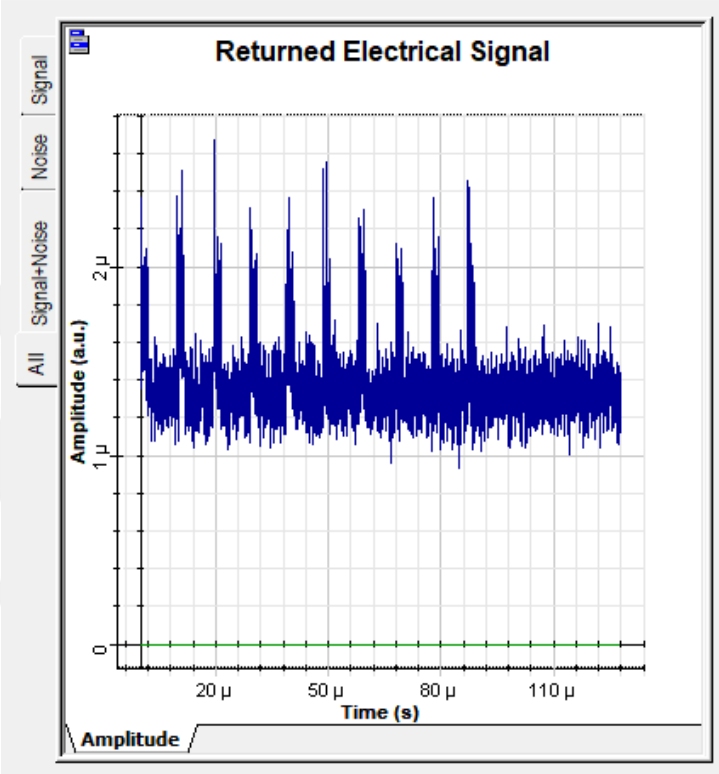

Figure 3.16 The returned backscattered electrical signal

3.6 Connector position detection

So far, a realistic model for observing OTDR response in OptiSystem is developed using time delayed fiber segments. This behavior can be used for tracking sudden changes over a fiber segment. To simulate this sudden change a 3 dB connector is used. Since the changes in backscattered power spectrum over time domain can be detected, it is possible to detect where a connector is placed as well. In this section, the connector is placed in between different fiber segments and backscattered signal spectrum is observed. Figure 3.17 shows an example of how a connector is placed after 1km segment over the FUT.

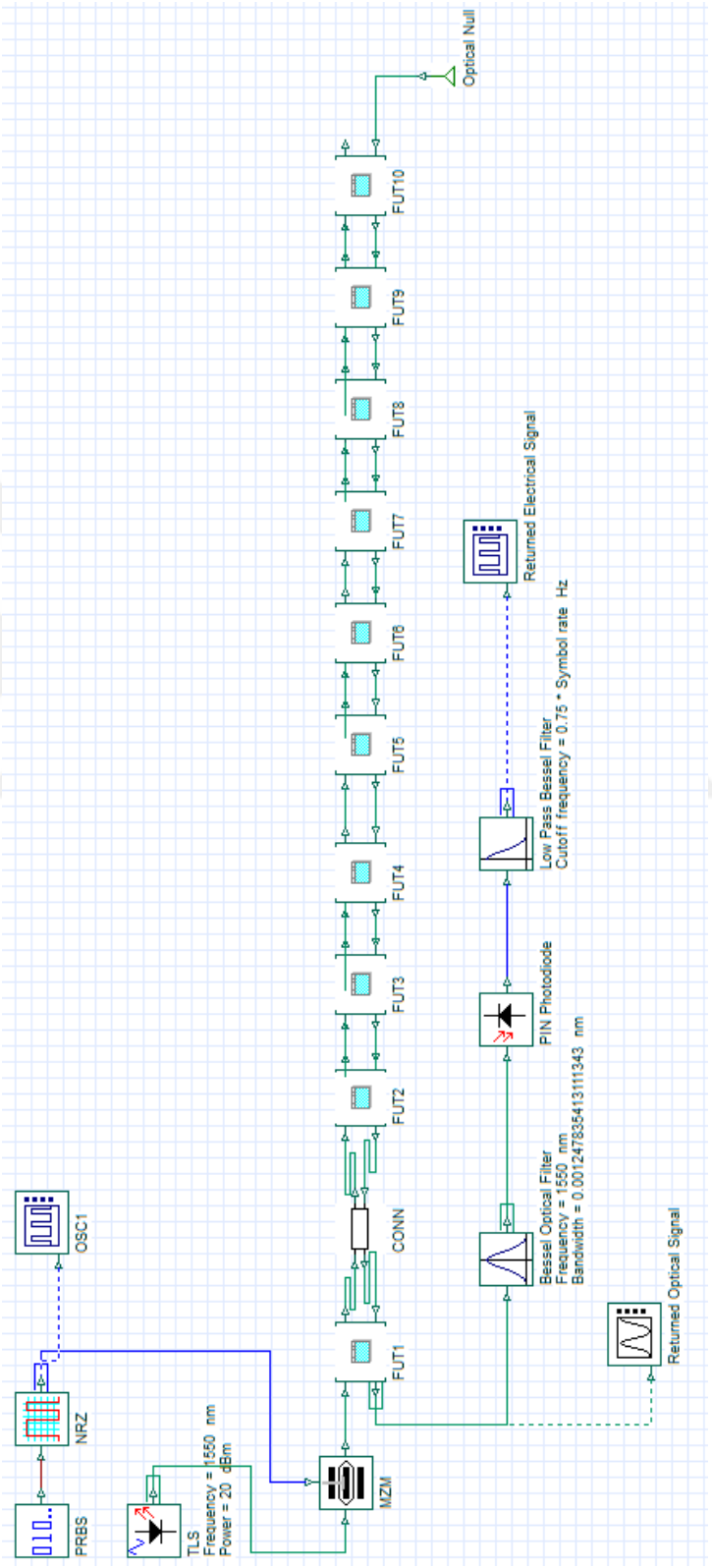

Figure 3.47 3dB connector in between 1st and 2nd segments

The connecter is placed in between: 1st and 2nd segments, 4th and 5th segments and finally 8th and 9th segments respectively. The received power spectrum is shown in figure 3.18.

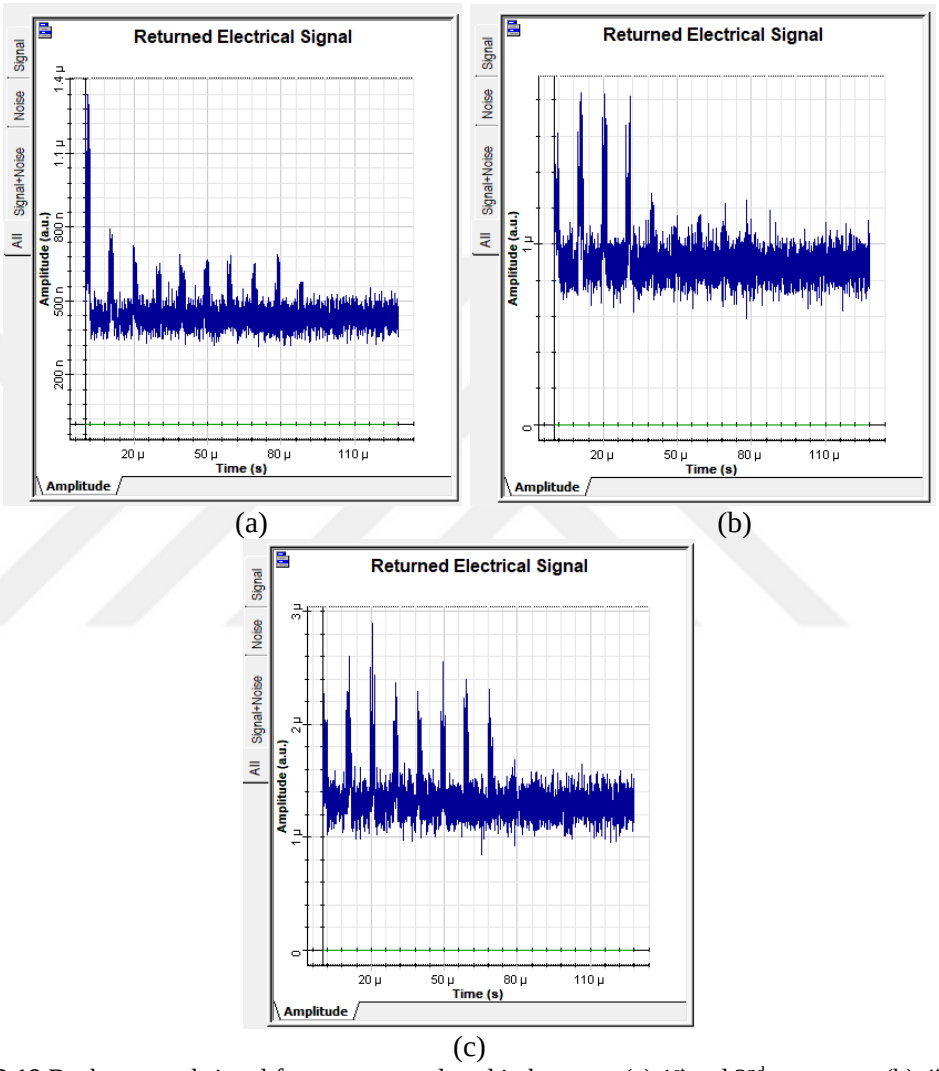

Figure 3.18 Backscattered signal for connector placed in between (a) 1st and 2nd segments, (b) 4th and 5th segments and (c) 8th and 9th segments

The amplitude drops in backscattered signal responses show where the connector is placed. Firstly, in figure 3.18 (a) there is a substantial power drop in between 1st and 2nd peaks. The first peak is placed at 4.83 µs and second peak is placed at 9.66 µs. The 4.83 µs time stamp denotes a 1 km distance and 9.66 µs time stamp denotes a 2 km distance. So, the connector is placed after 1 km. Secondly in figure 3.18 (b) the substantial power drop is in between 4th and 5th peaks. The fourth peak is placed at 19.32 µs and fifth peak

is placed at 24.15 µs. The 19.32 µs time stamp denotes a 4 km distance and 19.32 µs time stamp denotes a 5 km distance. So, the connector is placed after 4 km. Finally in figure 3.18 (c) the substantial power drop is in between 8^{th} and 9^{th} peaks. The eighth peak is placed at 38.64 µs and ninth peak is placed at 43.47 µs. The 38.64 µs time stamp denotes an 8 km distance and 43.47 µs denotes a 9 km distance. So, the connector is placed after 9 km.

3.7 Summary

In this section, an OTDR setup is designed and simulated in OptiSystem software. Then Rayleigh response of an SMF fiber is obtained. Then a lossy event detection mechanism is simulated with connectors attached in between different fiber segments. Connector locations were obtained successfully.

CHAPTER 4

REALIZATION OF RAYLEIGH OTDR FOR LOSSY EVENT DETECTION

4.1 Introduction

In this chapter, the previously simulated Rayleigh OTDR lossy event detection system is constructed in laboratory. The effects of pulse width and Vpp of input pulse laser on the OTDR system are observed. Different test fiber setups are experimented on, and the FC adapter connection locations are detected.

4.2 Laboratory Setup for Rayleigh OTDR Lossy Event Detection

The lossy event detection OTDR system simulated in previous chapter is constructed in laboratory. The laboratory setup is given in figure 4.1. Here P.L.: pulse laser, EDFA: Erbium Doped Fiber Amplifier, LF S.G.: Low frequency signal generator, FC ADPT.: Fiber channel adapter, FUT.: Fiber under test, OSC.: Oscilloscope, Bi.P.D.: Biased photo detector and P.C.: personal computer.

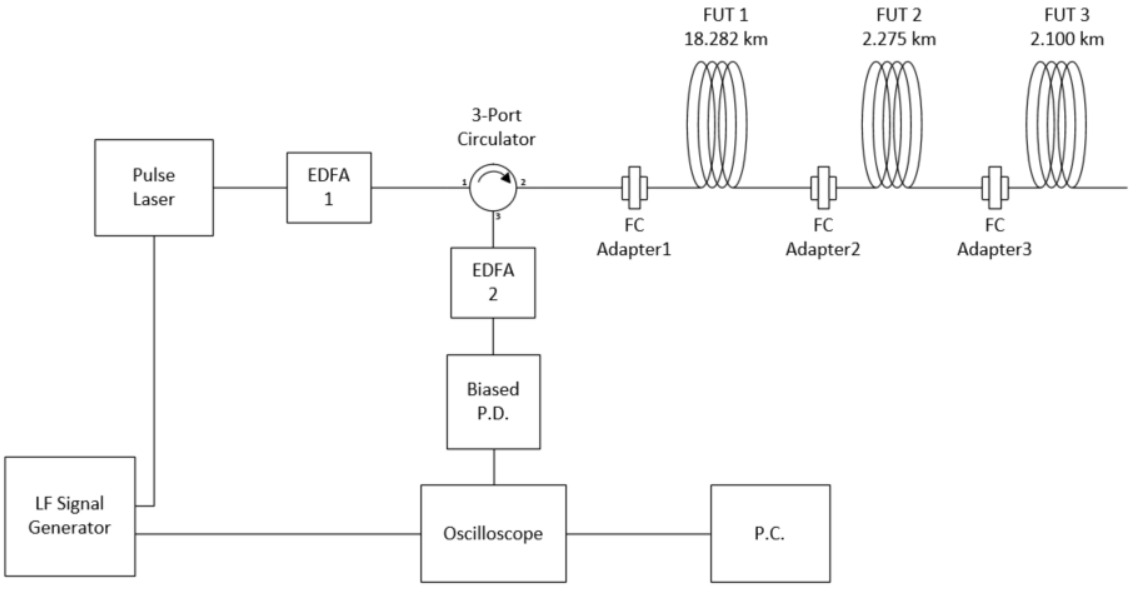

Figure 4.1 Rayleigh OTDR laboratory setup

Different from the simulation, CW laser and AOM were not used in the optical pulse generation, as an optical pulse laser was already available in the lab. The pulse laser (RF Optics, 1550nm) can generate 1550 nm pulse laser signals working with both internal and external triggers. When the internal trigger is activated, the laser works with on-board modulator to produce optical pulse in the limit of 50 ns pulse width and 5 kHz repetition rate. The external trigger enables the laser to be modulated via an LF electrical pulse.

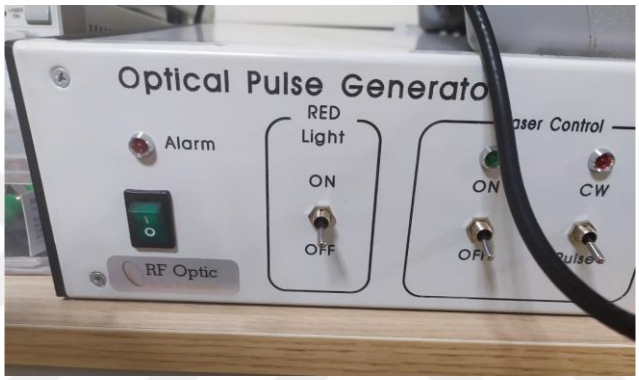

Figure 4.2 RF Optic Optical Pulse Generator

A low frequency signal generator (Agilent 33500B) is used to trigger the pulse laser. The channel1 output of the signal generator is connected to pulse laser external trigger input. Adjusting the signal generator's repetition rate and pulse width, the laser pulse is manipulated.

Figure 4.3 Agilent 33500B LF Signal Generator

The pulse input, however, by itself is very weak, due to the pulse laser's set amount of output power. The pulse laser power by itself was around -26 dB, which would not generate a sufficient Rayleigh reflection. To mitigate this issue an EDFA (EDFA1) was applied at the end of pulse laser. EDFA1 is an adjustable EDFA (YİMİ, tunable EDFA) which is capable of up to 30 dB gain and long temperature stability. The EDFA1 current was set to 275 mA, which corresponded to around 22 dB gain.

Figure 4.4 YİMİ Compact EDFA

The strengthened optical pulse is then sent to the FUT via a 1550 nm 3-port circulator. The pulse goes through port 1 to port 2 onto the FUT. Here the FUT is divided into multiple segments in the form of various length SMF spools, like in the simulation. The fiber segments are 2.275 km, 2.1 km and 18.282 km in length respectively. These segments are connected to each other with FC optical adapters, where these adapters are to simulate a source of significant loss over a fiber link.

Figure 4.5 FC Adapter connection

The reflected Rayleigh scattering signal is then sent to P.D. via circulator port 2 to port 3. Same as the optical pulse, the reflected Rayleigh signal was around -20dB in power, which was not detectable by the P.D. Therefore, another EDFA (EDFA 2) is used to amplify the signal. EDFA 2 (YİMİ, fixed power EDFA) has fixed gain around 20dB.

Finally, the amplified Rayleigh signal arrives at the P.D. to be converted into electrical signal. Then the converted electrical signal is sent to a high sampling rate oscilloscope (Agilent MSO-X 3054-A, up to 4 GSa/s). Normally a DAQ system is needed for data acquisition and averaging. However, since a high sampling oscilloscope was already available, this step is bypassed. The oscilloscope can average the reflected signal up to 65536 times. To correctly time data acquisition, the oscilloscope is triggered with the same LF signal that is used for modulating optical pulse laser.

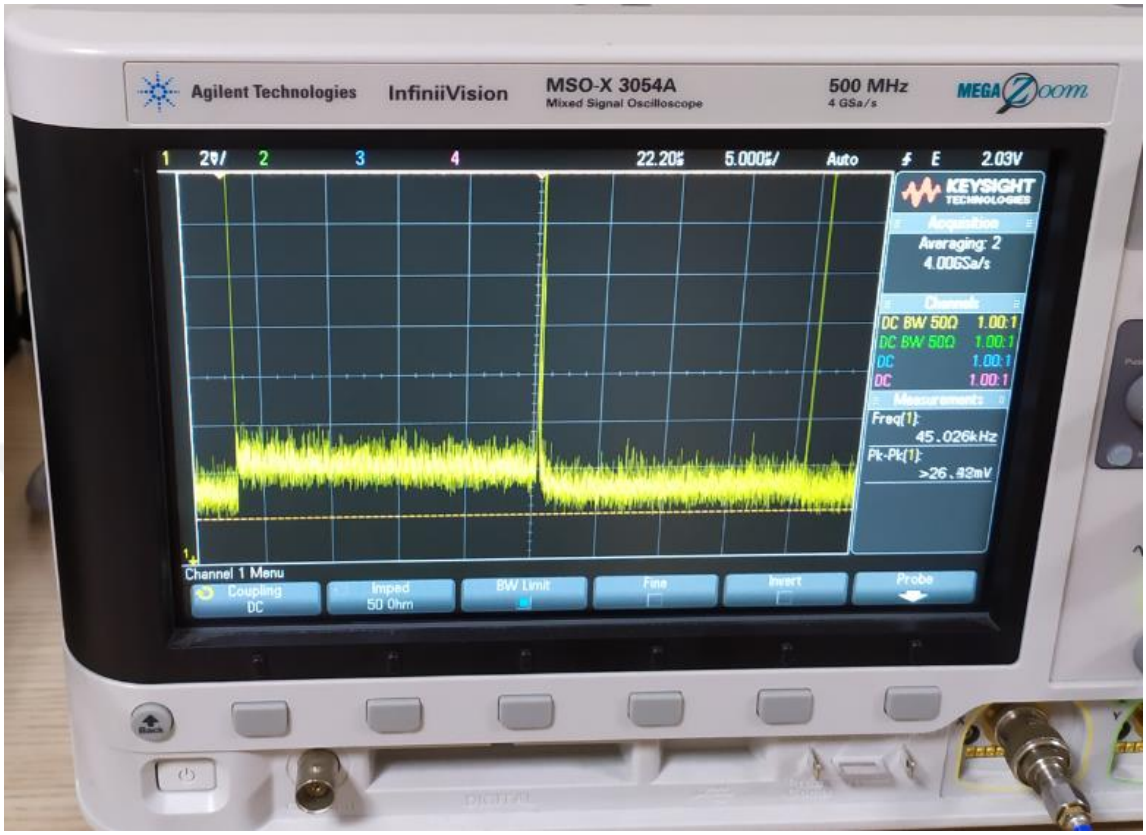

Figure 4.6 Agilent MSO-X 3054A 4 Gsa/s Oscilloscope

The acquired data is then sent to P.C. to get the OTDR distance-amplitude plot.

4.3 Remote Device Control Program

In fiber optic experiments, the laboratory devices require very sensitive adjustments. Even the slightest miss-alignments often result in unwanted shifts at the output. These types of shifts can easily misguide the engineer to misjudge the optical result.

Furthermore, fiber optic experiments demand many readings to get a meaningful data set. Each reading can have a unique set of laboratory device parameters. This means that after each reading, the laboratory devices must be setup again with different parameters. All these manual setups result in high wait times as each small adjustment time adds up.

To solve the time and misalignment issues of manual setup, a MATLAB code is created to control the devices remotely. Three devices are controlled: Signal generator, Oscilloscope and Pulse Laser.

ii) *ISignal Generator:*

First the USB communication object is created as a Keysight/Agilent Visa object with the proper device ID.

```
      SGENobj =
visa('AGILENT','USB0::2391::11271::MY52801056::0::INSTR');
      SGENobj.Timeout = 10;
      fopen(SGENobj);
```

Then the parameter changes are applied. The USB Visa connection for signal generator follows the SCPI commands. Fprintf commands are used for sending SCPI strings to the device. First the device remote memory is cleared. Then Trigger source is set to immediate to make oscilloscope and signal generator synchronized. Both channel outputs are turned off.

```
      Fprintf (SGENobj,'*CLS');
      fprintf (SGENobj,'TRIGger1:SOURce IMMediate');
      fprintf (SGENobj,'OUTP1 OFF'); fprintf (SGENobj,'OUTP2 OFF');
```

After that the channel1 signal waveform is set to pulse. The repetition rate frequency, peak to peak voltage and pulse width are set. Then channel1 is turned on.

```
      Fprintf (SGENobj,'SOURce1:FUNCtion PULSe');
      fprintf (SGENobj,'SOURce1:FREQuency 2000');
      fprintf (SGENobj,'SOURce1:VOLTage +3');
      fprintf (SGENobj,'SOURce1:FUNCtion:PULSe:WIDTh 20ns');
      fprintf (SGENobj,'OUTP1 ON');
```

ii) Oscilloscope:

Like signal generator, USB communication object is created as a Keysight/Agilent Visa object with the proper device ID.

```
      OSCobj=
visa('AGILENT','USB0::0x0957::0x17A2::MY52491374::0::INSTR');
  OSCobj.InputBufferSize = 1e8;
      OSCobj.OutputBufferSize = 1e8;
      fopen(OSCobj);
```

Oscilloscope reading mode is set to time domain. Then acquisition type is set to average.

```
Fprintf (OSCobj,':TIMebase:MODE MAIN');
avg =  256;
fprintf (OSCobj,':ACQuire:TYPE AVERage');
fprintf (OSCobj,':ACQuire:COMPlete 100');
fprintf (OSCobj,[':ACQuire:COUNt ' num2str(avg)]);
```

Then the channel1 reading is digitized and output data is read and stored.

```
Fprintf (OSCobj,':DIGitize CHANnel1');
fprintf (OSCobj,':WAVeform:SOURce CHANnel1');
fprintf (OSCobj,':WAVeform:FORMat ASCii');
fprintf (OSCobj,':WAVeform:POINts MAXimum');
fprintf (OSCobj,':WAVeform:DATA?');
y = fscanf(OSCobj);
```

iii) Pulse Laser:

The RF optics pulse laser, different from above, uses serial communication for remote control. The serial object is created via corresponding COM port. The pulse laser uses carriage return (CR) delimiter, therefore serial object's delimiter is set to CR.

```
PGobj = serial('COM7');
PGobj.Terminator = 'CR';
fopen(PGobj);
```

The pulse laser has unique set of string commands as opposed to SCPI. First the internal trigger is turned off to enable external triggering. Then Laser is turned on and continuous wave is disabled to get pulse output.

```
fprintf(PGobj,'IntTrig(OFF)');   fscanf(PGobj)
fprintf(PGobj,'Laser(ON)');      fscanf(PGobj)
fprintf(PGobj,'CW(OFF)');        fscanf(PGobj)
```

These three control subroutines allow successful communication with the laboratory devices. Using the above, a main routine is created. The code flowchart is given in figure 4.7.

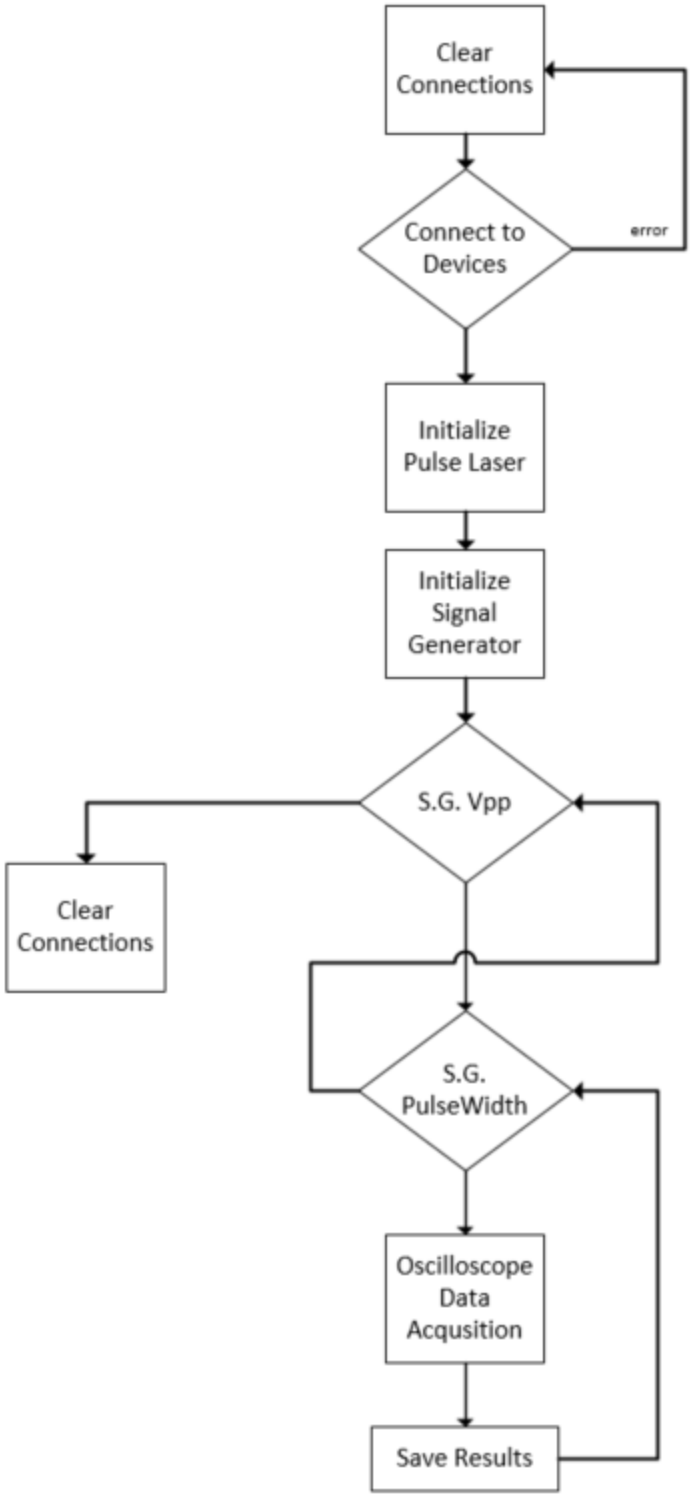

Figure 4.7 Remote control code flowchart

The main remote-control code first clears all previously established connections. This is done to eliminate connections overlap errors. Then signal generator, pulse laser and oscilloscope connections are established. Error handling is done to check if the connection is established. If for some reason connection is not established, the program goes back to clear connections block to later retry the connection. After connections are established, the pulse laser is initialized to work with external trigger signal. Then signal generator output signal is set to pulse with initial pulse width and repetition rate. Then a for loop is set for a set of peak-to-peak voltages for signal generator. The signal generator voltage level is set here. Inside this loop the pulse width of the signal generator is set with another for loop. The signal generator pulse width is set here. Inside this for loop, the oscilloscope is digitized, and data acquisition is taken with a set amount of averaging. Finally, the acquired data set is saved with a unique name for later accessibility. When all the loops finish the program closes and clears all the connections and finalizes the process.

The acquired time data is transformed into distance information using the same formula given in chapter 3.

With this code, all the data can be taken with a single run for back-to-back acquisitions with different parameter sets are saved in a unique way.

4.4 Connector Position Detection Over FUT

Using the laboratory OTDR setup and remote-control code, testing was done to detect the connection points of the adapters along the FUT. To test the accuracy of the OTDR setup, 3 FUT segments are connected in different combinations.

First, only 2.275 km and 2.1 km segments are connected to each other with and adapter. The test setup is shown in figure 4.8. A small pulse width of 16 ns is chosen as total OTDR length is around 4 km.

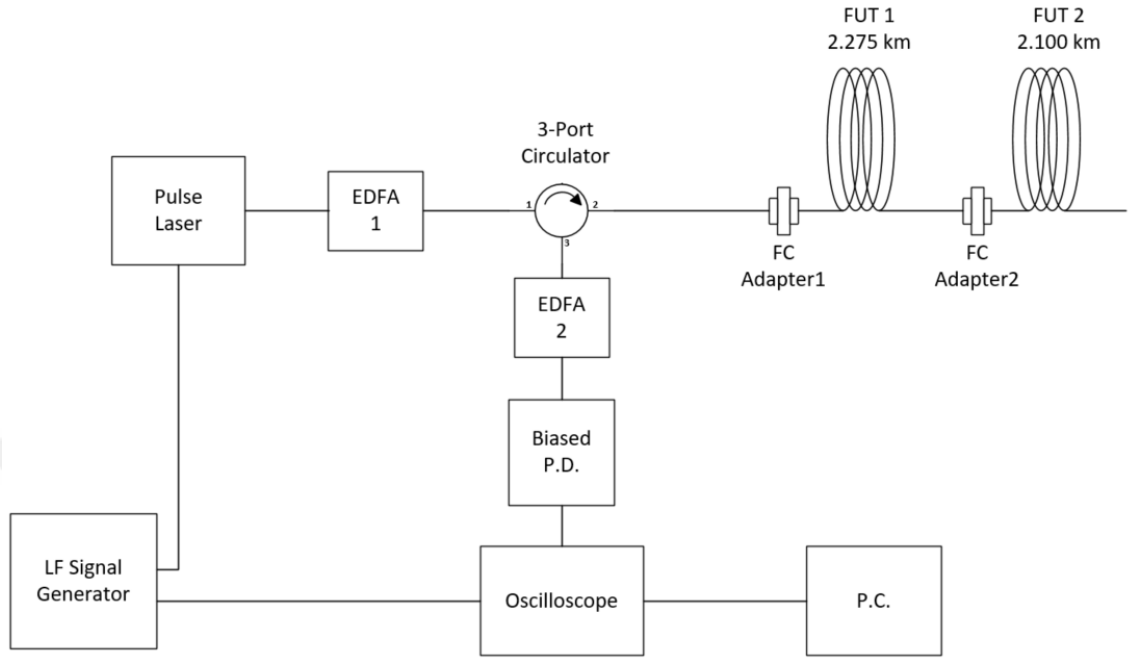

Figure 4.8 2.275km and 2.1km fiber segments connected back-to-back with an FC adapter

The resulting oscilloscope response is shown in figure 4.9. Notice that the converted electrical signal is very weak, especially with the attenuation slope in the vicinity of <<1mV.

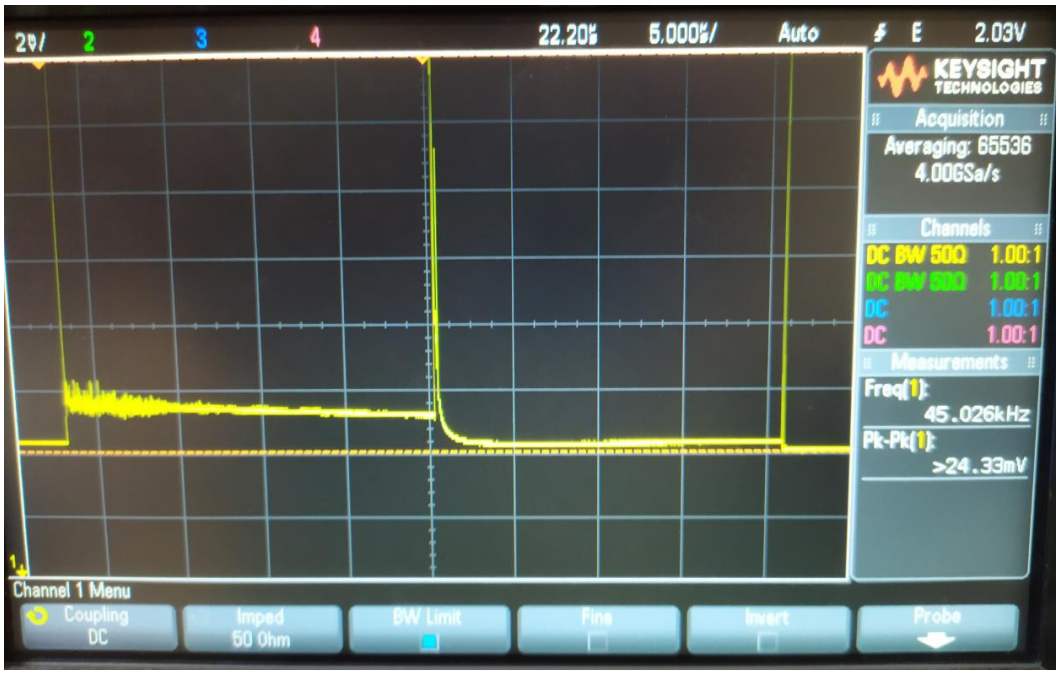

Figure 4.9 Oscilloscope response for 2.275km and 2.1km fiber segments

The received data is averaged 256 times and sent to P.C. The MATLAB plot for 2.275 km to 2.1 km OTDR response is shown in figure 4.10. We have three peaks here at; 37.33 m, 2301 m and 4403 m. the first two peaks correspond to two FC adapters and the last peak denotes the end of fiber reflection. In between first peak and second peak we have around 2.27 km. This shows that after the adapter in circulator port 2 there is a pure fiber length of 2.27 km, then another adapter is connected. In between the second and third peak we have around 2.1 km, again meaning that after the second adapter, there is a fiber length of 2.1 km. After the last peak we do not have any data until the new repetition, which is expected as the pulse finishes its journey over the fiber and waits for new pulse to be sent.

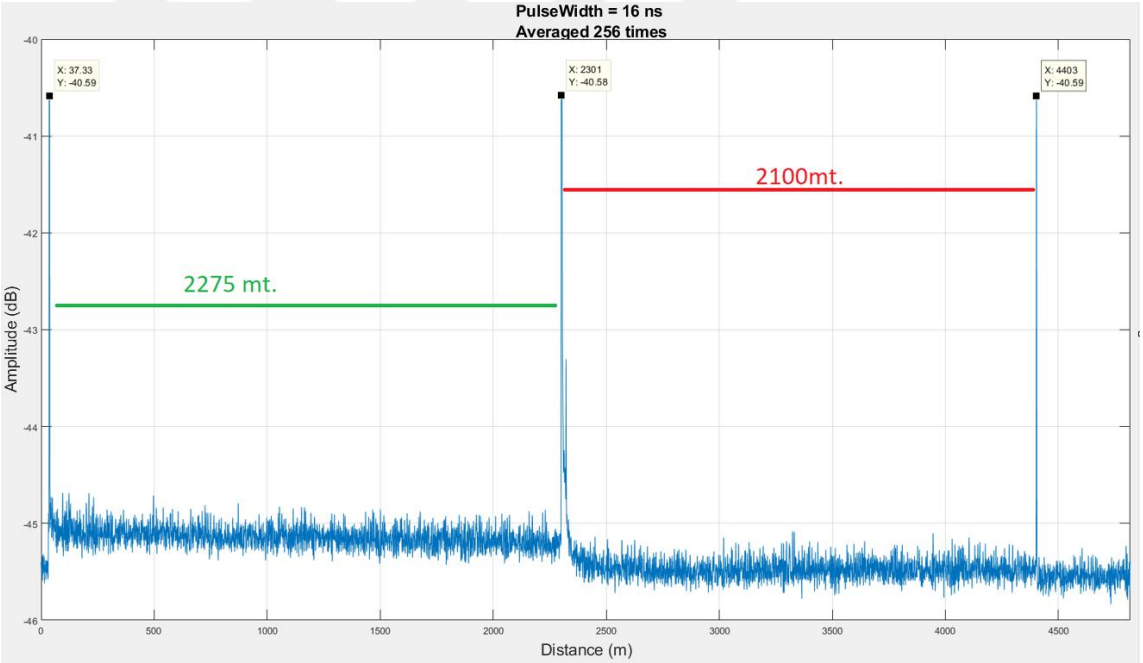

Figure 4.10 MATLAB data read for 2.275km and 2.1km fiber segments

Secondly 2.275 km, 18.282 km and 2.1 km segments are connected to each other with two FC adapters in between. The test setup is shown in figure 4.11. Here the pulse width is set to 50ns to compensate for the long OTDR length of around 22 km. Also, the repetition rate is decreased to 1 kHz to eliminate the pulse overlaps.

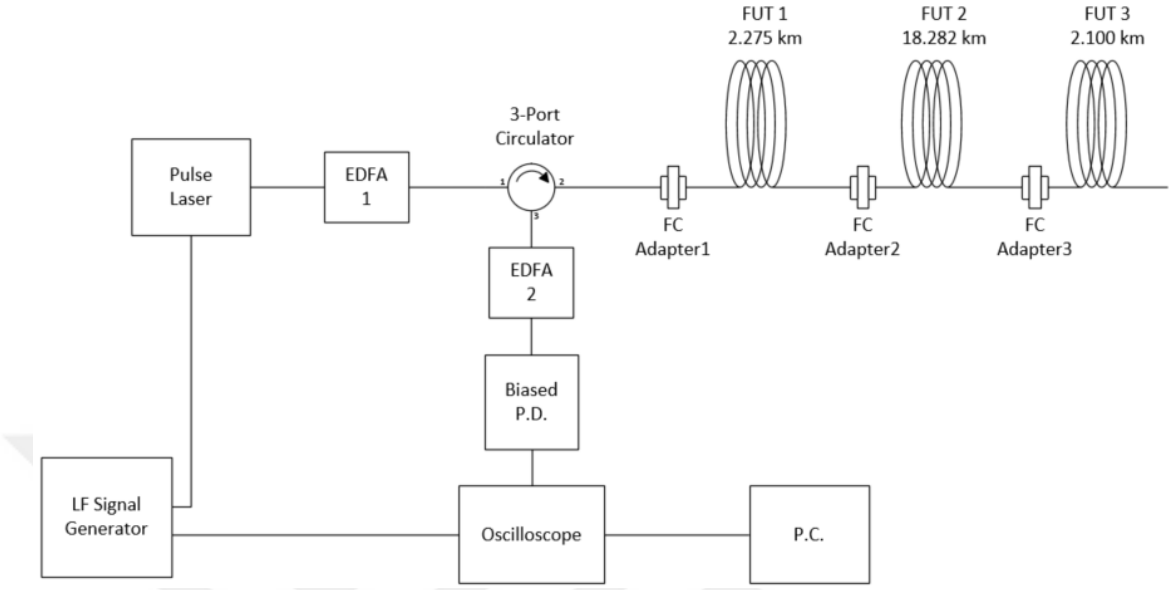

Figure 4.11 2.275km, 18.282 km and 2.1km fiber segments connected back-to-back with two FC adapters

The received data is averaged 256 times and sent to P.C. The MATLAB plot for 2.27 5km to 18.272 km to 2.1 km OTDR response is shown in figure 4.12. We now have four peaks at: 42.1 m, 2310 m, 20512 m and 22580 m. The first three peaks correspond to three FC adapters and the last peak denotes the end of fiber reflection. In between first peak and second peak we have around 2.27 km. showing that a fiber length of 2.27km is connected between the circulator port 2 adapter and second FC adapter. In between the second and third peak we have around 18.1 km, again meaning that after the second adapter, we have a fiber length of 18.1 km. In between the third and fourth peak we have around 2.1 km, once again meaning that after the third adapter, we have a fiber length of 2.1 km. After the fourth peak we do not have any data until the new repetition arrives.

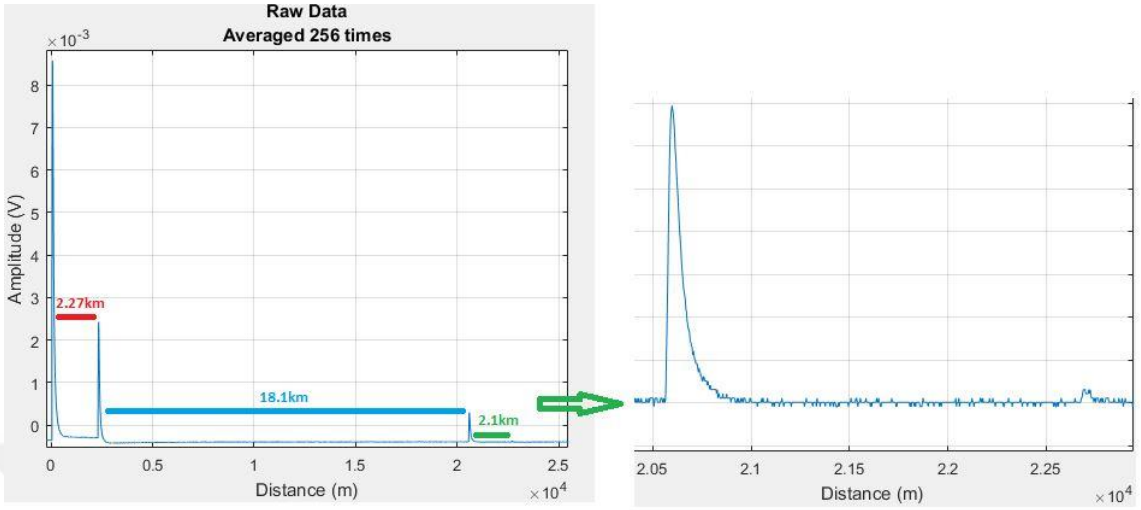

Figure 4.12 MATLAB data read for 2.275km, 18.282 km and 2.1km fiber segments

Finally, 18.282 km, 2.275 km and 2.1 km segments are connected to each other with two FC adapters in between. The test setup is shown in figure 4.13. Again, the pulse width is set to 50 ns and repetition rate to 1 kHz.

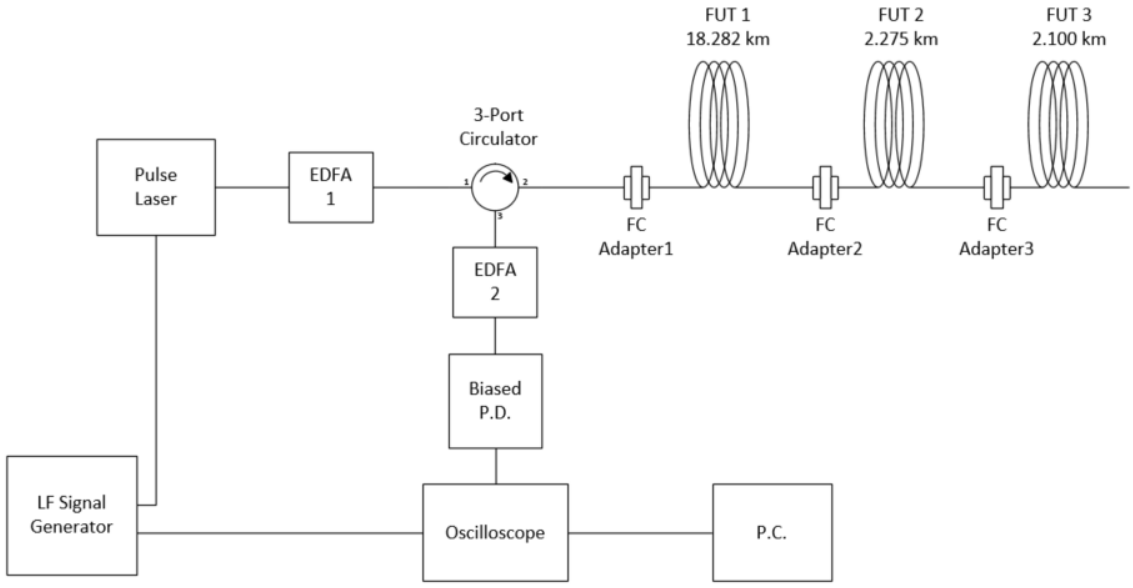

Figure 4.13 18.282 km, 2.275 km and 2.1 km fiber segments connected back-to-back with two FC adapters

The received data is averaged 256 times and sent to P.C. The MATLAB plot for 18.272 km to 2.275 km to 2.1 km OTDR response is shown in figure 4.14. We now have four

peaks at: 45.6 m, 18300 m, 20570 m and 22670 m. The first three peaks correspond to three FC adapters and the last peak denotes the end of fiber reflection. In between first peak and second peak we have around 18.2 km showing that a fiber length of 18.2 km is connected between the circulator port 2 adapter and second FC adapter. In between the second and third peak we have around 2.2 km, again meaning that after the second adapter, we have a fiber length of 2.2 km. In between the third and fourth peak we have around 2.1 km, once again meaning that after the third adapter, we have a fiber length of 2.1 km. After the fourth peak we do not have any data until the new repetition arrives.

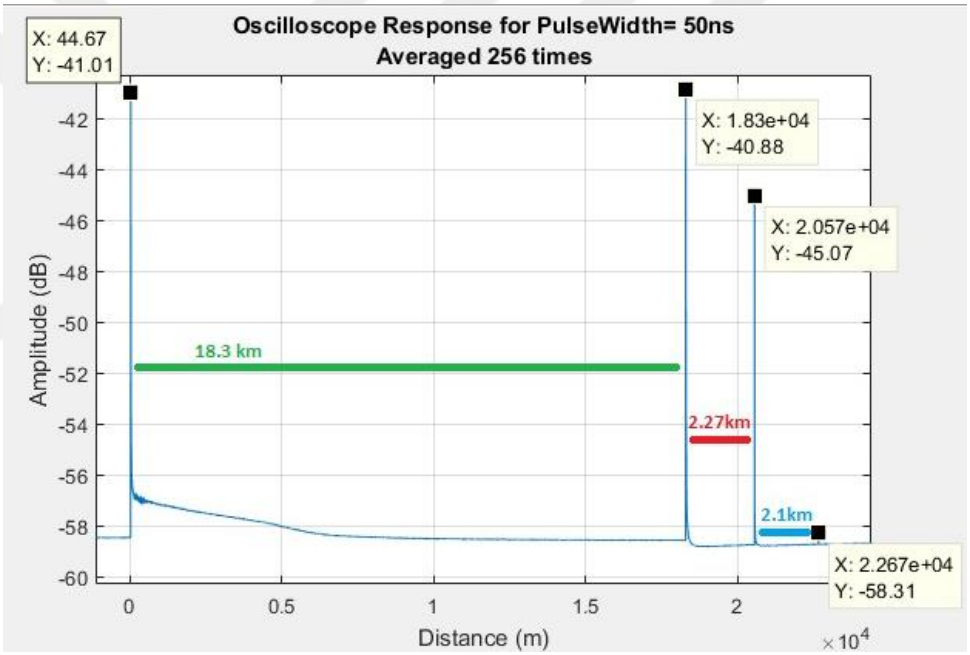

Figure 4.14 MATLAB data read for 18.282 km, 2.275 km and 2.1 km fiber segments

The OTDR attenuation slope can be best seen in the first 18.2 km fiber segment of this setup. The zoomed in attenuation slope is given in figure 4.15. The 0.2 dB/km attenuation slope can be seen over the first 5 km, then fiber seems to suffer harsh attenuation drop. The attenuation slope after another 2 km, then flattens like the readings in previous two setups.

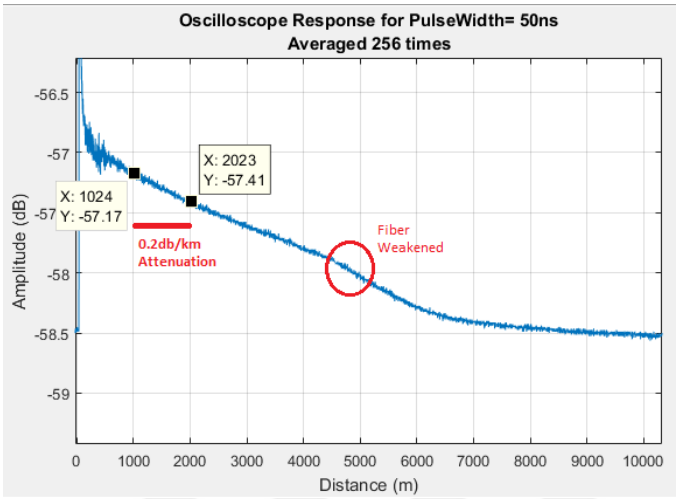

Figure 4.15 Zoomed in fiber attenuation over 18.282 km fiber segment

4.5 Effects of Pulse Width on OTDR System

The signal generator use in this setup can generate pulses in 16 ns width smallest. To observe the effects of pulse width over the OTDR system, the signal generator is set to 5 Vpp and pulse width is swept from 16 to 50 ns in 1ns steps. The result is shown in figure 4.16.

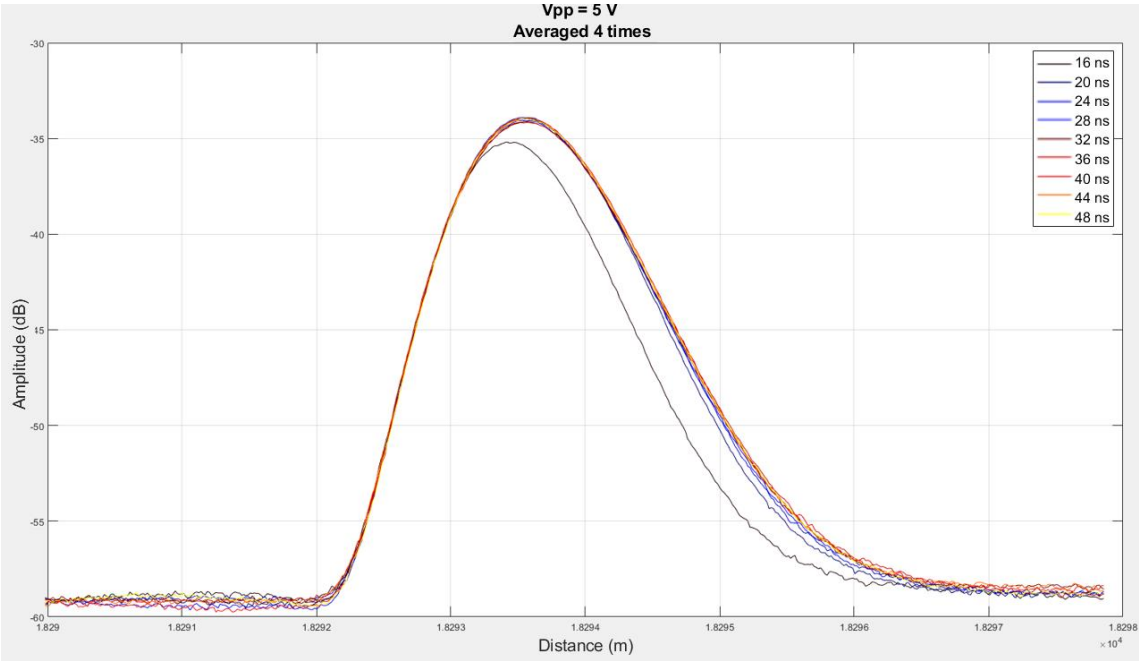

Figure 4.16 LF signal generator pulse width sweep from 16 to 48 ns

The pulse width changes did not affect the reflection widths of the adapters that much. The most notable changes happen from 16 ns to 24 ns sweep. The zoomed in response for this behavior is given in figure 4.17.

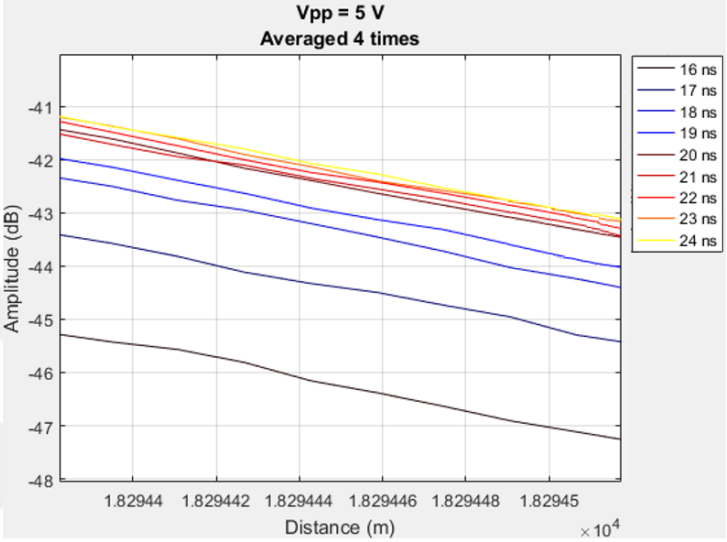

Figure 4.17 LF signal generator pulse width sweep from 16 ns to 24 ns zoomed in

Observing above plots, the changes come to a halt around 24 ns to 30 ns. However, lowering the pulse width to 16 ns, affect the overall power of the OTDR system, as the pulse laser power is dropping relatively to the pulse width.

4.6 Effects of Vpp on OTDR System

Then the effect of the peak-to-peak voltage of the LF pulse on OTDR system is observed. The pulse width is set at 30ns and Vpp is swept from 1.5 Vpp to 5 Vpp in 0.5 Vpp steps. The results are shown in figure 4.18. According to the results, the pulse laser does not generate laser output for lower than 2 Vpp LF pulses.

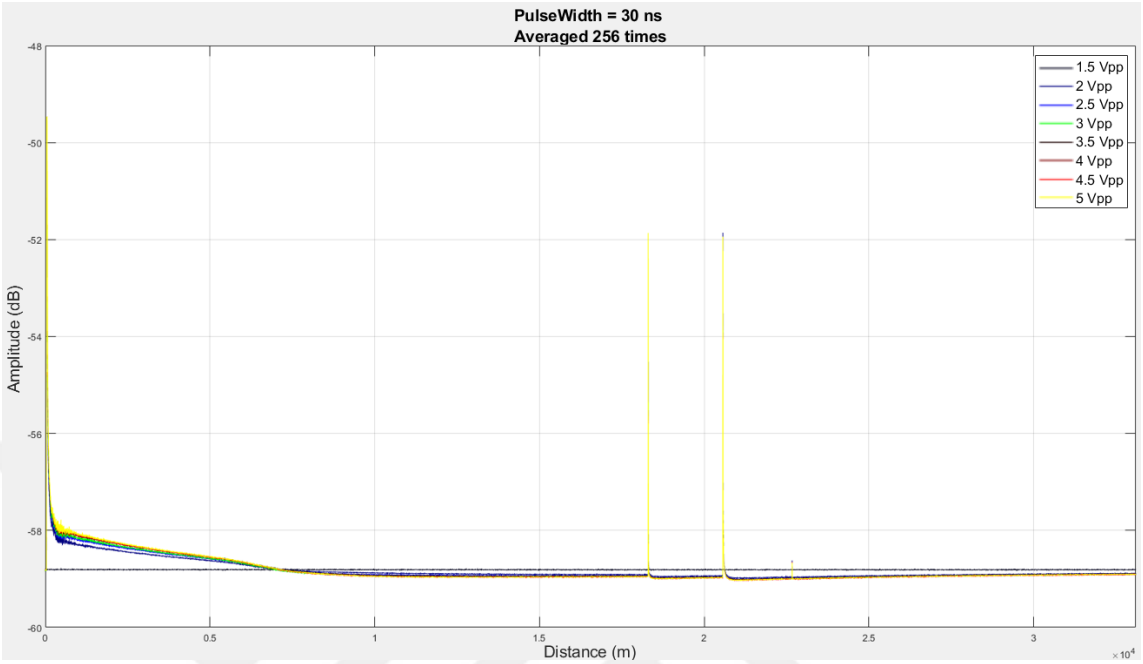

Figure 4.18 Experimented DP-SHFA Circuit Setup

The zoomed in response can be seen in figure 4.19. Here it is clear that, the photo detector flat lines at around -58.8 dB, which was the 7 km mark for the 18.282km to 2.275 km to 2.1 km fiber detection scheme. This shows that, the fiber weakening observed here, can be caused by the photo detector limits.

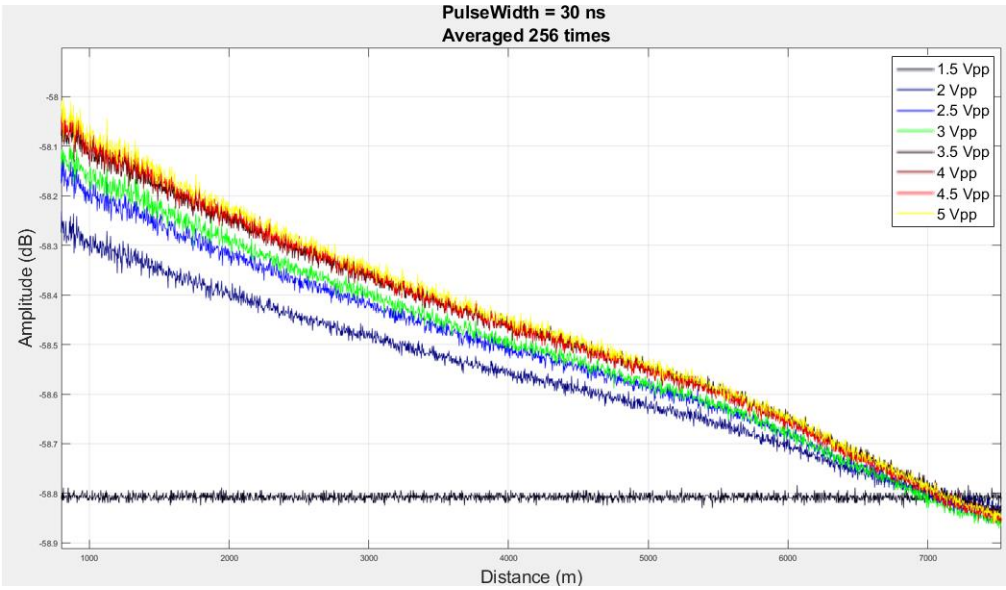

Figure 4.19 18.282km fiber segment zoomed in

4.7 Conclusion

In this chapter, the Rayleigh OTDR event detection system designed in simulation is realized. 3 dB FC/APC Adapters simulated lossy events. Adapters are connected in between different fiber spools. Fiber attenuation slope and connector points reflections peaks were detected successfully. Then the effects of LF signal's Vpp and pulse width on the scattered signal is observed. For Vpp, at least 2 Vpp LF signal is needed to create a meaningful Rayleigh trace. For the pulse width, at least 16 ns is needed. Although, the lower the pulse width the better the resolution is, lower than 16 ns pulse width does not create sufficient Rayleigh backscattering. Strong Rayleigh trace was acquired using 30 ns pulse width.

CHAPTER 5

PERFORMANCE ENHANCEMENT IN RAYLEIGH OTDR SYSTEM AND NONLINEAR FIBER AS TEMPERATURE SENSOR

5.1 Introduction

In this chapter, performance of the previously laboratory tested Rayleigh OTDR event detection system is tried to be improved. Effect of an isolator at the fiber end is observed. The OTDR intrusion point is replaced with splice. The detection events are changed from connectors to bad splice points. A GUI program is written in addition to previous remote-control code to better visualize the overall system.

Then, different types of nonlinear fibers, namely, HNLF, DSF and PMF are tested for their suitability as a potential R-OTDR temperature sensor medium. First, the Rayleigh backscattering characteristics of these fibers are observed and compared with a SMF. Then, 50 m of the fiber with the best Rayleigh backscattering characteristic is tested in a classical R-OTDR temperature sensor setup. The resulting temperature sensitivity is compared with that of SMF.

5.2 Isolator at the Fiber End

The end of the OTDR system is finalized with a C-band (1550nm) isolator, to observe the effect of eliminating fiber end Fresnel reflection. The test setup is given in figure 5.1.

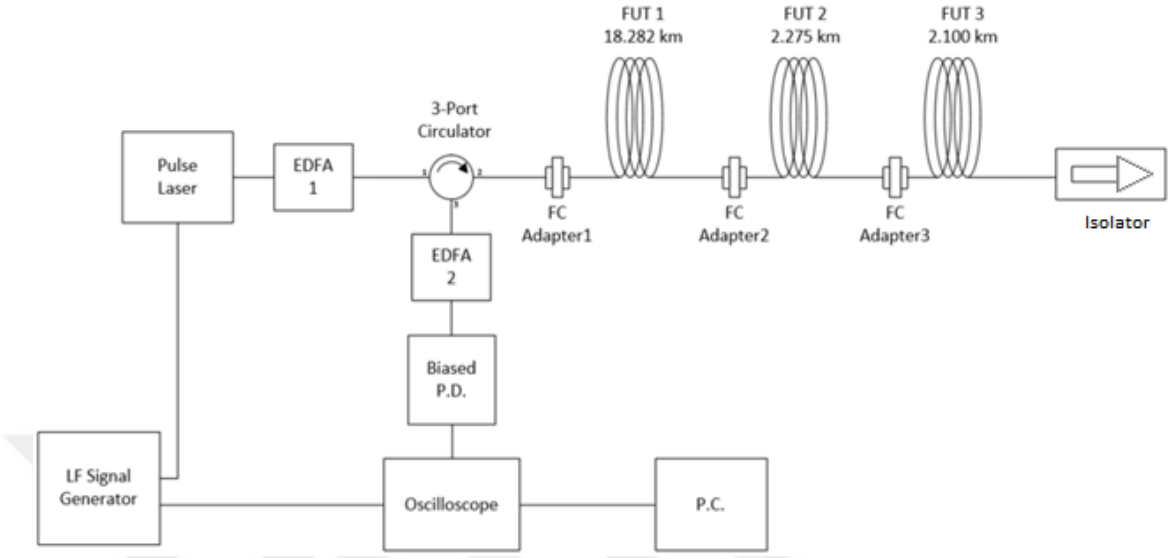

Figure 5.1 OTDR system setup finalized with an isolator at the end

The resulting signal is shown in figure 5.2. The Fresnel reflection at the end of the fiber is eliminated, as expected. However, the reflected back signal suffers from additional losses. These can be seen in figure 5.3, where the system responses of OTDR's with isolator and without isolator are compared to each other.

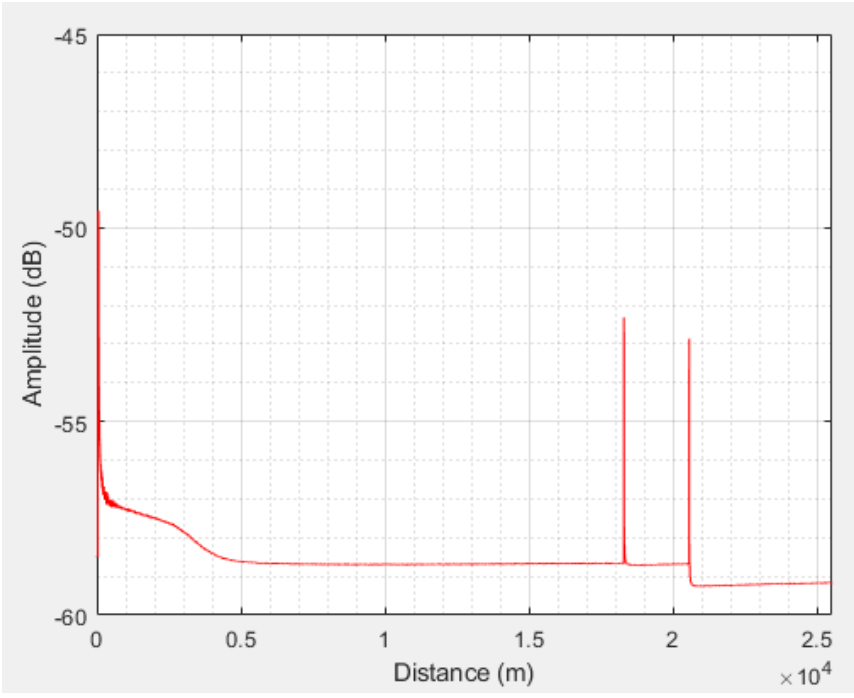

Figure 5.2 OTDR response of system finalized with isolator

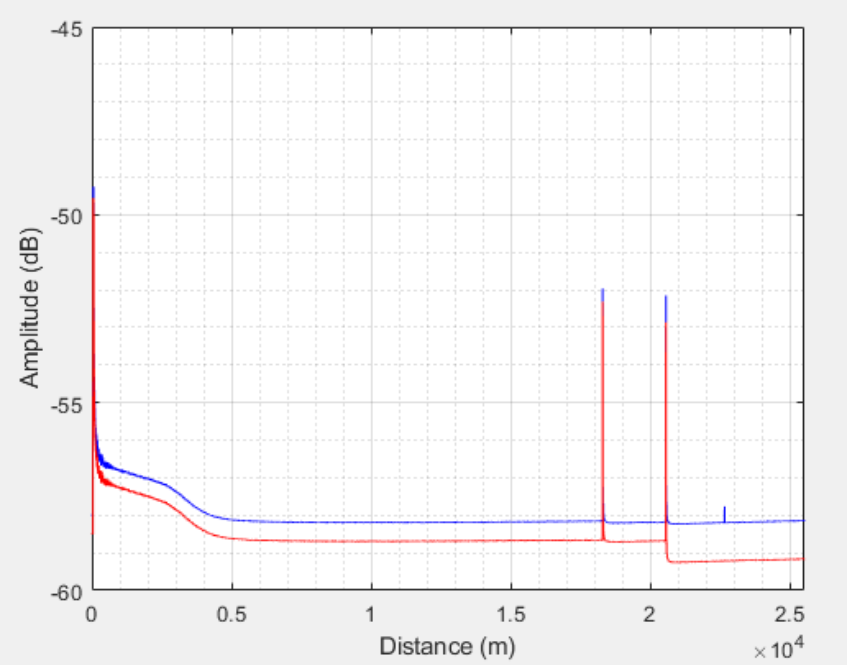

Figure 5.3 OTDR responses of system finalized with isolator (red) vs system without isolator(blue)

The addition of isolator at the fiber end eliminated the reflection coming from the fiber end, which makes the latest fiber segment irrelevant. The purpose of the OTDR is to locate every loss event throughout the entire fiber. Also, the overall reflected back signal is weakened by additional 0.5 dB, and at the end connector by 1 dB. Although the fiber attenuation is clearer, it is not advised to use isolator at the end of the fiber.

5.3 Splice at the OTDR Intrusion

When the OTDR graphs in chapter 4 are observed, too much of the signal is lost at the first connector. This makes the Rayleigh reflections weaker along the rest of the fiber. To negate this, the first connection point is replaced with a splice. The setup is given in figure 5.4.

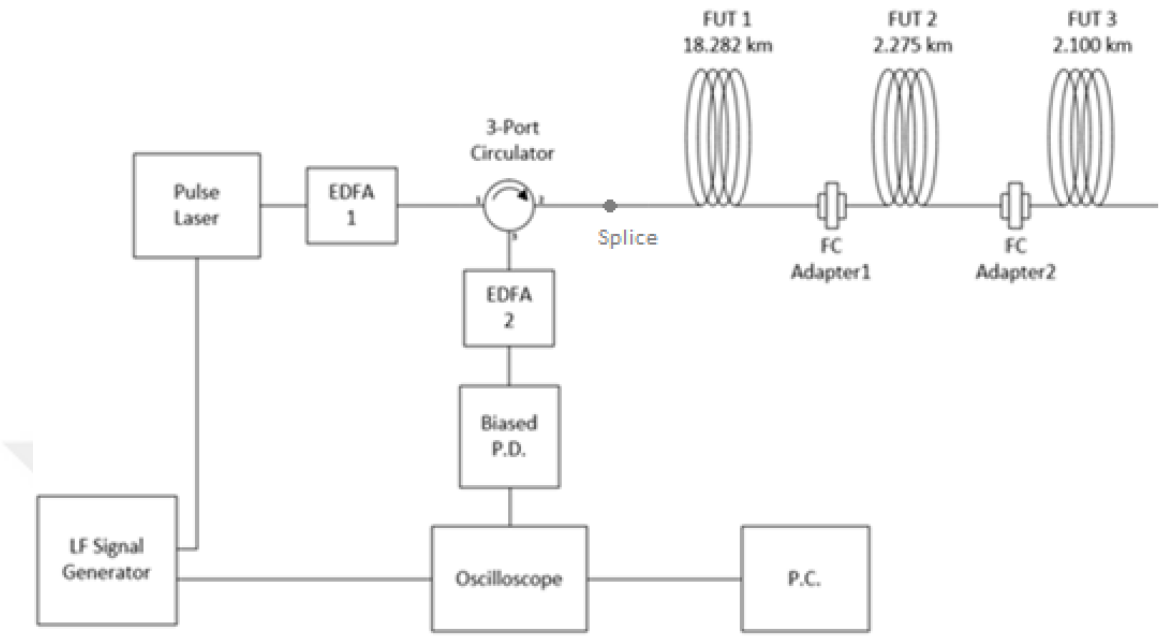

Figure 5.4 OTDR system with initial splice intrusion

The resulting signal is shown in figure 5.5. Comparison with the initial connector case is given in figure 5.6. The zoomed in response for the first 5 km is given in figure 5.7.

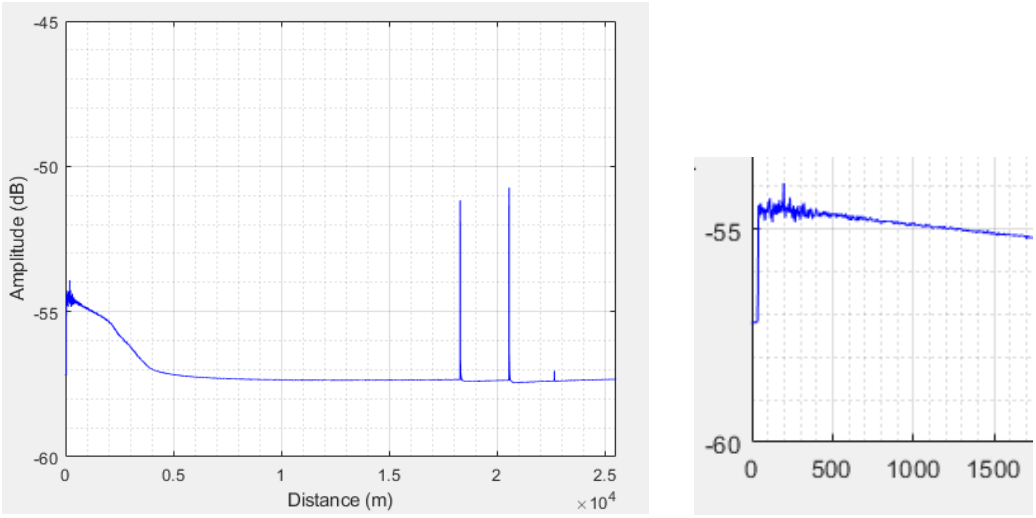

(a) (b)

Figure 5.5 (a) OTDR response of system with initial splice (b) Zoomed in response

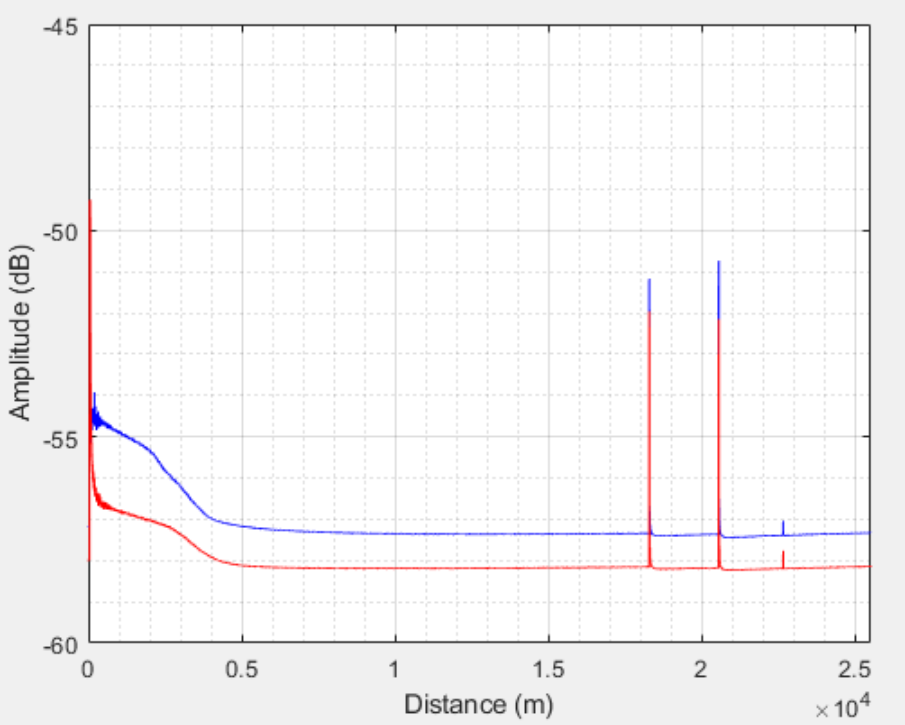

Figure 5.6 OTDR responses of system with initial splice (blue) vs system with initial connector (red)

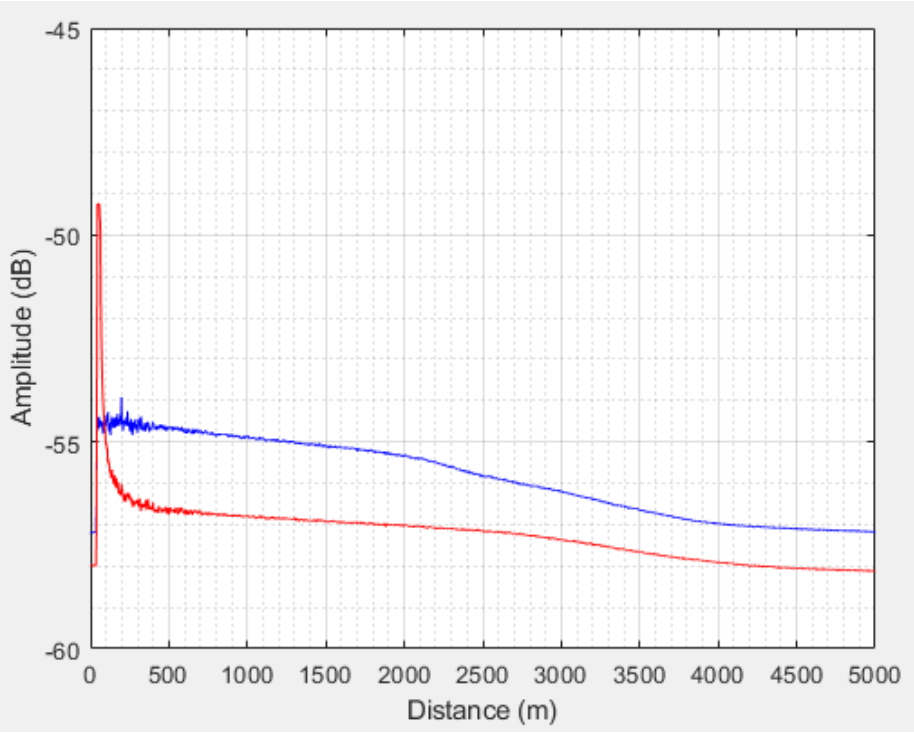

Figure 5.7 First 5km zoomed in OTDR responses of system with initial splice (blue) vs system with initial connector (red).

The replacement of the initial connection with splice results with a flatter reflection. When compared with the initial connector case the initial reflection peak is completely gone and the signal reflection is improved by a at least 2 dB. As the signal travels along the fiber, this gain is reduced to around 1dB. This proves that the Fresnel reflection at the first port of the first connector causes SNR deterioration.

The replacement of the splice at the beginning did not change the location detection by any margin. This can be seen in figure 5.6. All the connector points in between fiber segments are the same as the initial connector case.

However, the fiber attenuation is not improved by much. Still, after some distance the attenuation disappears and flatlines after passing through first connector.

Nonetheless, the replacement of splice significantly improved the reflected signal SNR, making the processing of data much easier.

5.4 Replacing Connectors with Bad Splices for Event Test Points

All the experiments up to this point showed that the connectors are causing too much signal loss for the OTDR system to process. Although connector positions are found precisely, the loss amounts cannot be quantized with this approach. To make a better event detection, the connector loss events are changed with intentional bad splice points. The first setup is given in figure 5.8. Here, a 2.1 km fiber segment is badly spliced to 18.282 km fiber segment.

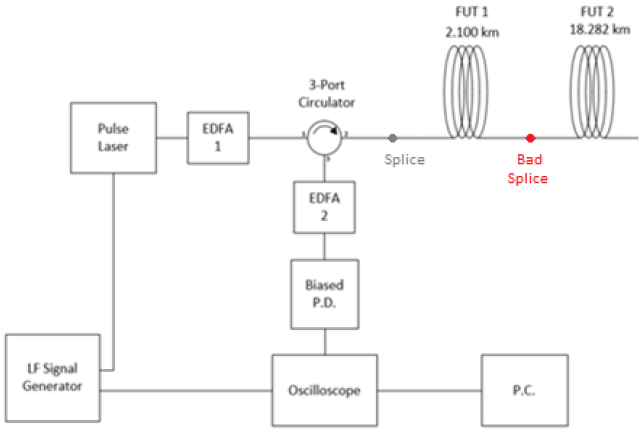

Figure 5.8 OTDR system with bad splice point for detection.

The resulting signal is shown in figure 5.9. After the 2.1 km segment we have a sudden drop in amplitude and then the 18.282 km segment goes until the fiber end. The OTDR response flatlines after 5 km, which is the same behavior as the previous experiments.

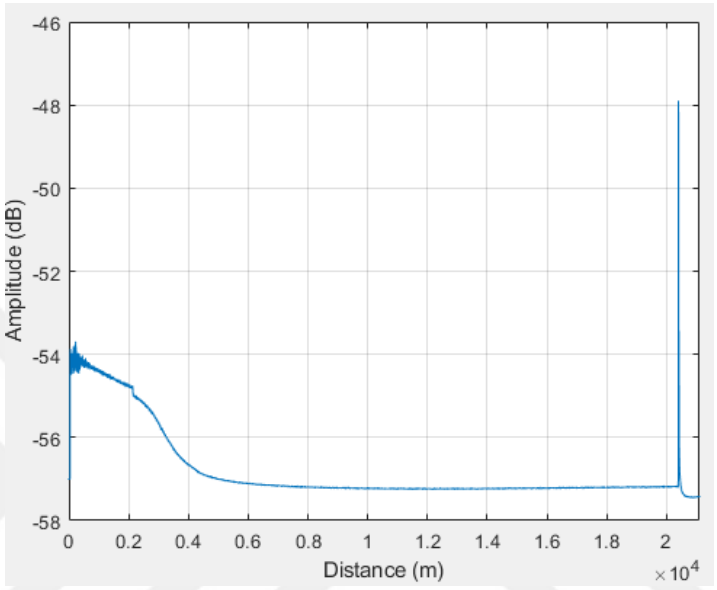

Figure 5.9 OTDR response for 2.1km badly spliced to 18.282 km

When zoomed in to the bad splice event (figure 5.10), the reflected signal suddenly drops by 0.22 dB. The attenuation slope before and after the bad splice event are the same 0.2 dB/km. The bad splice event happens exactly after 2.1 km from the fiber start.

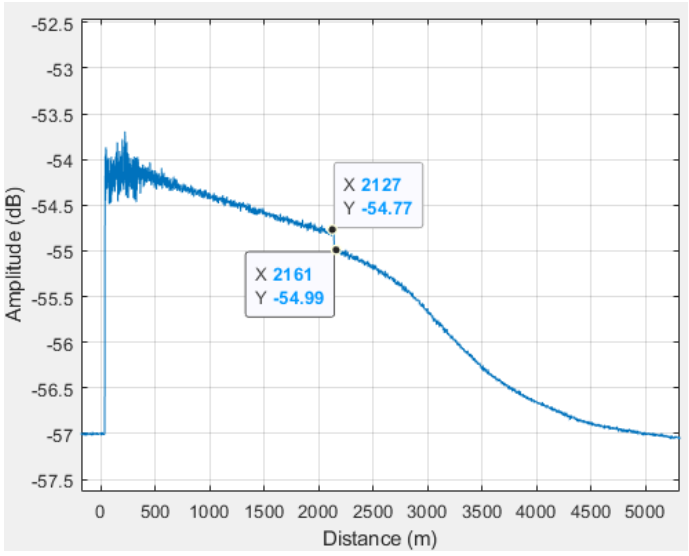

Figure 5.10 Event zoomed in for OTDR response for 2.1km badly spliced to 18.282 km

This experiment, together with all the previous experiments, suggest that the range limit of the OTDR is around 5 km. Any longer OTDR readings can show the location of connections but not the attenuation slope data. Therefore, the test fiber segments are shortened to overcome this. The next setup uses 2.1 km segment badly spliced to 271.87 m segment fiber as FUT. The setup is shown in figure 5.11.

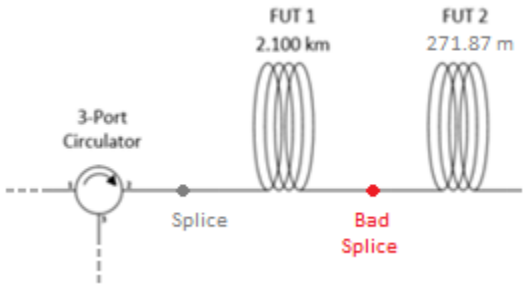

Figure 5.11 OTDR system for 2.1 km segment badly spliced to 271.87 m segment

The resulting signal is shown in figure 5.12. After the 2.1 km segment we have a sudden drop in amplitude and then the short 271.87 m segment goes till the fiber end. The OTDR response does not flatline and the attenuation slope stays steady till the end.

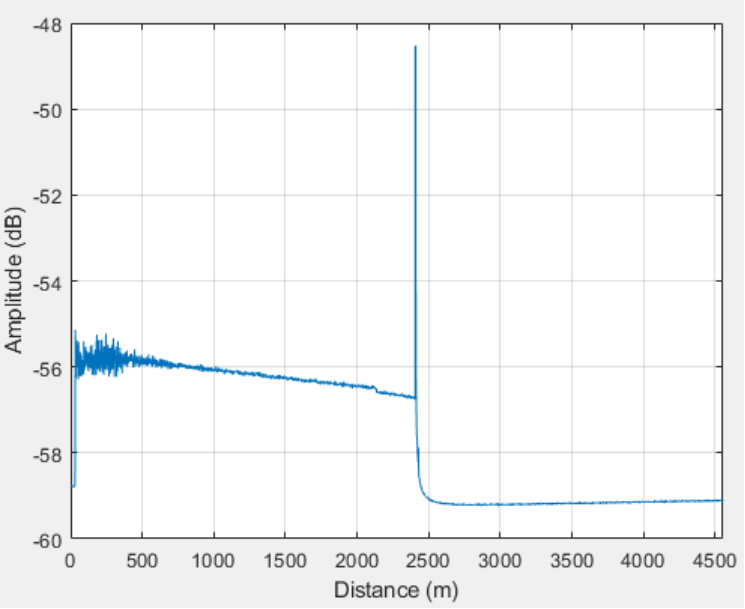

Figure 5.12 OTDR response for 2.1km badly spliced to 271.87 m

When zoomed into the bad splice event (figure 5.13), the reflected signal suddenly drops by 0.09 dB. The difference in amplitude drop compared to the previous case is caused by the difference at both bad splices. This shows that repeating the same bad splice process is hard as intentional bad splicing requires manipulating the fiber by hand during splicing.

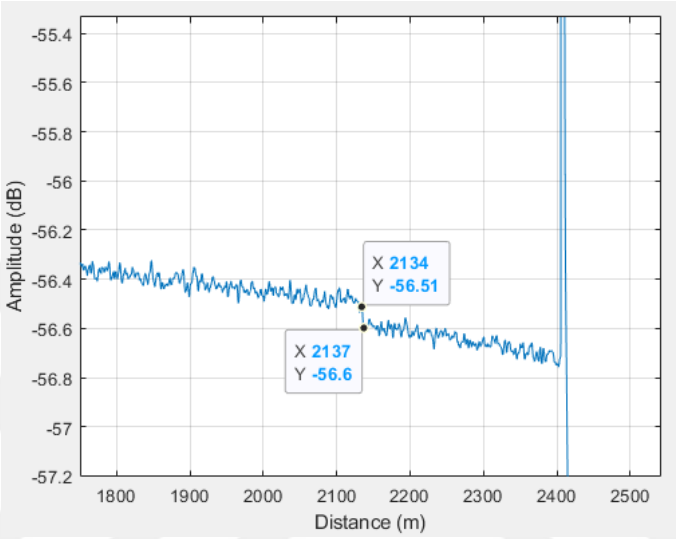

Figure 5.13 Event zoomed in for OTDR response for 2.1km badly spliced to 271.87 m

Finally, 2.1 km segment, 271.87 m segment and 2.27 km segment are all badly spliced to each other as FUT. The setup is shown in figure 5.14.

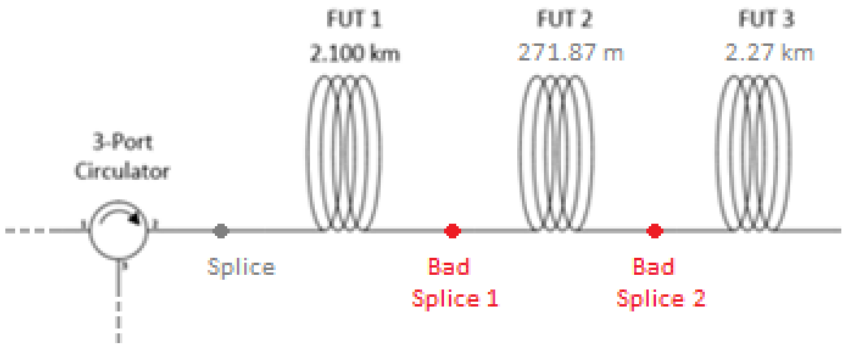

Figure 5.14 OTDR system for 2.1 km segment, 271.87 m segment and 2.27 km segment are badly spliced to each other

The resulting signal is shown in figure 5.15. After the 2.1 km segment we have the first amplitude drop then the second drop after 271.87 m segment. Then attenuation is steady till the fiber end for 2.27 km segment.

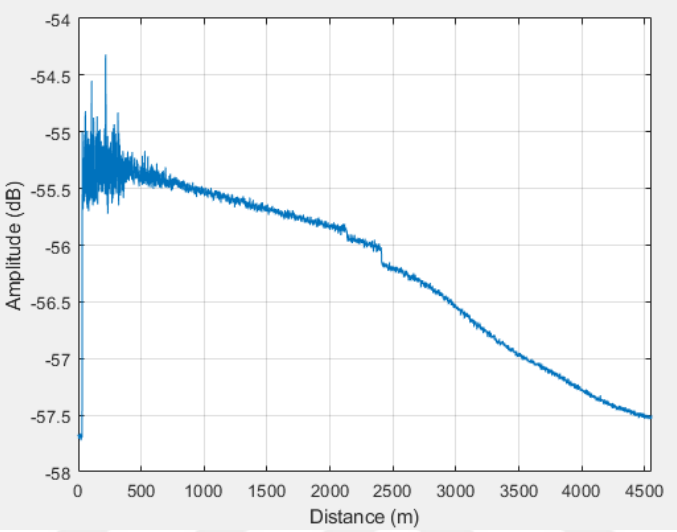

Figure 5.15 OTDR response for 2.1 km segment, 271.87 m segment and 2.27 km segment are badly spliced to each other

When we zoom into the bad splice event (figure 5.16), we can see that the first drop is by 0.09 dB at 2.127km and the second drop is by 1.01 dB at 2.408 km. Once again, the attenuation slope is preserved before and after the loss events. Additional loss events are detected successfully without flatlining of the attenuation response.

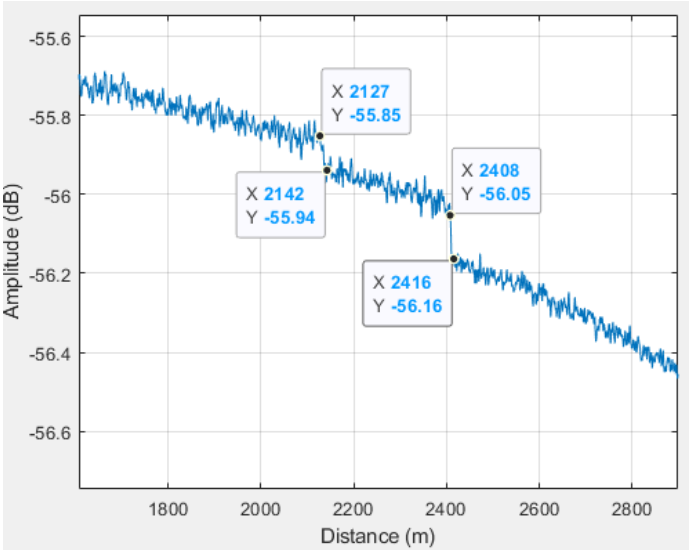

Figure 5.16 Event zoomed in for OTDR response for 2.1 km segment, 271.87 m segment and 2.27 km segment are badly spliced to each other

5.5 OTDR System GUI

To improve user interactivity and easier accessibility a GUI is designed in MATLAB 2020a (figure 5.17).

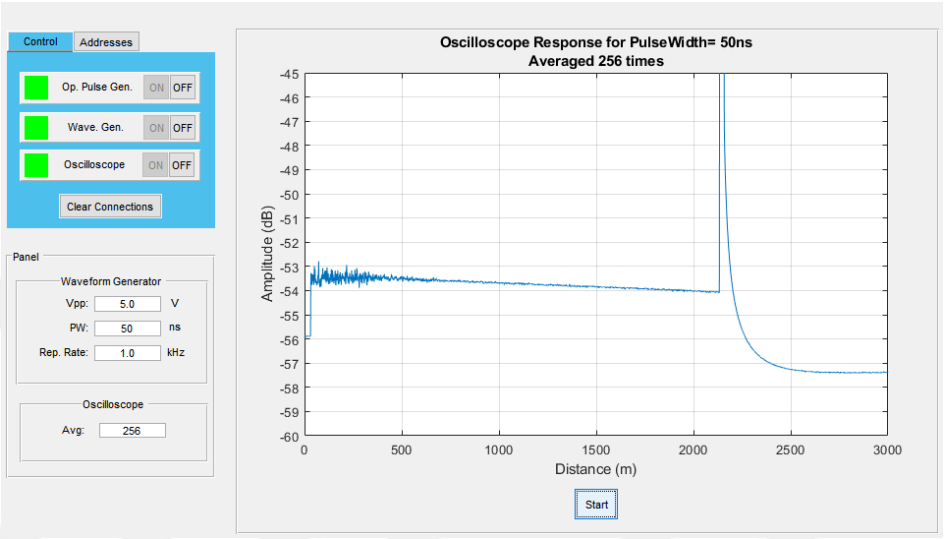

Figure 5.17 OTDR GUI

The control panel allows user to turn on/off devices mid experiments (figure 5.18). The light besides represents the status of the device; green ‘on’ and red ‘off’.

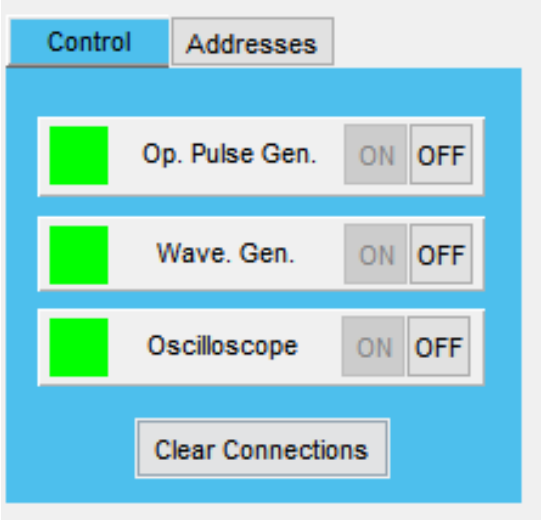

Figure 5.18 Control Panel

The addresses panel allows user to directly change device connection addresses from the GUI (figure 5.19).

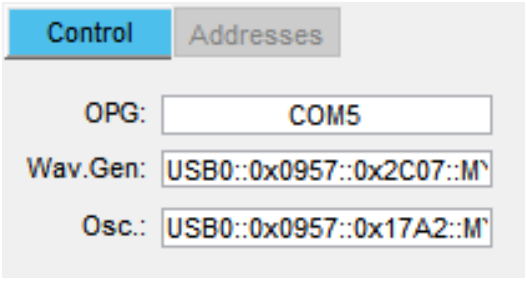

Figure 5.19 Addresses Panel

The parameters panel holds the OTDR parameters (figure 5.20). User can change any OTDR parameter from here. Also, if enabled, the amount of averaging on the oscilloscope can be changed here.

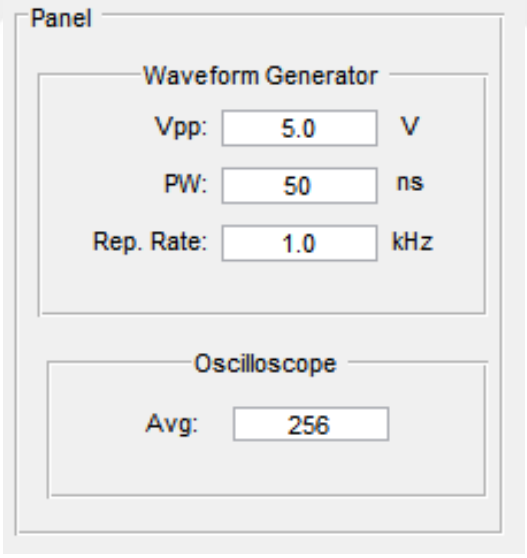

Figure 5.20 Parameters Panel

Finally, the axes panel shows the OTDR graph (figure 5.21). The start button initiates OTDR reading. Once complete, OTDR graph is displayed and the OTDR data is automatically saved in a predetermined folder with a time code.

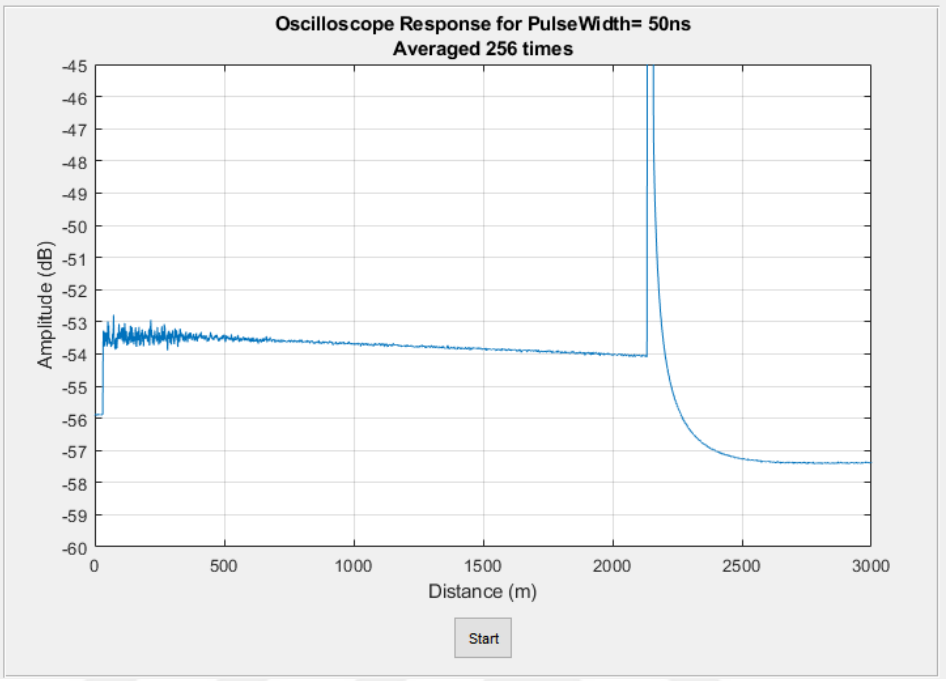

Figure 5.21 Axes Panel

5.6 Nonlinear Fibers as Temperature Sensing Medium in OTDR

The temperature sensitivity response of an R-OTDR sensor is highly dependent of the type of fiber used as FUT. Fibers with higher Rayleigh backscattering characteristics can be utilized to improve the temperature sensitivity. Therefore, observing different types of fibers for their Rayleigh responses would provide us with answers to if any accessible and cheap fibers can be used as testing medium.

5.6.1 Rayleigh Spectra for Different Fibers

The tunable laser source is connected to the 3-port circulator and then to the fiber under test. The circulator can operate in S+C+L band wavelength regions. The reflected back Rayleigh signal passes from the second port of the circulator to the third port. From there the signal reaches optical spectrum analyzer to be observed. The laser source is set to span wavelengths from 1530 nm to 1580 nm at -5 dBm power. The FUT is changed as: SMF (1 km), DSF (1 km), PMF (1 km) and HNLF (1 km). The setup is given in figure 5.22.

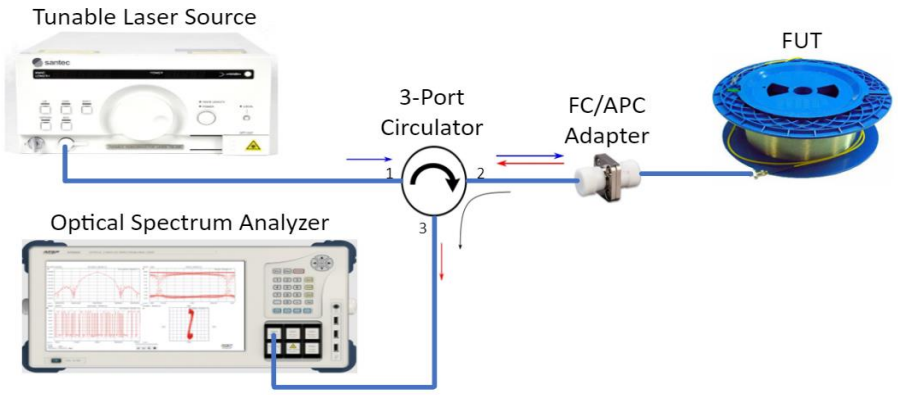

Figure 5.22 Rayleigh spectra test setup

The results are shown in figure 5.23. Although the HNLF yields promising Rayleigh backscattering signal at -39.83 dBm power, PMF offers the best response at -31.34 dBm.

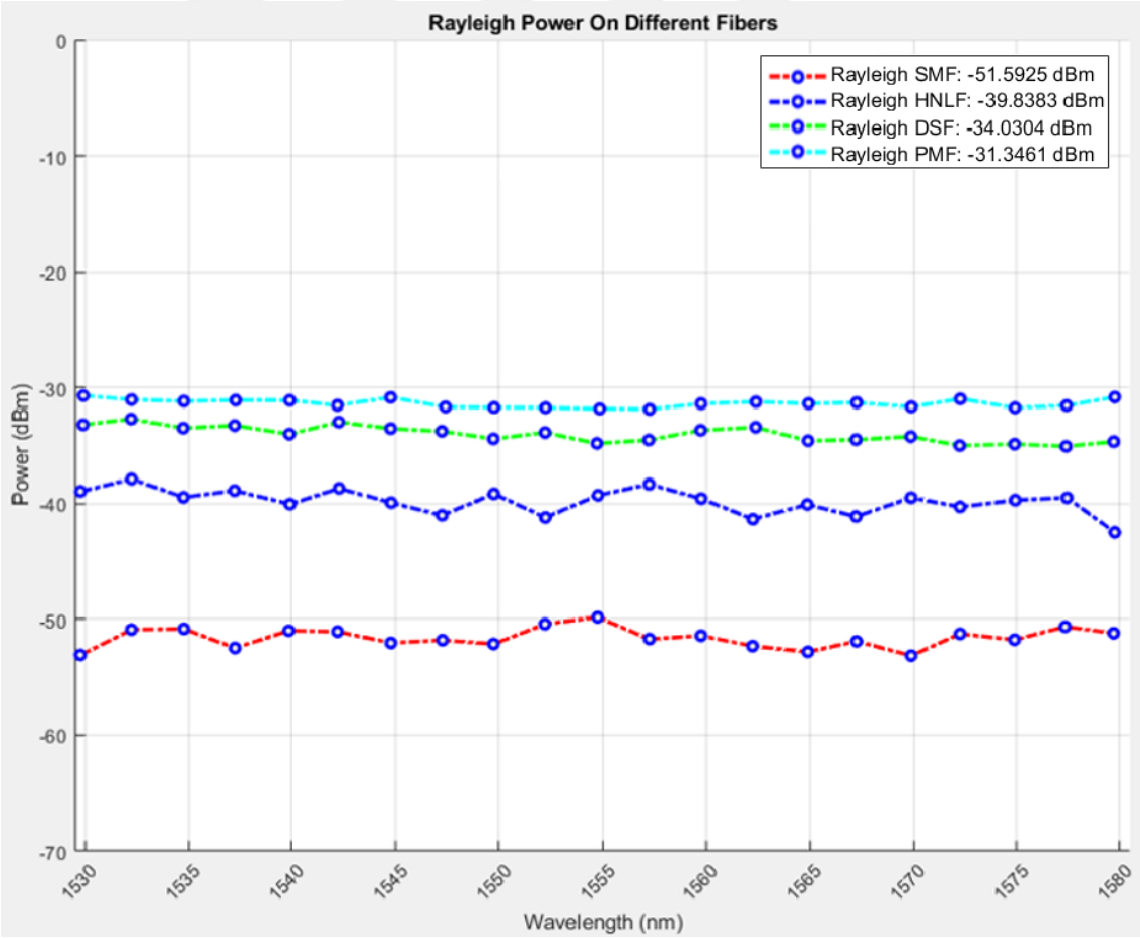

Figure 5.23 Rayleigh response results for SMF (1km), DSF (1km), PMF (1km) and HNLF (1km).

Since the PMF has the best Rayleigh response, it is tested in R-OTDR temperature sensor as 50m FUT and its temperature response is compared to that of 50m SMF FUT.

5.6.2 R-OTDR Temperature Test Results

The FUT are cut into 50 m segments for both SMF and PMF. They are put on the temperature test setup given in figure 5.24. The optical pulse generator (RF Optics) generates 1550 nm optical pulse signals which can be triggered either internally or externally. When the internal trigger is activated, the laser works with on-board modulator to produce optical pulse in the limit of 50ns pulse width and 5 kHz repetition rate. The external trigger enables the laser to be modulated via a Low Frequency (LF) electrical pulse. An LF signal generator (Agilent 33500B) is used to trigger the pulse laser. The channel1 output of the signal generator is connected to pulse laser external trigger input. The laser output is connected to EDFA1 (YİMİ, tunable EDFA) which can generate up to 30 dB gain and is capable of stabilizing temperature for long periods of time. The EDFA1 current was set to 275 mA, which corresponded to 22 dB gain. The amplified optical pulse is then sent to the FUT via a S+C+L wideband 3-port circulator. The pulse goes through circulator's port 1 to port 2 then onto the FUT. Here the FUT is divided into two segments; first a 2.275 km initial SMF which is used to mitigate the event dead zone of OTDR and to simulate a temperature event observed from a distance, then a 50 m temperature FUT segment. The reflected Rayleigh signal is then sent to Photo Diode (P.D) via circulator's port 2 to port 3. Same as the optical pulse, the reflected Rayleigh signal was around -20 dB in power, which was not detectable by the P.D. EDFA 2 (YİMİ brand, fixed power EDFA) is used to amplify the signal with a fixed gain of around 20 dB. Finally, the amplified Rayleigh signal arrives at the P.D to be converted into electrical signal. Then the converted electrical signal is sent to a high sampling rate oscilloscope (Agilent MSO-X 3054-A, up to 4 GSa/s).

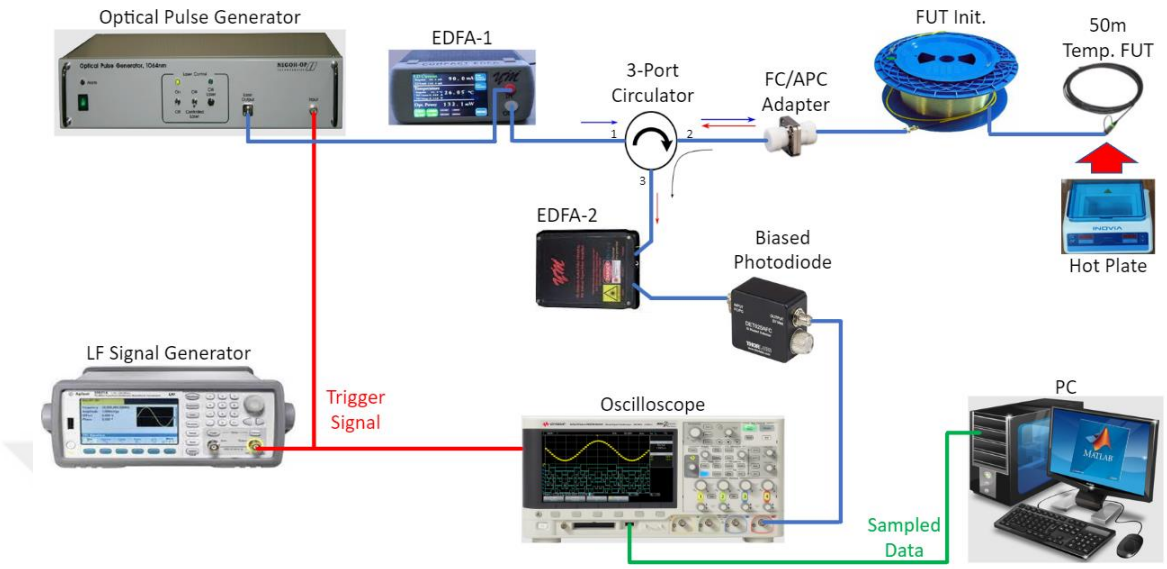

Figure 5.24 R-OTDR Temperature Sensor test setup. (LF: Low Frequency)

After the oscilloscope the signal arrives at the computer port and data is processed by MATLAB program. The program first clears all existing connections, if any. Then it connects to the oscilloscope via visa object and sets both input and output buffers. Then it connects to signal generator and optical pulse generator in that order. The signal generator is then sent the desired pulse width and repetition rate. Then pulse generator internal trigger is deactivated and is triggered with signal generator pulse. The pulse laser output is turned on. After a warmup period of 10 seconds, the oscilloscope is activated to acquire a window reading. The acquired data is then turned into numeric form and displayed on the screen. Since all the filtering, fitting, and averaging is done over the oscilloscope, no further data processing is needed. The flowchart of the program is given in figure 5.25.

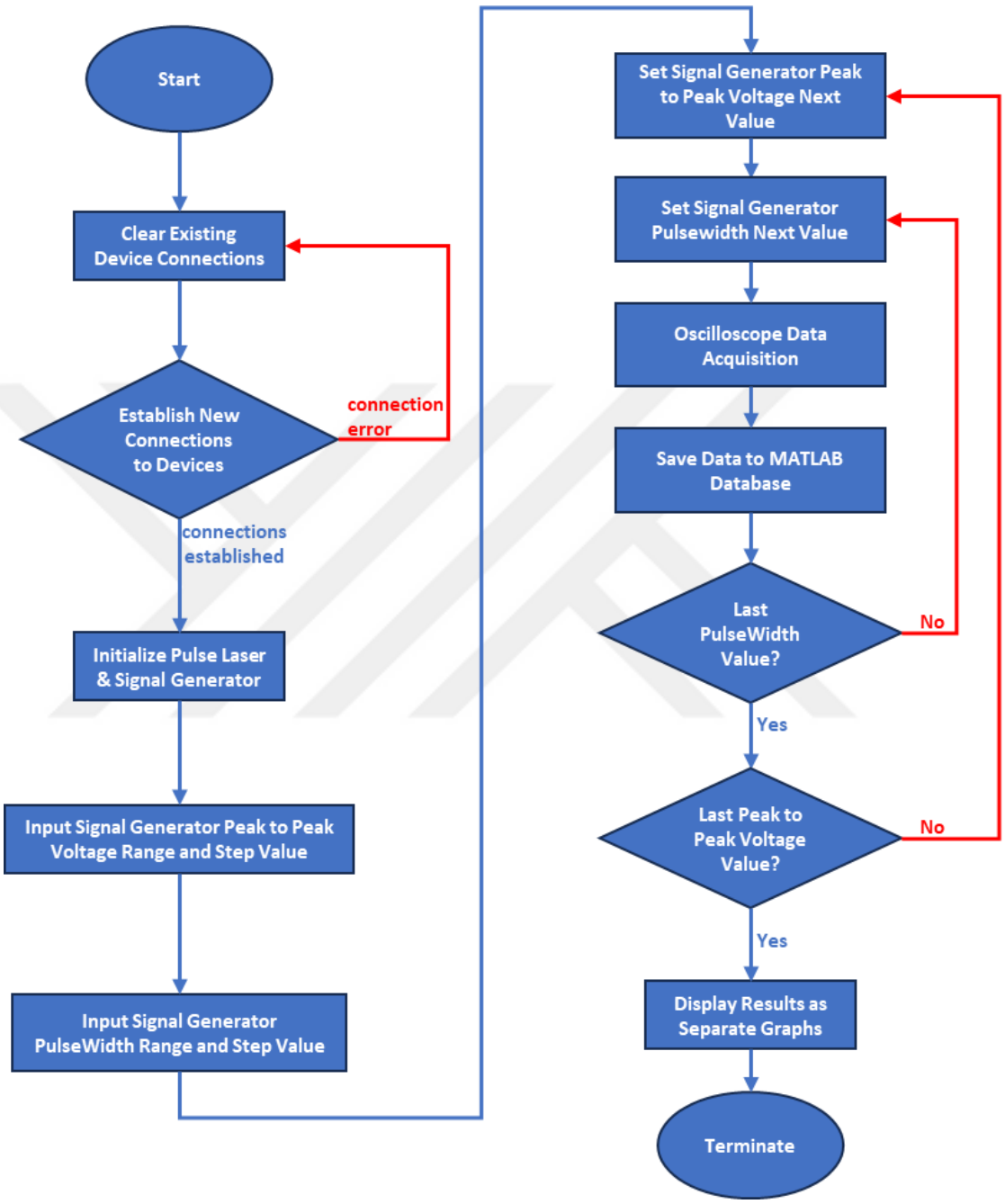

Figure 5.25 Flowchart of the MATLAB program [91]

Using the fully automated program the experiments have been repeated 100 times for each temperature value and the results are averaged.

The spatial resolution of the proposed setup is calculated with:

$$SR = \frac{c\tau}{2n} \tag{5.1}$$

where pulse width τ is 50nm. Which gives us a spatial resolution of approximately 5m.

The results for the 50 m SMF segment placed inside hotplate are given in figure 5.26. The hot plate temperature is changed respectively as 20 °C, 40 °C, 60 °C, 80 °C and 100 °C. The hotplate stayed at each temperature interval for over 10 minutes to get accurate repeatability of the experiment. The Rayleigh peak results are 20 °C -6.72 dB, 40 °C -6.68 dB, 60 °C -6.64 dB, 80 °C -6.61dB and 100 °C -6.56 dB [91].

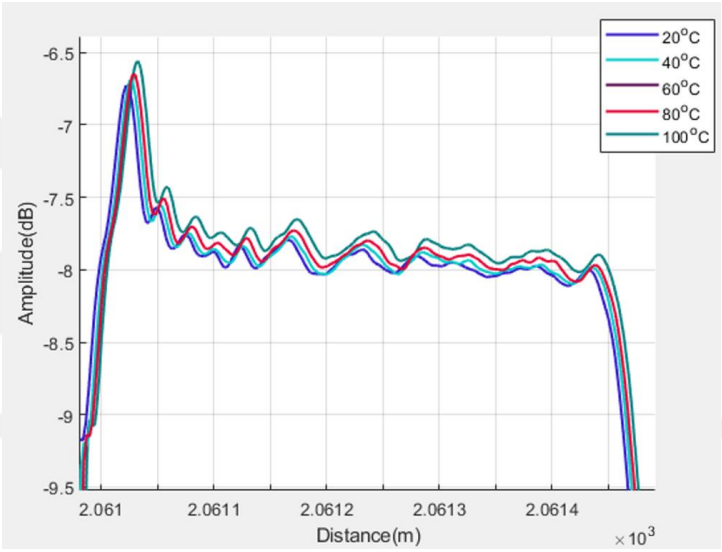

(a)

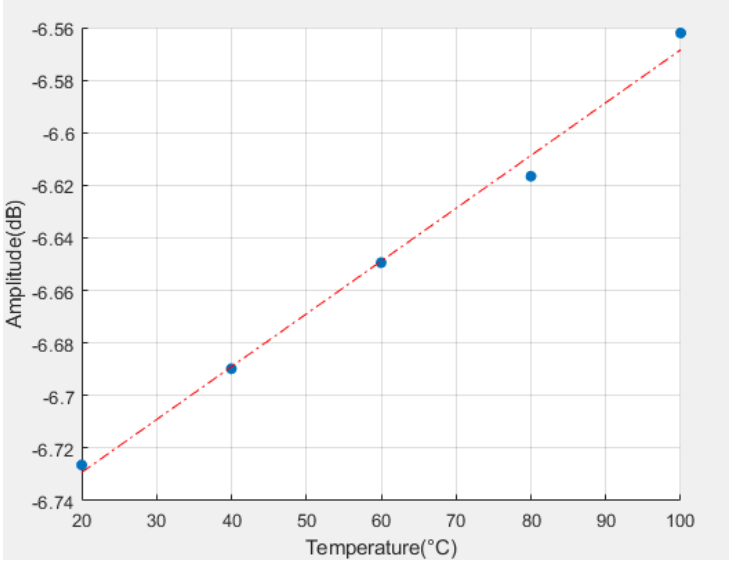

(b)

Figure 5.26 Rayleigh response of SMF vs temperature (a) Rayleigh response of 50m SMF vs temperature, (b) Rayleigh peak points vs. temperature

The linearity (R^2) of figure 5.26(b) is found as 0.9954.

Finally, the experiment is repeated for 50 m PMF segment with splice in between. The results are given in figure 5.27. The Rayleigh peak results are 20 °C -29.3118 dB, 40 °C -28.8579 dB, 60 °C -28.6929 dB, 80 °C -28.2343 dB and 100 °C -27.9739 dB [91].

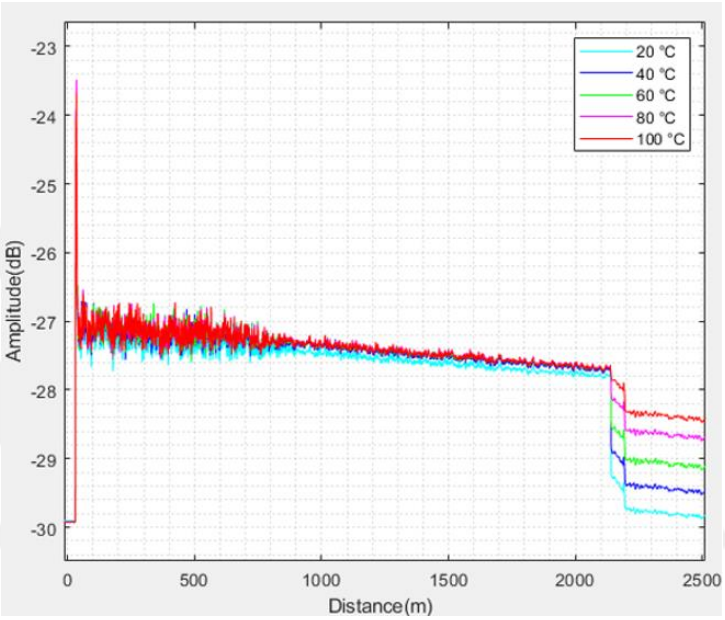

(a)

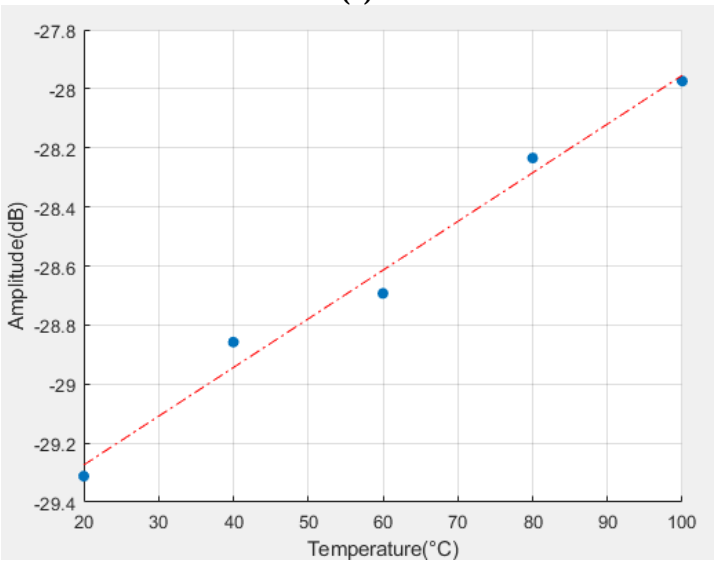

(b)

Figure 5.27 Rayleigh response of PMF vs temperature (a) Rayleigh response of 50 m PMF vs. temperature, (b) Rayleigh peak points vs. temperature

The linearity (R^2) of figure 5.27(b) is found as 0.9838.

The splice point drops can be clearly seen in figure 5.27. As stated above, these drop points have different values depending on the temperature. The temperature response is improved to 0.018 dB/°C [91].

5.7 Conclusion

The inclusion of isolator is observed in a Rayleigh OTDR setup. The addition improved the attenuation slope of the Rayleigh trace; however, dramatically lowered the end point of the fiber. Therefore, isolator is eliminated as a viable option for improvement.

The initial fiber insertion point was connected via an adaptor. In this study it was replaced with splice. The splicing significantly improved the backscattered signal power, in the levels of 2 dBm, without any loss in any fiber segments unlike isolator.

Then the event detection mechanism is changed from adaptors to intentional bad splices. These splice point drops and locations were detected successfully. Furthermore, the bad splicing made it possible for Rayleigh attenuation slope to continue even after loss events. Previously, with the adaptors, the Rayleigh slope was immediately disappearing after the first adaptor.

The remote-control code was updated to include a GUI for ease of use and faster repeatability of the experiments.

Finally nonlinear fibers' Rayleigh responses were observed. HNLF, DSF and PMF were investigated. The PMF showed most powerful Rayleigh backscattered signal in the order of -31.34 dBm. Then PMF was inserted into the temperature test setup. The temperature sensitivity was compared to SMF. Significant improvement was achieved, as the PMF showed 0.018 dB/°C compared to SMF's 0.002 dB/°C temperature sensitivity [91].

CONCLUSION

Within the scope of the thesis, a simulation is done for Rayleigh based OTDR system, which works very well in detecting the position of a sudden power drop over a length of fiber. However, the spatial resolution for power drop detection is directly related to the number and length of fiber segments, meaning shorter fiber segments would heavily increase the required processing time for the simulation. Moreover, the total number of iterations needed is directly dependent on number of fiber segments. Still, this approach proved to be promising as a novel idea of simulating OTDR with OptiSystem.

Then the simulated OTDR system is realized in laboratory. The lossy events were simulated with connectors. Through a set combination of different fiber spool segments, the connection points in between are successfully detected. Time-domain to spatial domain conversion and data reading were achieved successfully.

The remote-control codes synchronized the whole process. The data storing was automatized, making it possible to later accessing and processing previous data. The code allows for many more devices to be added in, which would make future complex projects much more manageable and less time consuming.

A biased photo detector was used for electrical conversion. The biased PD yielded very good readings at the connection points. Compared to other photo detectors, these are very cheap and even compatible to work with batteries. However, this conversion scheme become somewhat misguiding in the attenuation slope parts. The amount of power distributed here was very low compared to the reflection peaks. The biased photo detector seemed to flatten around -58.8 dB, therefore other than the first segment that had adaptor, it was not possible to get the attenuation slope.

To fix these issues, an isolator was tried at the end of the fiber under test as it would reduce the huge Fresnel reflection caused by the fiber end. However, the isolator completely

neutralized backscattering reading from the last fiber segment, which poses as a problem in an event detection OTDR system.

Then the first fiber segment entry point was spliced instead of using a connector. This significantly improved OTDR SNR. The elimination of first Fresnel reflection from the connector, strengthened the Rayleigh backscattered signal throughout the fiber. Other than the very first few 100 meters, the OTDR readings became very clear.

Next, connectors were replaced with bad splices as loss events, which further improved the OTDR SNR. Also, it provided a more readable event for signal processing and possible sensor applications, as the amount of amplitude drop was related to the amount of splice loss.

The remote-control program was upgraded with a GUI application for easier tracking of all the past experiment data. Previously all the devices were required to be online for the OTDR code to run. This caused repeatability problems for all devices were being connected and disconnected after every run, making them sometimes lag and result with program halt. With the new GUI, the devices establish connection at the request of the user and once connected, they stay connected until program is closed. This saved the troubling data transfer for continuous reestablishment of connections. Also, ‘try catch’ error and warning handling methods were applied to improve experiment safety. Previously one bad connection or device timeout was causing the entire experiment to halt. Now, at a possible device error or warning the experiment pauses and waits for the problem to be solved. Only after the problem is solved, experiment continues.

Finally, it has been investigated to make a simpler fiber optic temperature sensor compared to FBG, Brillouin and Raman based sensors. A classical R-OTDR temperature sensor is investigated as it is much easier to setup compared to COTDR setups.

As the type of the FUT would directly affect the temperature sensitivity, different types of candidate fibers are observed in an R-OTDR setup. First, Rayleigh backscattering responses for SMF (1 km), DSF (1 km), PMF (1 km) and HNLF (1 km) segments were observed. The Rayleigh responses were: HNLF had -39.83 dBm, DSF had -34.03 dBm

and PMF had -31.34 dBm. The PMF fiber segment showed the most promise among other fibers to be applied as a temperature sensing medium.

Then temperature sensitivity for 50 m SMF and PMF sections are observed in R-OTDR setup. The fiber attenuations and splice point drop for different temperatures were observed. The SMF segment had temperature sensitivity of 0.002 dB/°C, whereas the PMF had temperature sensitivity of 0.018 dB/°C.

The Brillouin sensors require analysis of both amplitude and frequency data of the backscattered signal. Although, it gives good temperature and strain readings, the process is very costly both in data processing and setup. Whereas, with Rayleigh OTDR sensors only amplitude data is enough to determine the temperature change. The issue with Rayleigh OTDR systems; however, is that the received signal is generally too weak to be meaningful as amplifying the signal would just amplify other loss factors. Therefore, a nonlinear fiber that has higher backscattering coefficient as temperature sensing medium was suggested in this work. Just by changing the FUT type to PMF a 9 times improvement was achieved in the temperature sensitivity. A small FUT length of just 50 m was used. Compared to other types of fiber sensors, no excessive data or frequency domain analysis was needed. Only averaging and a simple fitting was applied. Compared to Brillouin based sensors, this approach significantly reduced the computational power needed.

Overall, this thesis study showed that the complexities of the bulky, long fiber temperature sensors can be reduced with a simple R-OTDR based sensor which uses an alternative fiber PMF with a good Rayleigh backscattering response.

FUTURE WORKS

In this thesis study, the fiber end is left open as single point insertion OTDR systems have more functional use compared to OTDA systems. However, with the single insertion the adverse effects of Fresnel reflection from fiber end become apparent. To solve this, at the cost of giving up single entry scheme, passive nonlinear ring circulators may be applied at the end of the testing fiber. Any noise power would dissipate and get absorbed by the passive nonlinear ring circulator. Also, the ASE from EDFA blocks would get negated as well.

Another limiting factor was the opto-electronic conversion mechanism. The biased photodetectors used in this thesis study are not strong and would generally get flattened response around -58.8 dB. The dual biased photodetectors might improve the electrical conversion as they use coherent detection mechanism to get much better SNR. However, they are very costly compared to biased photodetectors.

Finally, the input laser signal may be strengthened with applying EOM or AOM to a CW laser. The optical pulse generator used in this thesis study had limitations as output power would only go so far. A strong CW laser modulated with a good EOM would theoretically yield better input power.

REFERENCES

[1] Udd, E. An overview of fiber-optic sensors. Rev. Sci. Instrum., *66*, (8), 4015-4030. 1995

[2] Grattan, K.T.V., Sun, T. Fiber optic sensor technology: an overview. Sensor Actuat A-Phys, *88*, (1-3), 40-61. 2000

[3] Yücel, M., Öztürk, N. F., Yücel, M., Göktaş, H. H., Gündüz, A. E. Design of a Fiber Bragg Grating based temperature sensor. 24th Signal Processing and Communication Application Conference (SIU), *24*, (1), 669. 2016

[4] Yücel, M., Öztürk, N.F., Torun, M., Yücel, M. Design and application of a fiber Bragg grating array-based temperature measurement system. Journal of the Faculty of Engineering and Architecture of Gazi University, *32*, (3), 957. 2017

[5] Kipriksiz, S.E., Yücel, M. Tilted fiber Bragg grating design for a simultaneous measurement of temperature and strain. Opt. Quant. Electron, *53*, (6), 1. 2021

[6] Yücel, M., Öztürk, N.F. Real-time monitoring of railroad track tension using a fiber Bragg grating-based strain sensor. Instrum. Sci. Technol., *46*, (5), 519. 2018

[7] Yücel, M., Göktaş, H.H., Yücel, M., Öztürk, N.F., Gündüz, A.E. Experimental analysis of the temperature dependence of the Brillouin gain spectrum in short-length single-mode fiber. Turk. J. Electr. Eng. Co., *25*, (5), 3881-3891. 2017

[8] Yücel, M., Yücel, M., Öztürk, N.F., Göktaş, H.H. The analyzes of the Brillouin scattering for the different fiber types. 23rd Signal Processing and Communication Application Conference (SIU), *23*, (1), 632-635. 2015

[9] Yücel, M., Gündüz, A.E., Göktaş H.H., Öztürk, N.F. Using single-mode fiber as temperature sensor. 24th Signal Processing and Communication Application Conference (SIU), *24*, (1), 461-464. 2016

[10] Yücel, M., Göktaş, H.H., Öztürk, N.F. The fiber optical sensing based on Brillouin scattering. 22nd Signal Processing and Communications Applications Conference (SIU), *22*, (1), 838-841. 2014

[11] Yücel, M., Yücel, M. The measurement of strain of a prototype pulley system using a Brillouin optical time domain analysis. Microw. Opt. Techn. Let., *64*, (1), 190-198. 2022

[12] M. Yonas, O. J. Claudio, D.P. Fabrizio, Aip. Conf. Proc., 7, (2019).

[13] Saxena, M.K., Raju, S.D.V.S.J., Arya, R., Pachori, R.B., Ravindranath, S.V.G., Kher, S., Oak, S.M. Raman optical fiber distributed temperature sensor using wavelet transform based simplified signal processing of Raman backscattered signals. Opt. Laser Technol., *65*, (1), 14-24. 2015

[14] Wang, Z., Sun, X.H., Xue, Q., Wang, Y.L., Qi, Y.L., Wang, X.S. An optical fiber-folded distributed temperature sensor based on Raman backscattering. Opt. Laser Technol., *93*, (1), 224-227. 2017

[15] Bao, X., Wang, X. Recent advancements in Rayleigh scattering-based distributed fiber sensors. Advanced Devices & Instrumentation, *2021*, (1), 1-17. 2021

[16] Palmieri, L., Schenato, L., Santagiustina, M., Galtarossa, A. Rayleigh-Based Distributed Optical Fiber Sensing. Sensors, *22*, (18), 6811. 2022

[17] Gifford, D.K., Soller, B.J., Wolfe, M.S., Froggatt, M.E. Distributed fiber-optic temperature sensing using Rayleigh backscatter. 31st European Conference on Optical Communication, *31*, (3), 511-512. 2005

[18] Iezzi, V.L., Loranger, S., Marois, M., Kashyap, R. High-sensitivity temperature sensing using higher-order Stokes stimulated Brillouin scattering in optical fiber. Opt. Lett., *39*, (4), 857-860. 2014

[19] Qiu, L., Zhu, Z., Li, T., Zhou, D., Dong, Y. High-Sensitivity Distributed Temperature Sensor Based on Brillouin Scattering with Double-Coated Single-Mode Fibers. IEEE Sens. J., *21*, (5), 6209-6216. 2021

[20] Minardo, A., Bernini, R., Lombera, R.R., Mirapeix, J., Higuera, J.M.L., Zeni, L. Proposal of Brillouin optical frequency-domain reflectometry (BOFDR). Opt. Express, *24*, (1), 29994-30001. 2016

[21] Karapanagiotis, C., Wosniok, A. Hicke, K., Krebber, K. Time-Efficient Convolutional Neural Network-Assisted Brillouin Optical Frequency Domain Analysis. Sensors, *21*, (8), 2724. 2021

[22] Zaynetdinov, M., See, E.M., Geist, B., Ciovati, G., Robinson, H.D., Kochergin, V. A Fiber Bragg Grating Temperature Sensor for 2–400 K. IEEE Sens. J., *15*, (3), 1908–1912. 2015

[23] Gurkaynak, I.A., Al-Mashhadani, T.F., Al-Mashhadani, M.K.S., Ali, M.H., Gunduz, A.E., Yucel, M., Göktaş, H.H., Zidan, K.A. An efficient wide flatness gain bandwidth with parallel hybrid fiber amplifier. Microw. Opt. Techn. Let., *64*, (2), 251-258. 2022

[24] Gurkaynak, I.A., Al-Mashhadani, M.K.S., Ali, M.H., Al-Mashhadani, T.F., Gunduz, A.E., Yucel, M., Göktaş, H.H. Widely flatness gain bandwidth with double pass parallel hybrid fiber amplifier. Opt. Quant. Electron., *53*, (7), 359. 2021

[25] Gurkaynak, I. A., Al-Mashhadani, T. F., Yucel M., Goktas, H.H. Broadly Flatness Gain Band with Double Pass-Serial Hybrid Optical Amplifier Utilizing Single Pump Unit. 8th International Conference on Electrical and Electronics Engineering (ICEEE), *8*, (1), 32-25. 2021

[26] Zhang, Z., Wu, H., Zhao C., Tang, M. High-Performance Raman Distributed Temperature Sensing Powered by Deep Learning. J. Lightwave Technol., *39*, (2), 654-659. 2021

[27] Ohashi, M., Kubota, H., Miyoshi, Y. OTDR techniques for measuring transmission characteristics of space-division multiplexing fibers. 25th Opto-Electronics and Communications Conference (OECC), *2020*, (1), 1-3. 2020

[28] Hazarika, D., Pegu, D.S. Micro-controller-based air pressure monitoring instrumentation system using optical fibers as sensor. Optical Fiber Technology, *19*, (2), 83-87. 2013

[29] Palma, A.J., Gonzalez, J.L., Asensio, L.J., Dolores, M., Ramos, F., Vallvey, L.F.C. Microcontroller-based portable instrument for stabilised optical oxygen sensor. Sensors and Actuators, *121*, (2), 629-638. 2007

[30] Omar, A.F., MatJafri, M.Z. Development of Optical Fiber Sensor for Water Quality Measurement. AIP Conference Proceedings, *1017*, (1), 398-402. 2008

[31] Zhang, Q., Liu, Q. Build intelligent home furnishing control system by microcontroller GSM and optical fiber sensor. Journal of Chemical and Pharmaceutical Research, *6*, (7), 1689-1696. 2014

[32] Uzenkov, O., Lee, P., Webb, D. An FPGA based Measurement System for a Fibre Bragg Grating (FBG) Strain Sensor. 2006 IEEE Instrumentation and Measurement Technology Conference Proceedings, *2006*, (1), 2364-2367. 2010

[33] Wild, G., Hinckley, S. Distributed Optical Fibre Smart Sensors for Structural Health Monitoring: A Smart Transducer Interface Module. 2009 International Conference on Intelligent Sensors, Sensor Networks and Information Processing (ISSNIP), *2009*, (1), 373-378. 2009

[34] Qin, Z. Distributed Optical Fiber Vibration Sensor Based on Rayleigh Backscattering. Ph.D. Thesis, Ottawa University. 2013

[35] Bao, X., Chen, L. Recent Progress in Distributed Fiber Optic Sensors. Sensors, *12*, (7), 8601-8639. 2012

[36] Barrios, F.R., Lopez, S.M., Sanz, A.C., Corredera, P., Castanon, J.D.A., Thevenaz, L., Herraez, M.G. Distributed Brillouin fiber sensor assisted by first-order Raman amplification. IEEE J. Lightw. Technol., *28*, (1), 2162-2172. 2010

[37] Soto, M.A., Bolognini, G., Pasquale, F.D. Optimization of long-range BOTDA sensors with high resolution using first-order bi-directional Raman amplification. Opt. Express, *19*, (5), 4444-4457. 2011

[38] Li, Y., Chen, L., Dong, Y., Bao, X. A novel distributed Brillouin sensor based on optical differential parametric amplification. J. Lightwave Technol., *28*, (1), 2621-2626. 2010

[39] Mafang, S.F. Brillouin Echoes for Advanced Distributed Sensing in Optical Fibres. Phd. Thesis, École Polytechnıque Fédérale De Lausanne. 2011

[40] Frazão, O., Correia, C., Santos, J.L., Baptista, J.M. Raman Fibre Bragg-grating laser sensor with cooperative Rayleigh scattering for strain–temperature measurement. Meas. Sci. Technol., *20*, (4), 5. 2009

[41] Martins, H.F., Marques, M.B., Frazão, O. Temperature-insensitive strain sensor based on four-wave mixing using Raman fiber Bragg grating laser sensor with cooperative Rayleigh scattering. Applied Physics B, *104*, (4), 957-960. 2011

[42] Bolognini, G., Park, J., Soto, M.A., Park, N., Di Pasquale, F. Analysis of distributed temperature sensing based on Raman scattering using OTDR coding and discrete Raman amplification. Meas. Sci. Technol., *18*, (10), 3211-3218. 2007

[43] Stokes, D.L., Vo-Dinh, T. Development of an integrated single-fiber SERS sensor. Sensors and Actuators, 69, (1-2), 28-36. 2000

[44] Palmieri, L., Schenato, L. Distributed Optical Fiber Sensing Based on Rayleigh Scattering. The Open Optics Journal, *7*, (1), 104-127. 2013

[45] Wosnioka, A., Nöthera, N., Krebbera, K. Distributed Fibre Optic Sensor System for Temperature and Strain Monitoring Based on Brillouin Optical-Fibre Frequency-Domain Analysis. Proceedings of the Eurosensors XXIII conference, *1*, (1), 397-400. 2009

[46] Kwona, H., Kim, S., Yeom, S., Kang, B., Kim, K., Kim, T., and others. Analysis of nonlinear fitting methods for distributed measurement of temperature and strain over 36 km optical fiber based on spontaneous Brillouin backscattering. Optics Communications, *294*, (1), 59-63. 2013

[47] Reshak, A.H., Shahimin, M.M., Murad, S.A.Z., Azizan, S. Simulation of Brillouin and Rayleigh scattering in distributed fibre optic for temperature and strain sensing application. Sensors and Actuators, *190*, (1), 191-196. 2012

[48] Gong, Y.D. Guideline for the design of a fiber optic distributed temperature and strain sensor. Optics Communications, *272*, (1), 227-237. 2006

[49] Lecoeuche, V., Webb, D.J., Pannell, C.N., Jackson, D.A. 25 km Brillouin based single-ended distributed fibre sensor for threshold detection of temperature or strain. Optics Communications, *168*, (1-4), 95-102. 1999

[50] Wait, P.C., De Souza, K., Newson, T.P. A theoretical based comparison of spontaneous Raman and Brillouin fibre optic distributed temperature sensors. Optics Communications, *144*, (1-3), 17-23. 1997

[51] Perez-Herrera, R.A., Lopez-Amo, M. Fiber optic sensor Networks. Optical Fiber Technology, *19*, (6), 689-699. 2013

[52] Sorin, W.V., Donald, D.K., Newton, S.A., Nazarathy, M. Coherent FMCW reflectometry using a temperature tuned Nd:YAG ring laser. Photonics Technol. Lett., *2*, (12), 902-904. 1990

[53] Venkatesh, S., Sorin, W., Donald, D., and Heffner., B.L. Coherent FMCW reflectometry using a piezoelectrically tuned Nd:YAG ring laser. Optical Fiber Sensors, *8*, (1), 1. 1992

[54] Shimizu, K., Horiguchi, T., & Koyamada, Y. Measurement of Rayleigh backscattering in single-mode fibers based on coherent OFDR employing DFB laser diode. Photonics Technol. Lett., *3*, (11), 1039-1041. 1991

[55] Huang, K.-Y., Carter, G.M. Coherent optical frequency domain reflectometry (OFDR) using a fiber grating external cavity laser. IEEE Photon. Technol. Lett., *6*, (1), 1466–1468. 1994

[56] Passy, R., Gisin, N., von der Weid, J.P., Gilgen, H.H. Experimental and theoretical investigations of coherent OFDR with semiconductor laser sources. J. Lightwave Technol, *12*, (9), 1622-1630. 1994

[57] Von der Weid, J.P., Passy, R., Gisin, N. Mid-range coherent optical frequency domain reflectometry with a DFB laser diode coupled to an external cavity. J. Lightwave Technol, *13*, (5), 954-960. 1995

[58] Tsuji, K., Shimizu, K., Horiguchi, T., Koyamada, Y. Coherent optical frequency domain reflectometry using phase-decorrelated reflected and reference lightwaves. J. Lightwave Technol, *15*, (7), 1102-1109. 1997

[59] Oberson, P., Huttner, B., Guinnard, O., Guinnard, L., Ribordy, G., Gisin, N. Optical frequency domain reflectometry with a narrow linewidth fiber laser. Photonics Technol. Lett., *12*, (7), 867-869. 2000

[60] Geng, J., Spiegelberg, C., Jiang, S. Narrow linewidth fiber laser for 100-km optical frequency domain reflectometry. Photonics Technol. Lett., *17*, (9), 1827-1829. 2005

[61] Oh, M.S., Park, H.S., Kim, B.Y. Optical frequency-domain reflectometry based on wavelength-swept mode-locked fiber laser. Photonics Technol. Lett., *15*, (2), 266-268. 2003

[62] Ndiaye, C., Hara, T., Ito, H. Profilometry using a frequency-shifted feedback laser. Conference on Lasers and Electro-Optics (CLEO), 3, (1), 1757-1759. 2005

[63] Clement, J., Maestre, H., Torregrosa, G., Fernández-Pousa, C.R. Incoherent Optical Frequency Domain Reflectometry Using Balanced Frequency-Shifted Interferometry in a Downconverted Phase-Modulated Link. 2018 International Topical Meeting on Microwave Photonics (MWP), 2018

[64] Kim, Y., Kim, M.J., Rho, B.S., Kim, Y.H. Measurement Range Enhancement of Rayleigh-Based Optical Frequency Domain Reflectometry with Bidirectional Determination. IEEE Photonics Journal, *9*, (6), 1-9. 2017

[65] Ai, F., Li, H., He, T., Yan, Z., Liu, D., Sun, Q. Simultaneous Distributed Temperature and Vibration Measurement with UWFBG based Coherent OTDR. 2018 Optical Fiber Communications Conference and Exposition (OFC), *7*, (1), 1. 2018

[66] Zhi, Y., Pengxiang, S., Yongqian, L. Research on COTDR for measuring distributed temperature and strain. 2011 Second International Conference on Mechanic Automation and Control Engineering, *2011*, (1), 590-593. 2011

[67] Marcon, L., Miguel, G.H., Miguel, S.A., Riccardo, V., Andrés, G.R. Analysis of disturbance-induced "virtual" perturbations in chirped pulse φ-OTDR. IEEE Photonic Tech. L., *32*, (3), 158. 2020

[68] Liu, T., Li, H., Ai, F., Wang, J., Fan, C., Luo, Y., and others. Ultra-high Resolution Distributed Strain Sensing based on Phase-OTDR. 2019 Optical Fiber Communications Conference and Exhibition (OFC), *1*, (1), 1. 2019

[69] Li, C., Tang, J., Jiang, Y., Cheng, C., Cai, L., Yang, M. An Enhanced Distributed Acoustic Sensor with Large Temperature Tolerance Based on Ultra-Weak Fiber Bragg Grating Array. IEEE Photonics J., *12*, (4), 1-11. 2020

[70] Boyd R. W. (1992), Nonlinear Optics, Academic Press, USA.

[71] Kenichi, S., Linqing, L. Distributed fiber optics sensors for civil engineering infrastructure sensing. Journal of Structural Integrity and Maintenance, *3*, (1), 1-21. 2018

[72] Picholle, E., Montes, C., Leycuras, C., Legrand, O., Botineau, J. Observation of dissipative superluminous solitons in a Brillouin fiber ring laser. Phys. Rev. Lett. *66*, (11), 1454-1457. 1991

[73] Lichtman, E., Friesem, A.A., Waarts, R.G., Yaffe, H.H. Stimulated Brillouin scattering excited by two pump waves in single-mode fibers: erratum. J. Opt. Soc. Am. B, *5*, (2), 259. 1988

[74] Taranenko, Y.N., Kazovsky, L.G. Three-wave envelope solitons: can the speed of light in the fiber be controlled. IEEE Photon. Technol. Lett. *4*, (5), 494-497. 1992

[75] Yu, F.T.S., Yin, S. Fiber Optic Sensors Based Upon the Fabry-Perot Interferometer. Fiber Optic Sensors, *76*, (2) 41-74. 2002

[76] Horiguchi, T., Shimizu, K., Kurashima, T., Tateda, M., Koyamada, Y. Development of a distributed sensing technique using Brillouin scattering. J. Lightwave Technology, *13*, (7), 1296-1302. 1995

[77] Bai, Q., Wang, Q., Wang, D., Wang, Y., Gao, Y., Zhang, H., and others. Recent Advances in Brillouin Optical Time Domain Reflectometry. Sensors, *19*, (8), 1862. 2019

[78] Schenato, L. A Review of Distributed Fibre Optic Sensors for Geo-Hydrological Applications. Appl. Sci., *7*, (9), 896. 2017

[79] Dakin, J.P., Pratt, D.J. Temperature distribution measurement using Raman ratio thermometry. Fiber Optic and Laser Sensors III, *566*, (1), 249. 1985

[80] Zeni, L. Optical fiber distributed sensors: a tool for in situ structural and environmental monitoring. Proceedings of the IWL 1st Italian Workshop on Landslides, *2009*, (1), 1. 2009

[81] Hetch, J. Understanding Fiber Optics Prentice Hall, Fifth Edition. USA, 215. 2006

[82] GN Nettest. Understanding OTDRs. (2000) Part#33881. Rev. A. February.

[83] Palmieri, L., Schenato, L. Distributed optical fiber sensing based on Rayleigh scattering. The Open Optics Journal, *7*, (1), 104-127. 2013

[84] Horiguchi, T., Kurashima, T., Tateda, M. Tensile strain dependence of Brillouin frequency shift in Silica optical fibers. IEEE Photonics Technol. Lett., *1*, (5), 107-108. 1989

[85] Fang, Z., Chin, K., Qu, R., Cai, H. Fundamentals of Optical Fiber Sensors Wiley. 2012

[86] Nakayama, J., Lizuka, K., Nielsen, J. Optical fiber locator by the step frequency method. Appl. Opt., *26*, (3), 440-443. 1987

[87] Dolfi, D.W., Nazarathy, M., Newton, S.A. 5-mm-resolution OFDR using a coded phase-reversal modulator. Opt. Lett., *13*, (8), 678-680. 1988

[88] MacDonald, R. Frequency domain optical reflectometer. Appl. Opt., *20*, (10), 1840-1844. 1981

[89] Udd, E. An overview of fiber-optic sensors. Rev. Sci. Instrum., *66*, (8), 4018. 1995.

[90] Grattan, K.T.V., Sun, T. Fiber optic sensor technology: an overview. Sensor Actuat A-Phys, *88*, (1-3), 46-47. 2000.

[91] Gunduz, A.E., Goktas, H.H. Analysis of temperature sensitivity of fibers with high nonlinear characteristics in Rayleigh backscattering based OTDR temperature sensor. Optoelectronics and Advanced Materials, *17*, (11-12), 484-489. 2023

PUBLICATIONS FROM THESIS

1. A. E. Gunduz, H. H. Goktas, “Analysis of temperature sensitivity of fibers with high nonlinear characteristics in Rayleigh backscattering based OTDR temperature sensor”, published December 4, 2023, OPTOELECTRONICS AND ADVANCED MATERIALS – RAPID COMMUNICATIONS Vol. 17, No. 11-12, November-December 2023, p. 484-489.
2. A. E. Gunduz, H. H. Goktas, M Yucel, “Connector Position Detection Simulation Using OTDR Analysis” 4th International Marmara Sciences Congress (IMASCON), 2020, Spring.


ANKARA YILDIRIM BEYAZIT ÜNİVERSİTESİ